DESIGN OF AUTOMOTIVE JOINTS: USING OPTIMIZATION TO TRANSLATE PERFORMANCE CRITERIA TO PHYSICAL DESIGN PARAMETERS

by

Min Zhu

Dissertation submitted to the Faculty of the

Virginia Polytechnic Institute and State University

in partial fulfillment of the requirements for the degree of

DOCTOR OF PHILOSOPHY

in

Aerospace and Ocean Engineering

APPROVED:

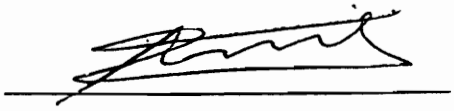

E. Nikolaidis, Chairman

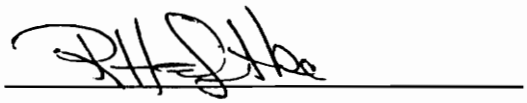

R. T. Haftka

O. F. Hughes

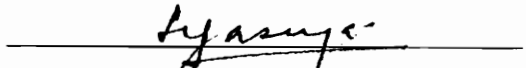

S. C. Jasuja

E. R. Johnson

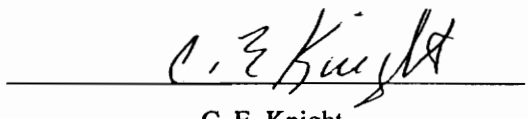

C. E. Knight

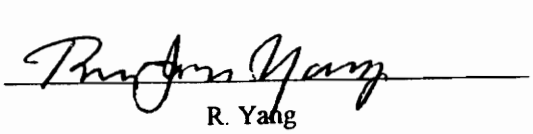

R. Yang

September, 1994

Blacksburg, Virginia

c.2

DESIGN OF AUTOMOTIVE JOINTS: USING OPTIMIZATION TO TRANSLATE PERFORMANCE CRITERIA TO PHYSICAL DESIGN PARAMETERS

by

Min Zhu

Committee Chairman: E. Nikolaidis
Aerospace and Ocean Engineering

(ABSTRACT)

In the preliminary design stage of a car body, targets are first set on the performance characteristics of the overall body and its components using optimization and engineering judgment. Then designers try to design the components to meet the determined performance targets and keep the weight low using empirical, trial-and-error procedures. This process usually yields poor results because it is difficult to find a good design that satisfies the targets using trial-and-error and there might even be no feasible design that meets the targets. To improve the current design process, we need tools to link the performance targets and the physical design parameters.

A methodology is presented for developing two such tools for design guidance of joints in car bodies. The first tool predicts the performance characteristics of a given joint fast (at a fraction of a second). The second finds a joint design that meets given performance targets and satisfies packaging and manufacturing constraints. These tools can be viewed as translators that translate the design parameters defining the geometry of a joint into performance characteristics of that joint and vice-versa.

The methodology for developing the first translator involves parameterization of a joint, identification of packaging, manufacturing and styling constraints, and establishment of a neural network and a response surface polynomial to predict the performance of a given joint fast (at a fraction of a second). The neural network is trained using results from finite element analysis of several joint designs. The second translator is an optimizer that finds the joint with the smallest mass that meets given performance targets and satisfies packaging, manufacturing and styling constraints.

The methodology is demonstrated on a joint of an actual car.

Acknowledgments

I sincerely thank my advisor, Dr. Nikolaidis, for his expert guidance, valuable suggestions and continuous encouragement throughout the development of this research. I thank all my committee members, R. T. Haftka, O. F. Hughes, S. C. Jasuja, E. R. Johnson, C. E. Knight, and R. J. Yang, for their time spent on my behalf. I also thank my fellow student, Xiandi Zeng, for his friendship and help during the years I was in Blacksburg.

I am thankful to the Ford Motor Company for funding this research.

Finally, I would like to express the deepest appreciation to my wife Xiaopin, for her continuous support and enormous encouragement throughout the entire Ph.D. program, and patience and understanding during the research and writing of this dissertation, and to my parents, Shanbao Zhu and Yuezhen Lu, for their discipline and inspiration throughout the formative years of my life.

Table of Contents

List of Tables

List of Figures

1. Introduction

The procedure for optimization of car bodies that is currently used by some automotive manufacturers uses a simplified model of a car body instead of a detailed model because the latter is too expensive and involves too many variables. Figure 1.1 summarizes this procedure. The simplified model represents components using *engineering parameters* such as stiffnesses of joints and moments of inertia of beams. Although the current procedure has helped design some recent car models, it has several drawbacks:

- The final optimum is defined using engineering parameters. It is difficult to develop design drawings from these parameters.

- The engineering parameters used to represent components might not correspond to a feasible design, that is a design that satisfies packaging and manufacturing constraints, because these constraints can not be linked directly to the engineering parameters.

- It is difficult to estimate the mass of a design from the values of the engineering parameters. As a result, crude, semi-empirical equations have to be used to estimate mass.

Due to the above drawbacks, the overall car body design process is very time consuming and in some cases leads to poor or even infeasible designs. Feasible design is a design that is manufacturable and satisfies packaging and styling constraints. To overcome these difficulties, we need a design tool that links the engineering parameters to the *physical design parameters* of the car body components. Physical design parameters, such as the dimensions of a beam, or the thickness of a plate, define directly the geometry of a component. Specifically, for given performance targets of each major car body component, we need a tool that determines the physical design parameters of a feasible design that satisfies these targets. This tool can be viewed as a translator because it translates given performance requirements expressed in terms of engineering parameters (for example cross sectional properties of a beam and stiffness of a joint) to values of the physical design parameters. The translators will make the optimization procedure more efficient and allow designers to obtain a truly optimum design of a car body because they will:

- help estimate the weight of a component accurately in optimization,
- ensure that the optimum engineering parameters that the optimizer yields correspond to feasible designs, and
- help designers find the actual designs of the components from the optimum engineering parameters.

Joints are important components of the car body because they affect significantly, and in some cases they even dominate, the static and dynamic behavior of a car. In this dissertation we propose a methodology to build translators for joints. Since there are many feasible joint designs for a given set of optimum performance targets, we propose to use

optimization to find the physical design parameters of the most efficient joint, that is the joint with the lowest mass, that satisfies these performance targets.

1.1 Background

1.1.1 Description of Vehicle Joints

A vehicle joint is a subassembly formed by several branch members that intersect together. It is a thin-walled structure that is formed by overlapping metal sheets fastened by spot welds. Figure 1.2 shows an example of a joint in a car.

1.1.2 Joint Models in Automotive Structures

Because of sharp discontinuity in the geometry of a joint and the loose fastening conditions, the joint connection itself will deform under load. Moreover, the thin-walled cross-section of the branches will severely deform in shear when it undergoes a twist moment (Vlasov 1961). Therefore, the end rotation of a branch will be different from the rotations of the other branches, which means that the joint is flexible. Hence, the conventional method of frame analysis with rigid joints can not be applied to predict the overall stiffness and dynamic behavior of a car body. Since 1970's, researchers have tried to understand the deformation mechanisms of joints and to develop simplified models to model the behaviors of joints. Chang (1974) proposed to use torsional springs to account for the joint flexibility in analysis of the overall car body stiffness. Lee and Nikolaidis (1991) developed procedures to estimate the parameters of simplified joint models that consists of springs using results of finite element analysis (FEA) of very detailed models

and/or from experimental measurements. Both studies demonstrated that the accuracy of a model of the overall car improves significantly if the model accounts for the joint flexibility. Nikolaidis and Lee (1992) developed a 3-D model that accounts for the flexibility, the offsets of rotation centers of joint branches, and the coupling between rotations of a joint branch in different planes.

Sunami et al. (1987, 1990) studied the joint stiffness of T- and L-shaped joints made of two box beams under in plane and out-of-plane bending, respectively. They used plates and stringers to model the joints and obtained analytical expressions of joint deflections using the shear flow theory (Vlasov 61). Their results agreed well with both experiment and FEA results. However, these approaches have limited application because they apply to rectangular cross-sections only and they can not account for structure imperfections such as service holes or details such as spot welds

Vlasov (1961) developed a theory for torsional deformation of a thin-walled beam using two sets of orthogonal functions (shape functions), one perpendicular to the cross-section and another lying in the plane of the cross-section, to describe the deformation of a cross-section. Nikolaidis and Zhu (1991) applied Vlasov's theory in inboard-outboard (I/O) bending of a T-shaped joint made of two box beams (Figure 1.3). Their results agreed well with those from FEA and from Sunami (1990). However, there are two major obstacles in applying Vlasov's theory in I/O bending of real joints. One is the difficulty to find the two suitable sets of orthogonal basis functions to represent the deformation of the cross-section. Another difficulties is the variation of the shape of the cross-section near the intersection of the joint branches.

Currently there are two types of models to simulate the behavior of joints in the design of car structures:

a) Simplified models

A simplified joint model is a very simple finite element model (FEM) that can be used to predict the static and dynamic behavior of a given joint. This model consists of springs, hinges and rigid elements, and it is defined in terms of engineering parameters, such as spring rates and coordinates of the positions of the hinges about which branches rotate. It has a small number of grids, usually less than 10. Figure 1.4 shows an example of a simplified 2-D joint model. Simplified models are used to represent joints in simplified (concept) FEM's of car bodies. These later models have about 2000 grids and are used in the early design stages.

Although the parameters of a simplified model can be estimated easily from tests, they represent conceptual rather than physical quantities that can be used to define a joint such as plate thicknesses and dimensions of members. Moreover, to develop a simplified joint model we need a detailed FEM or test data of a joint, which is not available in the early design stages. Therefore, we cannot directly use simplified joint models to guide design.

b) Detailed FEM of joints

These models account for many details, such as spot welds and openings. These models are used to predict the static and dynamic response of a given joint. Because of

their accuracy in predicting the static stiffness (error is less than 10%), they usually serve as reference for conceptual models when experimental data are lacking. They can also serve as useful tools in understanding the deformation mechanisms of joints. Figure 1.5 shows the detailed FEM model of the B-pillar-to-rocker joint model of a car. It has 1924 elements and 12,462 degrees of freedom.

Detailed FEM models are also of limited use in the early design stages because:

- They are expensive to develop and analyze. Therefore, we can not use them to evaluate many alternative designs.

- We can only use them to analyze a joint for which we have detailed drawings.

1.1.3 Translators for Design Guidance of Joints

In the early design stages of a car we use simplified model to optimize the car body. After the optimizer has yielded optimum values of the engineering parameters of the car body components, we need tools that relate physical design parameters, such as plate gages, with the performance characteristics of a joint, such as its stiffness (Figure 1.6). We call these tools translators. We may use these translators to predict the performance of a joint fast (within a few seconds or a fraction of a second, Figure 1.6, path A) or to translate specified performance characteristics of a joint to physical design parameters (Figure 1.6, path B). The first type of translators will allow designers to evaluate many designs fast in the early design stage of a car. The latter type (translators) will allow

designers to find the best joint, that is the joint with the lowest mass, that satisfies given performance targets.

1.2 Objectives

The objectives of this study are:

1. Develop a methodology for establishing a design guidance tool that predicts the performance of a given joint fast, with reasonable accuracy (Figure 1.6, path A).

2. Develop a methodology for translating specified performance targets for a joint, such as joint stiffness and mass into its physical design parameters (Figure 1.6, path B). This methodology will allow designers to find a joint, defined in terms of its physical design parameters, when they are given the desired performance characteristics of that joint. The found joint satisfies given packaging and manufacturing requirements.

In design of automotive structures, it is important to ensure that the B-pillar-to-rocker joint is adequately stiff in I/O direction (Figure 1.5), because the performance of this joint under I/O bending significantly affects the torsional rigidity of the overall car body. Hence, the above methodology will be applied to B-pillar-to-rocker joint. Only I/O bending will be considered in this study. However, the approach presented here is general and should apply to the forward-afterward (F/A) bending and the twisting cases of the B-pillar-to-rocker joint and also to other joints in automobile structures.

1.3 Outline

1.3.1 Outline of Methodology

The relations between physical parameters and performance of a joint are very complex. Except for the mass, which can be obtained based on the geometric information provided by design parameters, the performance of joint for a given set of design parameters needs to be evaluated using detailed FEA, which is very expensive.

In order to accomplish objective 1 in Section 1.2, that is to predict the performance of a given joint fast and inexpensively, we need to find an approximate tool to map the physical design parameters to the performance of the joint.

First, we parameterize the joint using a set of physical design parameters. This set is complete and contains only independent parameters. The term complete means that each set of these design parameters will define a joint uniquely while the term independent means that if we change only one parameter in a given set of parameter values defining a joint and keep the other parameters fixed, the new set will also define a valid joint design.

The total number of design parameters used in parameterization is relatively large (more than 30 for the B-pillar-to-rocker joint in this study). Therefore, it is difficult to map all of the design parameters to the performance of the joint. To circumvent this problem we use only a few parameters, which affect mostly the performance of a joint. To identify these parameters, we perform sensitivity analysis of joint stiffness with respect to all physical design parameters.

To accomplish the first objective of this study, we use response surface polynomials and neural networks to approximate the stiffness of a joint when the physical design parameters of that joint are given (path A, Figure 1.6). The coefficients of the polynomials and the weights of the Neural Networks are determined using results from FEA of several joint designs.

Once the objective 1 in Section 1.2 is accomplished, we have the tools to predict the joint performance in terms of a given set of design parameters. These tools are simple algorithms that can predict the joint performance very fast (in a fraction of a second). However, the relation between physical design parameters and performance characteristics of a joint is not one to one, because usually there are more than one joint design that fulfill the requirements set by the performance targets and other constraints such as packaging and manufacturing. We use the following two approaches to establish a translator that translates performance targets into the design parameters (objective 2, Section 1.2) :

a) Random Search

First, a set of random numbers uniformly distributed over the range from 0 to 1 is generated. The size of the set is equal to total number of physical design variables that define a joint. The random numbers are converted into design parameters so that the design parameters are uniformly distributed in their range of variation. Each set of random numbers corresponds to a set of design parameters, i.e., to a joint design.

A pool that contains many joint designs is created by generating a large number of the above sets of random numbers. Each design is screened against the performance targets and the packaging and manufacturing constraints. After screening, a small pool of feasible designs that satisfy the above requirements is obtained.

Finally, these feasible designs are ranked on the basis of the values of their performance characteristics. The first few designs are considered as a group of best designs. It is up to the designers to select the best design on the basis of the performance characteristics and shape of the feasible designs.

b) Numerical Optimization

Numerical optimization is used to find the design parameters of the lightest joint that satisfies the performance requirements and the packaging and manufacturing constraints.

One advantage of the random search approach is that it allows the designers to choose among several alternative good designs that satisfy all the packaging, manufacturing and performance requirements. On the other hand, numerical optimization usually converges to at least a local optimum. It usually yields a more efficient design than the random search.

1.3.2 Outline of Dissertation

The contents of this dissertation are arranged in the following order:

In Chapter 2, the deformation mechanisms of joint are investigated. The joint deformation of B-pillar-to-rocker joint is decomposed into deformation mechanisms.

In Chapter 3, the B-pillar-to-rocker joint is parameterized using a set of physical design parameters that define geometry of the joint. The design parameters are chosen such that they are meaningful to the designers. Then a generic model that can automatically output a FEM model of a joint, when the physical design parameters are given, is developed. Chapter 3 also compares predictions of joint performance obtained using the generic model and a detailed FEM.

In Chapter 4, the physical parameters are ranked on the basis of their effects on to the joint stiffness using the one-parameter-at-a-time method. The result of ranking is given for the joint in this study.

In Chapter 5, design modifications aimed at increasing joint stiffness in I/O bending are proposed based on the results of Chapters 2 and 4.

In Chapter 6, an algorithm that can predict the stiffness of a joint is developed. A few most significant parameters have been chosen to approximate the performance of a joint. The neural networks and response surface polynomials are used to map the design parameters to the joint stiffness. The learning algorithm used is backpropagation and the transfer function used is a tangent sigmoid function (also called hyperbolic tangent function). The number of unknown weights is close to but less than the size of the training data. The response surface polynomials used is a complete second order perfect

polynomial. A design of experiments method -- Box-Behnken's three level designs (Box and Behnken 60) has been chosen to create the training data base for Neural network and input data for response surface polynomials. The predictions of the stiffnesses of several joints using neural networks and response surfaces polynomials are compared with results from FEA to asses the accuracy of these tools.

In Chapter 7, an optimization scheme is proposed to minimize the mass of a joint. This scheme is applied to the B-pillar-to-rocker joint. Finally, a parametric study is performed to examine the effect of performance targets and the packaging and manufacturing constraints on the joint mass.

In Chapter 8, we give the concluding remarks of this study.

2. Deformation Mechanisms of Joints

In design of automotive structures, it is important to ensure that the B-pillar-to-rocker joint is adequately stiff in I/O direction. Indeed, the performance of this joint under I/O bending significantly affects the torsional rigidity of the overall car body. In some cases, requirements on adequate stiffness of the B-pillar-to-rocker joint dictate the design of that joint.

The flexibility of the B-pillar-to-rocker in I/O bending is due to the following factors:

- Bending deflection of the B-pillar
- Twist deflection of the rocker
- Shear deflection of the cross section of the rocker
- Deformation due to imperfections such as the spot welds and weld access holes
- Effects of other deformation mechanisms

In design of a joint, we usually start from a baseline design taken from an existing car model, evaluate several alternative design changes and choose and implement the ones that have the largest effect on the stiffness of the joint without significantly increasing the weight or cost. Therefore, it is important to know the relative importance of all deformation mechanisms because this will allow us to select and implement those changes

that affect the dominant mechanisms, thereby increasing the joint stiffness in the most efficient way.

In this chapter, we identify the deformation mechanisms that are responsible for the I/O flexibility of the B-pillar-to-rocker joint. We also quantify and compare the contributions of these deformation mechanisms to the joint flexibility.

In Section 2.1, we define the boundary of a joint. In Section 2.2, we describe the model of the joint subassembly of an actual car, the loading and constraints that are used in this study. In Section 2.3, we describe the physics of selected deformation mechanisms and how to quantify the effects of these mechanisms on the I/O flexibility. The results of this study are presented in Section 2.4.

2.1 Definition of the Joint Subassembly Used in This Study

A vehicle joint is defined as a region of structure, that contains the intersection or junction of two or more load-carrying branch members. This definition does not specify the lengths of the joint branches and the boundary conditions both of which are critical in determining the joint behaviors. Lee et al. (1991) demonstrated that the effect of the lengths of the joint branches on its behavior is significant because when the ends of a joint are constrained from warping and the in-plane deformation of the cross-sectional shape is constrained, the joint appears to be stiffer than it actually is, especially when the joint is subject to I/O bending. Consequently, a joint and the adjacent members are coupled. They also found that there is an upper threshold for the lengths of branch members. Beyond the threshold, the joint behaviors are not sensitive to the length of branch members. They

recommended to use a joint subassembly whose branch members exceed the aforementioned threshold. The stiffness corresponding to the threshold is called "effective stiffness". The advantages of using a subassembly are the following (Lee 1991):

- It provides an appropriate way to identify the important parameters that affect the response of the overall vehicle body or the subassembly.

- The effective stiffness represents the behavior of the joint in the overall car body more accurately than the stiffness of an isolated joint whose ends are constrained. The reason is that the isolated joint is usually considerably stiffer than the joint when it is part of the overall car body because the ends of the isolated joint are constrained in both tests and FEA analysis.

In this study, a joint subassembly whose branches are longer than the threshold, is used. Detailed information about this subassembly is given in the following section.

2.2 Description of the Joint Considered in This Study and Loading Condition

A 2-D frame structure of a car body is shown in Figure 2.1 in which the B-pillar-to-rocker joint is marked by a circle. We studied the B-pillar-to-rocker joint of an actual car. A detailed finite element model of this joint is shown in Figure 2.2. Figure 2.3 (a) is the side view of the model. The vertical and the horizontal members of this T-shaped joint are called B-pillar and rocker, respectively. An MSC/NASTRAN model is constructed by plate elements, CQUAD4 and CTRIA3 (Schaeffer 1979). There are 1924 shell elements and 12828 degrees of freedom in the model. There are structural imperfections, such as

spot welds and weld access holes in this model (Figure 2.3). The spot welds are modeled using rigid beam elements connecting the nodes of two or more plates that are spot welded.

The joint subassembly used in this study is formed by connecting the above joint model to the portions of the B-pillar and rocker shown in Figure 2.4. The lengths of the elongated parts are equal or large than the sensitivity threshold above which the stiffness is independent of the length (Section 2.1). Since the length of the B-pillar does not influence the joint stiffness, in the FEM of the subassembly, the B-pillar is connected to an equivalent beam whose length is equal to 500.0 (mm). This beam is placed on the extension of the shear axis of the B-pillar of the original joint. The model of this beam consists of 10 elements of the same length that is 50.0 (mm). The cross-sectional properties of this beam were chosen to be the same as those of the original portion of the B-pillar except for the cross product of moment of inertia that was assumed to be zero for the attached beam (Table 2.1). The elongated parts of the rocker have the same shape, material and physical properties as those of rocker sections at F1 and R1, respectively. The plates of the elongated parts of the rocker are also spot welded and the spot weld pitch is equal to that of the joint in Figure 2.2. The total elements and degrees of freedom of the subassembly are 3782 and 25464, respectively. The lengths of rocker and B-pillar of the subassembly are 1350 (mm) and 792 (mm) (measured from the center of the joint[1]), respectively. The I/O bending moment *Mx* acts at the tip of the pillar (Figure 2.4). The ends of rocker are clamped. In the following sections of this chapter, the deformation of the tip of the pillar is considered.

[1]Center of a B-pillar to Rocker joint is defined as the intersection of the normal to both the shear axes of the B-pillar and rocker, and the shear axis of the rocker.

2.3 Deformation Mechanisms

For the above mentioned joint subassembly under I/O bending, the resulting deformation at the tip of B-pillar (Figure 2.4) is due to the effects of the following deformation mechanisms:

- Bending of the B-pillar
- Twist of the rocker
- Shear deformation of the rocker cross-section
- Deformation due to imperfections such as spot welds and weld access holes
- Other unknown mechanisms

In I/O bending the rocker can be considered as a thin-walled beam undertaking a twist moment (Sunami et al. 1987). Besides twist deflection (St. Venant torsion), the rocker undergoes shear deformation that is induced by the deformation of the contour of the rocker section (Sunami et al. 1987 and Vlasov 1961). Figure 2.5 shows the shear and twist deformation of a rectangular section of a beam when applying a force couple to the vertical walls of the beam.

Bending of the B-pillar also contributes to the total deflection. Bending can be analyzed by classical beam theory.

The contribution of the spot welds is coupled with that induced by the shear deformation. To simplify the analysis of the deformation mechanisms, the deflection due to spot welds is considered as part of the shear deformation of the rocker.

Based on the aforementioned discussion, the total rotational deflection (angle) at the tip of the B-pillar under I/O bending (for either spot welds or continuous welds case) is,

$$\Phi_{tip} = \Phi_s + \Phi_t + \Phi_p + \Phi_o + \Phi_r \tag{2.1}$$

Where,

Φ_{tip} is total deflection at the tip of the pillar,

Φ_s is shear deflection of rocker,

Φ_t is twist deflection of rocker,

Φ_p is bending deflection of B-pillar,

Φ_o is deflection due to weld access holes,

Φ_r is the remaining component of the deformation (residual deformation) that can not be attributed to the above mechanisms. This residual deformation is due to some unknown effects.

We used the following procedure to estimate the components of the deflection due to shear deformation of the rocker, twist of the rocker and weld access holes: (In all the cases that are described below, the response of the joint was calculated using FEA.)

(A) Shear deformation of the rocker cross section

We clamped both ends of rocker at R2 and F2 positions (Figure 2.4), applied the I/O bending moment M_x to the tip of pillar and calculated the resulting deflection Φ_{tip}. Then we constrained the shear deformation of the rocker cross section by putting a pair of bulkheads within the rocker at positions F3 and R3 (Figure 2.4). These bulkheads have little influence to the twist rigidity of the rocker and do not restrain the warping deflection of the section. We calculated the deflection of the tip Φ'_{tip} of the modified joint under the same moment M_x. Assuming that the shear deformation of the rocker across section is zero when putting bulkheads in the rocker we can conclude that the reduction in the tip deflection is equal to the shear deflection of the rocker.

(B) Twist of the rocker

The twist deflection of the rocker is the angular rotation of the joint center when the twist moment M_x is applied at the center of the joint. Due to the complexity of the structure at the joint connection, it is difficult to apply the twist moment M_x at the joint center to obtain the twist of rocker Φ_o directly. To overcome this problem, we apply a moment at one end of the rocker, which is left free to rotate, we use the twist of that end to calculate the joint deflection and use the following procedure to obtain the twist of rocker at the joint center when both ends are clamped..

We clamped one end of the rocker and attached a panel to the other end that was left free. Then we applied a twist moment to this end. No load was applied to the tip of the

B-pillar. The deflection obtained at the free end was used to calculate the rocker twist rigidity approximately by St. Venant theory:

$$GJ = \frac{M_x L}{\Phi_{free}} \tag{2.2}$$

Where:

GJ is the twist rigidity of rocker

M_x is the moment applied at the free end of rocker

L is the length of rocker

Φ_{free} is the angular deflection at the free end of rocker.

Figure 2.6 (a) shows an example of the rocker subjected to a twist moment M_x on the plane of the section O, which passes through the centers of the joint. Both ends of rocker are clamped. GJ is the twist rigidity of the rocker. The rocker length measured from one end of rocker F2 to section O is d_f while the length measured from another end of rocker section R2 to section O is d_r. The rotational deformation due to moment M_x at section O is Φ_t.

The above rocker can be separated into front and rear parts (Figure 2.6 b). In Figure 2.6 (b) M_{xf} and M_{xr} are moments applied to front and rear parts, respectively while Φ_{xf} and Φ_{xr} are the angular deflections of front and rear parts, respectively. By using comparability condition (Deflection of point O is the same for both front and rear parts) and St. Venant theory, we obtained the following equations:

$$L = d_f + d_r \tag{2.3}$$

$$M_x = M_{xf} + M_{xr} \tag{2.4}$$

$$\Phi_t = \Phi_{xf} = \Phi_{xr} \tag{2.5}$$

$$\Phi_{xf} = \frac{M_{xf} d_f}{GJ} \tag{2.6}$$

$$\Phi_{xr} = \frac{M_{xr} d_r}{GJ} \tag{2.7}$$

By solving equations (2.2) to (2.7), we got

$$\Phi_t = \Phi_{xf} = \Phi_{xr} = \frac{M_x L}{GJ} \frac{d_f d_r}{L^2} = \Phi_{free} \frac{d_f d_r}{L^2} \tag{2.8}$$

where Φ_t is the angular rotation of rocker due to moment M_x applied at the section O (Figure 2.6 a).

(C) Weld access holes

We used plates that had the same material properties and thickness as those in the vicinity of the opening to cover the openings. Here we made up only for the two relatively larger openings as described in Section 2.2 (Figure 2.3 b). The difference in the deflection of the tip of the B-pillar before and after covering the openings was attributed to the effect of the openings, i.e.,

$$\Phi_o = \Phi_{tip} - \Phi_{no} \tag{2.9}$$

where Φ_{no} is the rotation of the assemble with its openings covered.

2.4 Results of Decomposition of Joint Deflection in I/O Bending

We calculated the static response of the B-pillar-to-rocker subassembly under an I/O bending moment M_x equal to 24,500 N.mm which is a typical loading condition used to evaluate the joint stiffness by Sunami (1987). We considered four cases. In the first three cases, the rocker was clamped at F2 and R2 (Figure 2.4). The resulting deflections at the tip and the root of the B-pillar are presented in Table 2.2. Case (1) is for the original joint model and its deflection is due to openings, spot welds and shear deformation. In case (2), we covered the openings of the original joint model. In case (3), we constrained shear deformation of the original model using transverse bulkheads at positions R3 and F3 (Figure 2.4). In case (4), we applied a twist moment at one end of rocker and calculate the twist of the rocker using the procedure described in Section 2.3 (B). Table 2.3 shows the twist deformation at the free end of the rocker when twist moment M_x is applied to the free end and the other end of rocker is clamped.

The results of the breakdown of the joint deformation are shown below:

(A) Deflection due to shear deformation of the rocker cross section

The shear deflection of rocker is the difference of Φ_{root} in cases (1) and (3) (Table 2.2),

$$\Phi_s = \Phi_{root,case\,1} - \Phi_{root,case\,3} = 5.294 * 10^{-3} rad.$$

(B) Deflection due to twist of the rocker

The twist deflection at the free end of rocker is (Table 2.3),

$$\Phi_{free} = 0.5218 * 10^{-3} rad. \tag{2.10}$$

From Figure 2.6 (a) and (b), d_f = 760 mm, d_r = 590 mm and L = 1350 mm. Using formula (2.8),

$$\Phi_t = 0.1284 * 10^{-3} rad. \tag{2.11}$$

(C) Deflection due to openings

The deflection due to opening is the difference of Φ_{root} between cases (1) and (2) (Table 2.2),

$$\Phi_o = \Phi_{root,case\,1} - \Phi_{root,case\,2} = 0.040 * 10^{-3} rad. \tag{2.12}$$

(D) Deflection due to B-pillar bending

From Table 2.2, we observe that the pillar deflection was the same in all three cases,

$$\Phi_p = \Phi_{tip} - \Phi_{root} = 0.117 * 10^{-3} rad. \quad (2.13)$$

We can also estimate Φ_p from classical beam theory,

$$\Phi_p = \frac{M_x L_p}{EI} \quad (2.14)$$

where

M_x is the bending moment (24,500 N.mm),

L_p is the length of the B-pillar from root to the tip (500 mm),

E is the Young's modulus ($2.1 * 10^5 N / mm^2$),

I is the I/O bending moment of inertia (487.480 mm^4)

Substituting into (2.13), we get

$$\Phi_p(theory) = 0.120 * 10^{-3} rad. \quad (2.15)$$

which is close to the value obtained by (2.13).

(E) Residual deflection

According to equation (2.1), the residual component of deformation is

$$\Phi_r = \Phi_{tip} - \Phi_t - \Phi_s - \Phi_p - \Phi_o = 0.5126 * 10^{-3} rad. \quad (2.16)$$

Figure 2.7 shows the contribution of each deformation mechanism to the total deflection of the tip of pillar of the subassembly. We observe that shear deflection dominates because it contributes over 86.9% of the total deflection. The twist deflection of the rocker, the bending deflection of the B-pillar and the deflection due to openings contribute 2.1%, 1.9% and 0.7%, respectively. The residual deflection is about 8.4%.

On the basis of above the observations we draw the following conclusions:

- For the joint studied the effect of shear deflection of the rocker is dominant -- it contributes about 87% of total deflection in I/O bending.

- The twisting deflection of the rocker, bending of B-pillar and the deflection due to the openings is less important.

- An effective way to increase the stiffness of the joint is to put two transverse bulkheads in the rocker near the center of the joint.

The above conclusions agree with those reported by Sakurai and Kamada (1988).

3. Parameterization of A Joint and Development of Generic Model

When a designer designs a joint of a car, he or she usually starts from an existing joint model and modifies it to reach specified performance targets. The designer needs to know which factors affect the performance targets and by how much. The designer could do a better job if he or she could represent a joint using a set of physical design parameters and had a relation between these parameters and the performance of the joint.

The process of finding a set of parameters to represent a joint is called parameterization of a joint. There are many ways to select the physical design parameters. However, a good set of parameters should fulfill the following requirements:

The parameters should be associated to physical quantities (dimensions, plate thickness) so that they can be understood easily by designers. Conceptual engineering parameters such as stiffness and lengths of rigid elements do not satisfy these requirements. Only important parameters, i.e., parameters that affect significantly the joint performance should be included in this set. It should be possible to estimate the joint performance with good accuracy using the values of the parameters (good accuracy means that the error between predictions and measurements is less than 10%).

In design, one needs to evaluate many alternative designs using FEA or tests. However, due to the complexity of the structure of a joint, it is very time consuming to create a FEM model of a joint. For instance, it takes several weeks or months to create

and validate a typical detailed joint model. Hence, the designer has to either consider fewer alternative designs or rely on his or her experience without analyzing a detailed FEM model. Hence, it is essential to have a generic procedure that can create a FEM model of a given joint fast based on given physical design parameters on the joint. The model created by the generic model should be detailed enough to represent the joint reasonably accurately but should not contain unnecessary construction details.

In this chapter, we parameterize a group of B-pillar to rocker joints that have a particular type of construction. Then, we propose a way to construct a generic model. Finally, we demonstrate how to apply the parameterization procedure and the generic model to an actual joint of a car.

In Section 3.1, we give a general idea of parameterization of a joint using physical design parameters. In Section 3.2, we describe the construction characteristics of the joint model and propose a way to create a generic model. In Section 3.3, we give the results of parameterization and the results of applying the generic model to the B-pillar to rocker joint used in this study.

3.1 Parameterization of a Joint

Parameterization of a joint is the procedure of finding a set of independent physical design parameters that is complete, i.e., only one joint corresponds to a set of values of these parameters. To parameterize a joint, one has to find out how many independent parameters are needed and choose these parameters.

We will use the following example of a rocker cross section shown in Figure 3.1 to demonstrate the procedure for parameterizing a joint. The rocker section shown in Figure 3.1 has 5 vertices. Panel BC is parallel to the Y axis while panel CD is parallel to the Z axis. All panels have the same thickness t.

3.1.1 Determine the Number of Independent Parameters

The above mentioned problem is equivalent to determining how many parameters are needed to define the geometry of the joint and the thicknesses of its plates uniquely. For the example rocker section shown in Figure 3.1, we can use the concept of analytical geometry to define the geometry. In this section, panel BC is parallel to Y axis and panel CD is parallel to the Z axis. The thickness of all the sides is constant. Let's select vertex E as the origin of the Cartesian coordinate system YZ. Each vertex is determined by its Y and Z coordinates. To define the shape of rocker cross section is equivalent to defining the y, and z coordinates of the other four vertices A, B, C and D, A(y), A(z), B(y), B(z), C(y), C(z), D(y) and D(z). Here (y) and (z) denote the Y and Z coordinates of vertex. We also have two constraints:

$$B(z) = C(z) \tag{3.1}$$

$$C(y) = D(y) \tag{3.2}$$

Hence, the total parameters needed to determine the coordinates of the other four vertices and therefore the section geometry are 6 (8-2=6). Considering that there is one

more physical parameter, the thickness of the plate, we need 7 (6+1=7) independent parameters to define the rocker cross section.

3.1.2 Choose Physical Design Parameters

There are many ways to choose physical design parameters that should not only be meaningful to the designer but also allow us to estimate the most important performance targets, such as stiffness and moment of inertia. For the rocker section shown in Figure 3.1, dimensional parameters $a - f$ and t can be used to define the cross section.

3.2 Construction Characteristics of the Joint Model and Generic Model

Parameterization of a joint yields a set of physical design parameters to define a joint uniquely. We also need a tool to generate a FEM using these parameters. In this section, we develop such a tool.

3.2.1 Construction Characteristics of B-pillar to Rocker Joints

Figure 3.2 shows the cross sections of B-pillar and rocker of the joint model used in this study. The joint consists of five components: the outboard panel (B-pillar and rocker share the same outboard panel), rocker inboard panel, B-pillar inboard panel, rocker shear panel and B-pillar reinforcement. The dark dots denote the spot welds which connect the five components together.

3.2.2 Generic Model

One way to develop a FEM model of a joint is to mimic the way the joint is constructed. First we model each component. Then we connect all components by appropriate welding, spot weld or continuous weld, to form the final joint model.

In order to create the FEM model of a joint fast, we propose a procedure to convert the physical design parameters to a FEM model of the joint automatically. We call the FEM model created by this procedure *generic model*. According to this procedure, the physical design parameters are converted to coordinates of the vertices of each component. Then a FEM model of each component is created. Finally, all components are connected by appropriate welding to form the joint model. Figure 3.3 presents a the flow chart of the procedure for developing a generic model.

3.3 Application to the Joint Assembly in This Study

3.3.1 Parameterization

We simplified the following characteristics of the joint model used in this study.

- Rocker section
- Openings
- Blending curve of B-pillar to rocker linkage
- Linkage length of B-pillar to rocker
- B-pillar

Figure 3.4 (a) and (b) show the rocker section of the joint subassembly (Figure 2.4) before and after the simplification. The folded parts marked by circles in Figure 3.4 (a) are simplified by straight lines.

The openings in the original model (Figure 2.3 b) are not considered in parameterization since their effect on the joint stiffness corresponding to inboard-outboard bending is very small (Section 2.4).

Figure 3.5 shows the blending curves of B-pillar to rocker connection of original model and how it was simplified. By comparing the results from the simplified joint model and a detailed FEM, we found that the simplification in Figure 3.5 has little influence on I/O stiffness.

Figure 3.6 is a sketch of the top view of the joint used in this study. The linkage lengths of B-pillar to rocker of the original model are shown in Figure 3.6 (a). RPL_O and RPL_I are the linkage lengths of outboard side and inboard side, respectively. We simplify this using the average of these two linkage lengths as the linkage length used in parameterization (Figure 3.6 b). Moreover, since the contribution of B-pillar to joint flexibility is very small (less than 2%), we use an equivalent beam of constant rectangular cross section to represent the B-pillar (Section 2.2).

On the basis of the above simplifications, we parameterize the joint assembly used in this study (Figure 2.4) using 35 independent physical design parameters. Figures 3.7 to 3.9 show a side view of the joint sub-assembly, the rocker cross section and the area near

the linkage of the B-pillar and rocker of the generic model and the parameters defining this model.

We further replace parameters B1, B2 and B4 by B1/B2, B2 and B4/B1, respectively. The reason for this is that, as we will show in Chapter 4, parameters B1/B2 and B4/B1 affect significantly the joint stiffness.

The values of the parameters of the joint subassembly used in this study (Figure 2.4) are listed in Table 3.1.

3.3.2 Generic Model

By using the procedure described in Figure 3.3, we can create the detailed FEM model of a joint with a given set of physical design parameters. We developed a program that can convert the physical design parameters into FEM model called generic model (MSC/NASTRAN data deck) ready to run. Figure 3.10 shows the FEM model created based on the values of parameters in Table 3.1. The model has 3211 shell elements and 21510 degrees of freedom. In order to check the validity of the generic model, we decomposed the joint deflection in I/O bending using the generic model and compared the results with respect to those of FEM model of the original joint subassembly as shown in Figure 2.4.

We calculated the static response of the B-pillar to rocker subassembly under an I/O bending moment M_x equal to 24,500 N.mm. We considered three cases. In the first two cases the rocker was clamped at F2 and R2 (Figure 2.4). The resulting deflections at

the tip and the root of the B-pillar are presented in Table 3.2. The shear deformation of the rocker section was constrained as explained in Section 2.3 (A). In case (1) no deformation mechanisms were constrained. In case (2), we constrained the original model from deforming in shear. In case (3), we calculated the twist of the rocker using the procedure described in Section 2.3 (B). Table 3.3 shows the twist deformation at the free end of the rocker when twist moment M_x is applied to the free end while the other end of rocker is clamped.

Using the method described in Section 2.4, we obtained the components of deformation corresponding to each deformation mechanism that are shown in Table 3.4. The corresponding values from the detailed (component) model, which were presented in Figure 2.7 are also shown in Table 3.4 for comparison.

From Table 3.4 we can see that order of importance of the deformation mechanisms and their contributions to the total deformation are roughly the same for the generic and the FEM model of the original joint subassembly. Specifically, the largest contribution is due to shear of the rocker cross section and is about 90% of the total deflection; the contributions of B-pillar and twist of rocker are both about 2% of the total deflection; the residual is 4% and 8.5% for the generic and the FEM model of the original joint subassembly, respectively. If we use the results from the FEM model of the original joint subassembly as reference, the relative changes in total deflection, the contribution of the B-pillar, the twist of rocker and the shear of the rocker are -6.9%, 0%, -28% and 1.21%, respectively. Even though the change in the twist of the rocker is large, the contribution of twist to the total deflection of the joint is small (about 2%).

The mass of the joint predicted using the generic and the FEM model of the original joint subassembly was found to be 11.208 and 11.319 kilogram, respectively. The change in the prediction of the mass from the generic model was only 1%.

On the basis of the above observations, we conclude that the generic model can predict the deflection and mass of the joint with reasonable accuracy.

4. Identification of Important Physical Design Parameters on Joint Stiffness

As was mentioned earlier, the stiffness of a joint affects significantly the performance of a car. In the previous chapter the B-pillar-to-rocker joint was parameterized using 35 independent parameters, which define completely its geometry. It is important to find out which parameters affect most the stiffness of the joint and by how much, because this will allow us to develop a simple design oriented model. In order to find the most important physical design parameters we perform sensitivity analysis of the joint stiffness in I/O direction with respect to the design parameters.

In this chapter, we use the one-parameter-at-a-time method to calculate the sensitivities and effects of parameters on stiffness and rank the parameters according to their sensitivities and effect on stiffness. In this method, we vary one-parameter-at-a-time around a baseline value and keep the rest of parameters fixed at their baseline values.

In Section 4.1, we define the stiffness of a joint in I/O direction. In Section 4.2, we briefly describe the one-parameter-at-a-time method that is used to calculate the sensitivities and effects of joint stiffness with respect to the physical design parameters. In Section 4.3, we calculate the sensitivities and effects of physical design parameters used in this study and rank the parameters based on their sensitivities and effects, respectively.

4.1 Definition of the Stiffness of Joint in I/O direction

From Section 2.3 we know that the angular deflection of the tip of beam connected to B-pillar in I/O direction consists of the following components:

- bending deflection of the B-pillar,
- twist deflection of the rocker,
- shear deflection of the cross section of the rocker,
- deformation due to imperfections such as the spot welds and service holes,
- effects of other deformation mechanisms.

Thus the total rotational deflection (angle) at the tip of the B-pillar under I/O bending is obtained from the following equation, which is the same as equation (2.1):

$$\Phi_{tip} = \Phi_s + \Phi_t + \Phi_p + \Phi_o + \Phi_r \tag{4.1}$$

Let M_x be the moment applied at the tip of the B-pillar in the I/O direction (Figure 2.4). To calculate the joint stiffness we remove the effect of bending deflection of the B-pillar and twist deflection of the rocker from the total deflection of the tip of the B-pillar since these two deflections can be calculated separately using strength of materials and these deflections can not be attributed to the flexibility of the joint. We define the stiffness of the joint in the I/O direction as follows:

$$K_{I/O} = \frac{M_x}{\Phi_{tip} - (\Phi_t + \Phi_p)} = \frac{M_x}{\Phi_s + \Phi_r + \Phi_o} \tag{4.2}$$

where $K_{I/O}$ is the stiffness of the joint in the I/O direction.

4.2 Method for Calculating the Sensitivities of Joint Stiffness with respective to Design Parameters and the Effects of These Parameters - One-parameter-at-a-time Method

Since a joint can be represented by a set of physical design parameters as described in Chapter 3, the stiffness of joint in the I/O direction is a function of these physical design parameters:

$$K_{I/O} = K_{I/O}(x_1, x_2, ..., x_n) \tag{4.3}$$

where $x_1, x_2, ..., x_n$ is a set of physical design parameters used to define a joint.

One-parameter-at-a-time method calculates the change of $K_{I/O}$ when only one parameter varies (the other parameters are fixed at their baseline values).

We used the logarithmic sensitivity derivatives of the stiffness with respect to the parameters and the effects of the parameters on the stiffness to assess the importance of the parameters. The logarithmic sensitivity derivative of the stiffness, $K_{I/O}$, with respect to the parameters x_i is defined as follows:

$$\text{Logarithmic Sensitivity of } K_{I/O} \text{ with respect to } x_i = \frac{x_i(0)}{K_{I/O}(0)} \frac{\partial K_{I/O}}{\partial x_i} \tag{4.4}$$

where $x_i(0)$ and $K_{I/O}(0)$ are the values of x_i and $K_{I/O}$ that correspond to the baseline joint. Equation (4.4) gives changes in $K_{I/O}$ with respect to x_i normalized by $K_{I/O}$. We will use term **sensitivity** for the logarithmic sensitivity derivatives in this dissertation. The derivative of $K_{I/O}$ with respect to x_i is estimated using central finite difference:

$$\frac{\partial K_{I/O}}{\partial x_i} \approx \frac{\delta K_{I/O}}{\delta x_i} \tag{4.5}$$

where $\delta K_{I/O}$ is the change in stiffness due to a change δx_i in parameter x_i.

The **effect** of x_i on $K_{I/O}$ is defined as the change in $K_{I/O}$ due to a change in x_i normalized by baseline stiffness:

$$\text{Effect of } K_{I/O} \text{ with respect to } x_i = \frac{\Delta K_{I/O}}{K_{I/O}(0)} \tag{4.6}$$

where

$$\Delta K_{I/O} \approx K_{I/O}(x_1, x_2, \ldots, x_i + \frac{\Delta x_i}{2}, \ldots, x_n) - K_{I/O}(x_1, x_2, \ldots, x_i - \frac{\Delta x_i}{2}, \ldots, x_n) \tag{4.7}$$

where $x_i, i = 1,...,n,$ are the values of the parameters corresponding to the baseline design, and Δx_i is the range in which parameter x_i is expected to vary if we consider different possible designs. Note that the sensitivity and effect with respect to parameter depends on the values of the parameters. In this study, the effects were calculated by varying the parameters about the values that corresponding to the baseline design.

4.3 Ranking of Parameters Using Sensitivities and Effects

In this study, we used one-parameter-at-a-time method to calculate the sensitivities and effects of stiffness in I/O direction with respect to physical design parameters. Then, we ranked the parameters based on the sensitivities and effects, respectively. The generic model was used to predict the stiffness of the modified joint designs.

Thirty five physical design parameters are used to describe the joint assembly in this study (Figures 3.7 to 3.9). We fixed 8 of the 35 parameters: the length of the rocker RL, the length of B-pillar PL, the distance between B-pillar blending curve and front end of the rocker X_ini (Figure 3.7), the angle between the B-pillar and Rocker α_p (Figure 3.7), and width of the flanges of rocker and B-pillar ZZU, ZZL, ZZM (Figure 3.8) and W (Figure 3.9). We were not interested in studying Rl, PL, X_ini and α_p since they are global parameters that define the global configuration of the joint subassembly. We fixed ZZU, ZZL, ZZM and W since they are width of flanges that are usually fixed in real joints due to manufacturing constraints. Table 4.1 shows the values of the fixed parameters. The sensitivities and effects of the rest 27 physical design parameters were evaluated. The ranges in which parameters varied for evaluating the sensitivities of these parameters are $\pm 5\%$ from their baseline values ($\delta x_i = 5\% x_i$). The ranges for evaluating the effects of the

parameters ,$\pm\Delta x_i$, were chosen so that the parameters reach their lower and upper bounds dictated by the packaging and manufacturing constraints. Table 4.2 lists the names of the parameters x_i and their corresponding *baseline* values, ranges used for calculating sensitivities, δx_i, and ranges of these values used in calculating effects of the 27 parameters. Here, baseline means generic model of the joint subassembly shown in Figure 2.4.

Table 4.3 shows the normalized $K_{I/O}$ at $x_i \pm \delta x_i$, the estimated sensitivities and the results of ranking of parameters based on their sensitivities. The normalized $K_{I/O}$ was obtained by dividing its current value by that of the baseline joint. Table 4.4 gives the normalized $K_{I/O}$ for the lower bound, $(x_i - \Delta x_i)$ and upper bound, $(x_i + \Delta x_i)$ of x_i, the effects obtained using (4.6) and the ranking of parameters based on their effects. We notice from Tables 4.3 and 4.4 that the top 5 ranking parameters for both sensitivities and effects contains the same group of parameters. These top 5 ranking parameters are (from most to least significant): B1/B2, T1, B4/B1, RPL, B2 for ranking by sensitivities and B1/B2, T1, RPL, B4/B1, B2 for ranking by effects.

We also calculated $K_{I/O}$ for several values of each parameter to identify nonlinearities in the relation between the parameters and $K_{I/O}$. We found that the variation of $K_{I/O}$ with respect to H3 and α_1 is not monotonic at the baseline point. Figure 4.1 shows the relation of normalized $K_{I/O}$ with H3 and α_1. We then calculated sensitivities of effects of H3 and α_1 using backward and forward differences. Table 4.5 shows the sensitivities of H3 and α_1 using backward and forward differences. Comparing the sensitivities in Table 4.5 with those in Table 4.3, α_1 should be ranked in position 7 or 6 in Table 4.3 whereas H3 should be ranked in position 5 if we use sensitivities obtained by backward or forward

differences in Table 4.5. For this reason, we consider H3 and α_1 among the first 7 most important parameters.

5. Design Modifications to Increase Joint Stiffness in I/O Bending

The I/O stiffness of B-pillar to rocker joint is an important performance target in design. On the basis of the results of Section 2.4 and Section 4.3, we propose some design modifications that should be effective in increasing the I/O stiffness of the joint. The proposed design modifications are divided into two parts. One called "generic modifications" applies to any T-shaped thin-walled joints. The other called "specific modifications" applies only to the joint used in this study.

Sections 5.1 and 5.2 describe the general purposed modifications and the specific modifications , respectively.

5.1 Generic Modifications

In this section, we consider I/O bending of a T-shaped joint formed by two thin-walled beams. As it was mentioned in Section 2.4, the shear deformation of the rocker is the most important deformation mechanism because it is responsible for roughly 90% of the total deflection of the joint. Sunami et al (1987) studied the I/O stiffness of T-shaped joints made of two intersecting box beams. They also found that the shear deformation of horizontal member is a dominating factor that affects the I/O stiffness of the joint (contributing over 80% to joint stiffness). The reason for the large shear deformation of rocker is partly due to the discontinuity of the structure between load carrying members (B-pillar and rocker) at the joint connection. This is due to the fact that the panels of the

vertical and the horizontal members are not flush. Figure 5.1 shows this discontinuity of the structure in a simplified T-shaped joint. In Figure 5.1, the major load applied from the B-pillar to the rocker on the top panel of rocker is normal to this panel. Since the top panel of rocker is thin, it deflects considerably under I/O bending. Hence, the rocker section will have large shear deformation under I/O bending.

We proposed the following "generic design modifications" for strengthening the structure at the connection part of joint to reduce the shear deformation of the rocker of a T-shaped joint.

- Introduce 2 transverse bulkhead in the outboard cell of the rocker (Figure 5.2). These panels can be spot welded or seam welded to the outboard panel of the rocker.

- Extend the B-pillar so that it forms a cap inside the rocker (Figure 5.3).

- Add a plate in the rocker as shown in Figure 5.4. This plate will reinforce the linkage between the rocker and the B-pillar thereby reducing the shear deformation of the rocker.

Figure 5.5 shows the effect of 2 transverse bulkheads (Figure 5.2) on the stiffness of the joint used in this study (Figure 2.4). These bulkheads are spot welded to the outer panel of the rocker. We used both the generic model and the detailed FEM to derive the results in Figure 5.5. It is observed that this modification increases the stiffness of the joint by 102%. We also found that the efficiency of the joint (stiffness over mass)

increases by approximately 101%. It is also observed that the generic model and the FEM model of the original joint subassembly are in good agreement.

Figure 5.6 shows the effect of 2 transverse bulkheads, which are continuously welded to the inboard panel, outboard panel and the shear plane, on the stiffness of a continuously welded joint. We used the generic model to derive the results in this figure. It is observed that this modification increases the joint stiffness by approximately 14 times.

5.2 Specific Design Modifications for the Joint Used in This Study

In this section, we consider the joint that is part of an actual car that is used in this study. As it was mentioned in Section 4.3, the most significant parameters are B1/B2, T1 and RPL (Figure 3.8, Figure 3.9). Table 5.1 gives the effects (Table 4.4) of these parameters on I/O stiffness based on the ranges considered in Table 4.2. We can see from Table 5.1 that the I/O stiffness increases 187%, 124% and 19.5%, respectively when B1/B2, T1 and RPL vary from their lower to upper bounds used in this study. Figure 5.7 explains why B1/B2 is a very important parameter. The load of B-pillar on the top panel of the rocker can be simplified as a force pair F-F as shown in Figure 5.7 (a). This top panel in Figure 5.7 (a) is further simplified as a simply supported beam that has a unit span. Force F acts at B1/B2 from the left end B. For B1/B2 being greater than 0.5, the larger B1/B2 is, the smaller the deflection at point C will be.

Figures 5.8 and 5.9 show the proposed modifications. These modifications include the following:

- Increase the thickness of the outer cell of the rocker, T1 (Figure 5.8).

- Increase B1/B2 (Figure 5.8).

- Increase the radius of the blending curve, thereby increasing the length of the linkage between the B-pillar and the rocker (Figure 5.9).

5.3 Summary

For the joint consisting of two thin-walled beams, we proposed to reinforce the structure at the connection area between B-pillar and rocker (Figure 5.2 to Figure 5.4). For the joint whose geometric contour of rocker section is similar to that used in this study, we also propose to increase values of B1/B2, T1 and RPL.

However, there are concerns about manufacturing difficulties and increasing cost for the proposed generic modifications. For example, the spot welds which connect the bulkhead with the rocker outer panel will affect the appearance of this panel. This is not important in case that the outer surface of the rocker is covered with plastic modeling, but is unacceptable for a car whose outer rocker surface is exposed. Due to the possible increase in complexity and the cost associated with these modifications, we decided not consider them further in this dissertation and focus on a joint design whose type of construction is shown in Figure 2.2.

Note that the above proposed design modifications should be subject to the constraints of performance, such as moments of inertia of rocker section, manufacturing and packaging constraints that will be discussed in Chapter 7 in detail.

6. Development of Algorithm to Predict the Stiffness of Joints

The stiffness of joints is usually estimated using finite element analysis (FEA) or experiments. Both methods are time consuming and expensive. Therefore, it is difficult to use them in optimization where we need to analyze many design alternatives fast. Instead, approximate methods should be used to predict the joint stiffness. In this study, we use response surface polynomials, and artificial neural networks, to predict the stiffness of a joint.

Methods using response surface polynomials are well established. The area of artificial neural networks (also called neural networks) is relatively new. Neural networks can be used to approximate any function or functions of several input variables. This is the case with the joints; due to the packaging and manufacturing constraints, the physical parameters of the joints can vary only in narrow ranges. Neural networks have proved to be very effective in approximating input -- output relations when the input variable range is limited.

In this chapter, we use a response surface polynomial and a neural networks to map the design variables of a joint to its stiffness. The polynomial and neural network can be used as design tools for predicting the stiffness of a given joint fast (Objective 1, Section 1.2).

In Section 6.1, we describe two approximate mapping methods: response surface polynomials and artificial neural networks. In Section 6.2, we describe Box's three-level designs that are used to collect data for fitting response surface polynomials and training neural networks. In Section 6.3, we introduce the coefficient of variation as the metric for evaluation of the accuracy of the approximate methods. In Section 6.4, we present the results of application of response surface polynomials and neural networks to the B-pillar to rocker joint used in this study.

6.1 Prediction of Stiffness Using Approximate Methods

As described in Chapter 3, a joint can be represented by a set of physical design parameters. We want to find a relation between these physical design parameters and the stiffness of the joint. Thus, we want to establish the following relation:

$$K = K(x_1, x_2, ..., x_n) \tag{6.1}$$

where K is joint stiffness and $x_i (i = 1, 2, ..., n)$ is a set of independent physical design parameters. For convenience, we also call x_i's *design variables* in the following discussion.

The relation of equation (6.1) is very important at the early design stage of the joint since it can guide the designer to get a better design. FEA method can be used to map one **particular** set of parameters to stiffness with good accuracy. However, it will be impractical to use FEA method to map all possible combinations of parameters to stiffness since the number of these combinations is too large and the FEA method is very time

consuming. To overcome this problem, we propose to use the following two approximate methods to map the set of physical design parameters of a joint to the stiffness with acceptable accuracy: response surface polynomials and artificial neural networks. Due to the large number of packaging and manufacturing constraints that a joint must satisfy, the range in which physical parameters describing the joints can vary is narrow. Detailed descriptions of the response surface polynomials and artificial neural network are given in Sections 6.1.1 and 6.1.2.

6.1.1 Response Surface Polynomials

We rewrite the equation (6.1) in the following form:

$$K = f(x_1, x_2, ..., x_n) + \varepsilon \tag{6.2}$$

where f is a selected function to approximate K and ε is the error of the approximation. The surface represented by f is called *response surface*. Usually, a lower-order polynomial in some region of the independent design variables is chosen for f. Of course, one polynomial model can hardly approximate f over the entire space of the independent design variables but it usually works well in a small region of design variables. The following equation gives a complete second-order polynomial

$$f = \beta_0 + \sum_{i=1}^{n} \beta_i x_i + \sum_{\substack{i=1 \\ i \le j}}^{n} \beta_{ij} x_i x_j \tag{6.3}$$

β's are the model parameters to be found using regression least squares. The parameters can be estimated more efficiently if proper experimental designs are used to collect the data. Designs for fitting response surfaces are called *response surface designs* and they will be discussed in Section 6.2. We use complete second-order polynomials in this study.

6.1.2 Artificial Neural Networks

Artificial neural networks are mathematical models inspired by the neurons in human brain. Artificial neural networks perform various tasks such as mapping, memorization, and image processing. Hajela and Berke (1992), Berke et. al. (1992), and Swift and Batill (1991) have shown that neural networks may have significant potential in analysis and design of structures. In the following we review some important characteristics of neural networks. Hecht-Nielsen (1990), Obermeir and Baron (1989), and Caudill (1992A-B) provide an overview of neural networks.

Architecture of Neural Networks

Artificial neural networks consist of interconnected processing elements called neurons. Each neuron receives inputs through interconnects. An interconnect has a weight attached to it. It scales the signal that passes through it by this weight. Each neuron produces an output that is a function of the sum of its inputs. We may have several layers, each of which consists of several neurons connected in parallel (Figure 6.1). The layers are usually connected in series, so that the outputs of one layer are fed to the next layer. A neural network has an input and an output vector. These vectors consist of

numbers. The input is fed to the first layer of neurons that is called input layer. The last layer, whose output is the output of the network, is called output layer.

A mathematical model of a single neuron is shown in Figure 6.2. The input p (a row vector) is transmitted throughout a connection that multiplies its strength by weight w (a row vector), to form the product wp^T. The weighted input wp^T plus b (a number called *bias*) is the argument of the transfer function F, which produces the output a. The transfer function is typically a sigmoid function or tangent-sigmoid (hyperbolic tangent) function. The following equation describes a tangent-sigmoid function

$$y = F(x) = \frac{e^{2x} - 1}{e^{2x} + 1} = \tanh(x) \tag{6.4}$$

Figure 6.3 is a plot of the above tangent-sigmoid function.

Applications of neural networks

A neural network transforms an input to an output. We may use a neural network to simulate a multi input-output system and predict the system response to a given input.

First, we layout the structure of the neural networks including number of layers and number of neurons for each layer. Then, we select the transfer function for each neuron and decide whether to consider the bias for the neuron. Finally, we choose the learning algorithm to determine the parameters of a network using known sets of input and output vectors, called training sets. We provide these training sets to the network,

assign some initial values to its parameters and run the network (which adjusts its parameters according to the learning algorithm and sum of the square error criteria) over and over until the output is satisfactorily accurate. This procedure of determining the network parameters is called *training*.

Once we have trained a neural network, we may use it to estimate the response of the system to any input even if that input does not belong to the training set. Of course, this input should be within the range of variation of input vector used in training.

There are several algorithms that are used to train the neural networks, that is to find the appropriate weights and biases of the neurons to minimize the sum of square error of the network. These algorithms are called learning algorithms. The most popular algorithm is called *backpropagation* (Rumelhart D. E. et al 1986). This algorithm adjusts the values of the network weights and biases in the direction of steepest descent with respect to the error. The changes in each weight and bias are proportional to that element's effect on the sum of square error of the network. The differentiability of the transfer function, such as tangent-sigmoid function, enables the implementation of the steepest descent that is the key part of the backpropagation algorithm.

Some advantages of neural networks

Neural networks are usually more effective than algebraic polynomials, because they approximate functions more smoothly near the boundary of the domain of the independent variables than polynomials.

We do not need to program neural networks. We teach them to give satisfactory answers by providing them with known inputs and outputs. Thus, the user can treat a neural network as a black box. All he or she needs to do is to input the training sets. Thus, neural networks are easier to use than artificial intelligence codes, which need to be programmed by the user. However, it is up to the user to select the architecture and the learning algorithms that are most suitable for the user's problem.

6.2 Experimental Designs for Fitting Polynomials and Training Neural Networks

The preparation of the data for fitting the function is as important as choosing the function for the regression model. The model parameters can be estimated more efficiently if proper *experimental designs* are used to collect the data. Experimental design is a process of planning experiments (set up the levels of the design variables) so that appropriate data can be collected. Experimental design is more efficient than traditional one-parameter-at-a-time method in collecting data. For second-order polynomials, an experimental design must have three levels for each variable so that the model parameters can be estimated (Montgomery 1976). The most commonly used experimental designs for fitting polynomials are known as Box-Behnken designs. These will be described in the next section. The same experimental designs were used for training the neural networks and fitting the polynomials in this study.

6.2.1 Box-Behnken's Three Level Designs

Box-Behnken designs (Box-Behnken 1960) require that all variables can only be set at three possible levels, namely "low level", "nominal level" and "high level", respectively.

Table 6.1 gives these designs from 3, 4, 5 and 7 independent variables. We will use a matrix for 3 variables to explain Box-Behnken designs. In this matrix, the "low level", "nominal level" and "high level" correspond to -1, 0 and +1, respectively. The three columns of the matrix correspond to three independent variables. The rows are the settings of variables corresponding to the runs of the experiments. Notice that shorthand notation of the runs. The first row in the matrix is (± 1 ± 1 0), which represents the following four runs: (+1,+1,0), (+1,-1,0), (-1,+1,0) and (-1,-1,0). The design is an incomplete design, which means that it does not include all the possible combinations of the levels of the independent variables. For a 3 variable case, the number of runs for complete design is 27 while that for Box-Behnken designs is 13. Another property of the design is that it is *orthogonal blocked* which means that the runs represented by each column in the matrix are orthogonal with respect to each other (i.e., the dot product of any pair of columns is zero). We also notice from Table 6.1 that the number of runs increases rapidly as the number of independent variables increases. For example, the number of runs increases from 13 to 57 as independent variables increase from 3 to 7. The data collected by Box-Behnken designs will be used for fitting response surface polynomials and training neural networks. Figure 6.4 shows the experiments corresponding to the design matrix for 3 factors.

6.3 Metric for Evaluation of the Accuracy of the Response Surface Polynomial and Neural Network

Suppose we have analyzed m joint designs using FEA and an approximate method (response surface or neural network). Then we have m pairs of estimates obtained from FEA and the approximate method. We define the following quantity

$$b_i = \left(\frac{K_{predicted}}{K_{FEA}}\right)_i \qquad (i = 1,2,...,m) \tag{6.5}$$

where $K_{predicted}$ and K_{FEA} are stiffnesses predicted by an approximate method and FEA, respectively. If the prediction of the approximate method is close to that of FEA, the value of b_i is close to 1. Furthermore, we define the following statistical quantities:

$$\bar{b} = \frac{1}{m}\sum_{i=1}^{m} b_i \tag{6.6}$$

$$SSE = \sum_{i=1}^{m} (b_i - \bar{b})^2 \tag{6.7}$$

$$\sigma = \sqrt{\frac{\sum_{i=1}^{m} (b_i - \bar{b})^2}{m}} \tag{6.8}$$

$$\text{cov} = \frac{\sigma}{\bar{b}} \tag{6.9}$$

where $\bar{b}$, SSE, σ and cov are the *mean, sum of square errors, standard deviation* and *coefficient of variation* of b.

We choose cov as the metric for evaluation of the two approximate methods used in this study because it measures the scatter in the error of the approximate method. The smaller the value of the cov, the more accurate the predictions of the approximate method are.

6.4 Application of Approximate Methods to B-pillar to Rocker Joint

In this study we will investigate how suitable response surface polynomials and neural networks are in predicting the I/O stiffness of a joint when we specify its physical design parameters. We use Box-Behnken designs for fitting response surface polynomials and training neural networks. Then, we generate testing data for testing response surface polynomials and neural networks in estimating stiffness. The testing data are obtained by varying all physical design parameters randomly in their variation ranges and by predicting the stiffness using FEA. The cov of b mentioned in Section 6.3 will be used to evaluate the results.

As mentioned in the previous section the number of runs to collect data will increase rapidly as the numbers of independent variables increase. We can not afford to use all the physical design parameters that describe the joint. On the other hand, based on the results of Section 4.3, we know that only some of the physical design parameters are important to the I/O stiffness of the joint. Hence, we plan to select the number of

parameters to represent joint step by step. First, we select the first 3 most significant parameters on I/O stiffness to represent the joint stiffness from Table 4.4. We use Box-Behnken designs to collect data and check the results of both methods. Then, we include the next significant parameter in the ranking to represent the I/O stiffness. We check the results again to see if the results converge. Finally, we select the number of parameters at which the *cov* of b starts to converge. Notice that as the number of independent variables in the relation between stiffness and the variables increases the number of experiments needed to establish the polynomial or the neural network increases.

6.5 Results

First we selected parameters to describe the joint and determine their ranges of variation. Thirty-five parameters were used to describe the joint used in this study. We considered that 27 parameters vary, which are shown in Table 4.2. The rest 8 parameters were fixed at their baseline design values since they are either global parameters in which we were not interested or parameters that are usually fixed in a real joint (see Section 4.3 and Table 4.1).

Then we selected parameters to represent I/O stiffness of joint step by step as described the previous section. In Section 4.3, we ranked the parameters based on their *effects* on the I/O stiffness of the joint used in this study. Table 6.2 gives the first 7 based on the conclusions of Section 4.3. We used the first 3, 4, 5 and 7 parameters to represent the I/O stiffness of the joint.

6.5.1 Data Preparation

For each number of parameters used to represent the joint stiffness, we used Box-Behnken designs (Table 6.1) to create the data for fitting/training polynomials/neural networks.

We also created a group of testing data for checking the results of fitted polynomials and trained neural networks. Fifty data points were created by randomly varying the 27 parameters in their ranges (the ranges are given in Table 4.2). The results from FEA of the joint designs corresponding to these 50 data points were used as the reference with respect to which the results of the two approximate methods were compared.

All of the above data points were *feasible* designs of the joint (A design is feasible if it satisfies all the packaging and manufacturing constraints. The constraints will be described in Section 7.3.2).

6.5.2 Structure of the Polynomials and Neural Networks

Polynomials

We used second order complete polynomials to approximate the joint stiffness. Table 6.3 shows the number of unknown regression coefficients for 3, 4, 5 and 7 parameters. The reason for this is that the ranges of physical design parameters are narrow and the stiffness changes smoothly as the variables change in their ranges.

Neural Networks

There are many possible selections of the structure of the neural networks. However, we should keep the unknown weights of the networks less than the number of data points used in training the network because otherwise the network will simply tend to "memorize" the training data points. For 3 parameter case, we tried to use different combinations of the number of inner layers and the number of neurons for each inner layer to form different networks. The neural networks with one inner layer and the total number of unknown weights being close to the number of training data points gave the best results. Hence, we followed this rule to select the neural networks used in this study. Figure 6.5 shows an example of such a neural network. Table 6.4 shows the number of unknown weights for 3, 4, 5 and 7 parameters. We also tried to use sigmoid ($y=(1+e^{-x})^{-1}$) and tangent sigmoid function (6.3) as the transfer function for the neurons. Both functions worked well for the 3 parameter case. Hence, we chose tangent-sigmoid function as the transfer function in this study for the neurons in the input and hidden layer. The transfer function of a neuron in the output layer was linear.

6.5.3 Results Fitting/Training and Testing

The regression coefficients were obtained using MATLAB (1992) pseudo inverse function while the neural networks were trained using a backpropagation algorithm.

Fitting/Training

We compared the predictions of the joint stiffness used in training by comparing the polynomials and neural network predictions with FEA predictions. Figure 6.6 gives the

results of *cov* versus number of parameters used to represent I/O stiffness of the joint for fitted polynomials and trained neural network. From Figure 6.6, we observed that the minimum value of *cov* is about 3.5% and 5.6% for neural networks and polynomials respectively. Figure 6.7 compares the prediction of polynomials, neural networks and FEA when 7 parameters are used. From Figure 6.6, we observed that the values of *cov* for neural networks are less than those of polynomials, which means that the neural network fits training data better than polynomials do in this case. The reason is that the number of unknown weights of the neural networks is larger than the coefficients of the polynomials (Tables 6.3 and 6.4). Moreover, it seems that the *cov* of the polynomials does not convergence for the fitting/training data set. The reason for this is that for different number of parameters used to represent joint stiffness, the fitting/training data set is different. Hence, we should not expect the convergence of these data sets.

Testing

We predicted the stiffness of the joint designs corresponding to the 50 point testing data set using both approximate methods and compared them with predictions obtained from FEA. Figure 6.8 shows the *cov* versus number of joint parameters that the polynomials and neural networks use to predict stiffness. Figure 6.9 compares the prediction of polynomial, neural network and FEA for the set of 50 point testing data when 7 parameters are used. When using polynomials, the *cov* ranges between 9% and 12.01%. The minimum value of *cov* corresponds to a polynomial with 5 parameters and is about 9%. The *cov* corresponding to the neural network reduces monotonically as the number of design parameters increases and the *cov* converge to a value that is approximately equal to 7.79%. From Figure 6.8, we observed again that neural networks

fit the random testing data better than the polynomials. We also observed that testing results of neural networks converge after using the first 7 most important parameters to predict the joint stiffness.

We also checked the predictions of polynomial and neural network for the 7 parameter case using a different number of testing data. We used a sliding window with width equivalent to 25 data points to choose data points from the 50 testing data points mentioned above. We will call the points point 1, ..., point 50. First, the window covered the first 25 data points of the 50 testing data points (points 1 - 25). Then, we moved the window one data point forward to cover points 2 to 26. Finally, the window covered points 26 to 50. In this way, we obtained 26 different testing data sets. Since the 50 testing data points were created randomly, the obtained 26 data sets were also random. We used these data sets to predict the stiffness of the joint designs using the fitted polynomial and the trained neural network. The *cov*'s of the polynomial and neural network corresponding to this data set are given in Table 6.5. The maximum values of *cov* for polynomial and neural network were 12.03% and 8.01%, respectively, while the minimum values of *cov* were 11.54% and 7.58%, respectively. Again, we observed that the prediction of neural network is slightly better than that of polynomials.

On the basis of the above observed results, we draw the following conclusions:

1. Both approximate methods can predict the stiffness of the joint used in this study with acceptable accuracy.
2. The predictions of neural networks are slightly more accurate than the response surface polynomials for the example of the set of 50 randomly generated data in this Chapter.

3. The first 7 most important parameters (Table 6.2) are adequate to represent the I/O stiffness of the joint.

7. Development of a Translator for Finding a Joint That Meets Given Performance Targets

In the preliminary design stage of a car, we need a design tool that for a given set of requirements on the joint behavior and geometry finds the most efficient joint that satisfies these requirements. Most efficient joint means joint with lowest mass. The given set of requirements includes performance targets, such as moments of inertia, twist rigidity and stiffness of joint and packaging and manufacturing constraints. This problem can be solved using optimization. Objective function is the mass of the joint. Constraints are performance targets and the packaging and manufacturing constraints. Design variables are the physical design parameters of joints. Since some of the constraints are nonlinear (for example the relation between stiffness and dimensions), the optimization problem is non-linear.

In this study, we use two schemes to optimize joints: sequential quadratic programming method and random research method. There is no intention to explore the methods for optimization in this study. The optimization schemes were selected on the basis of availability concerns.

In Section 7.1, we describe the above mentioned two optimization schemes. In Section 7.2, we apply the two schemes to the B-pillar-to-rocker joint used in this study. In Section 7.3, we formulate the optimization problem for the two methods. Finally, the results of the two optimization schemes are presented in Section 7.4.

7.1 Optimization Schemes

The standardized minimization problem with single objective function can be expressed in the following form,

$$\begin{aligned} &\textbf{Minimize} && f(\mathbf{x}) && \mathbf{x} = (x_1,...,x_n)^T \\ &\textbf{Such that} && g_j(\mathbf{x}) = 0, && j = 1,...,m_e \\ & && g_j(\mathbf{x}) \geq 0, && j = m_e + 1,...,m \\ & && \mathbf{x}_l \leq \mathbf{x} \leq \mathbf{x}_u \end{aligned} \tag{7.1}$$

where $\mathbf{x}$ denotes a vector of design variables, $\mathbf{x}_l$ and $\mathbf{x}_u$ are vectors of the lower and upper bounds of design variables, $f(\mathbf{x})$ is the objective function and $g_j(\mathbf{x})$ are constraints. All of the above functions are assumed to be continuously differentiable.

7.1.1 Random Search Method

The random search method is a classic method in optimization. In this method, many randomly generated designs are compared to find the best design. In each design, the values of the design variables are drawn from the distributions over the range of variation of these design variables. Then, the objective function and the constraints are evaluated. The method accepts a feasible design as a candidate design and rejects an unfeasible one. Feasible design is a design that satisfies the constraints. For a large number of randomly generated designs, a pool of feasible designs can be obtained. By ranking the

designs in the pool on the basis of the values of their objective function, this method can give a set of good designs, which are close to the optimum.

7.1.2 Sequential Quadratic Programming

The sequential quadratic programming method (Wilson 1963, Han 1977, Powell 1977) is based on a theorem that states that the optimum of (7.1) is equivalent to the minimum of the Lagrangian function in the tangent subspace, which is formed by vectors orthogonal to the gradients of the active constraints. On the basis of an iterative formulation, this method establishes subproblems by using a quadratic approximation of the Lagrangian and by linearizing the constraints. A line search is used along the search direction to find a new iteration point. This method is quite efficient for solving nonlinear optimization problems.

7.2 Application to B-pillar-to-rocker Joint

We applied the optimization scheme to the B-pillar-to-rocker joint of an actual car. This joint was described in Section 2.2. The physical design parameters of this joint were presented in Table 4.2. We tried to minimize the mass while the stiffness in I/O bending and the cross sectional properties of the branches did not fall below some given lower limits.

Although we considered only the I/O bending stiffness in this study, we needed to ensure the stiffness in the F/A bending to be sufficient large. We fixed the thickness of the B-pillar to rocker transition part (T4, T5 and T6) and also values of AU, BU and PF1

(Figure 3.9) to their values in the baseline model. Hence, there are 21 design variables (Table 7.1) that are chosen from 35 physical design parameters (Figure 3.7 to Figure 3.9). The rest (14) of the physical design parameters are fixed (Table 7.2). The ranges of design variables are chosen based on practical limitations in design of joint. The objective function is the mass of the joint that is the mass of the rocker plus the transition part from rocker to B-pillar. There are 24 constraints that consist of 13 packaging and 6 manufacturing constraints and 5 constraints on performance targets. The constraints were established by interacting with industrial designers.

7.3 Optimization Problem Formulation

The optimization problem is formulated in the form described by formula (7.1). This section will describe the problem formulation in detail.

7.3.1 Objective Function

The objective function is the mass of the rocker plus the transition part from rocker to B-pillar. When a set of design variables is given, the geometry of a joint is determined. The mass of the joint can be calculated using a relatively simple equation that we developed for the mass. The objective is to minimize mass because this will help reduce the cost and weight of the car. It will also help increase mileage, acceleration and improve handling.

7.3.2 Packaging and Manufacturing Constraints

The packaging constraints are related to the arrangement and interaction of car body components in space. An example of such a constraint is that B2-B4 (Figure 7.1) should be large enough so that step H5 in the outboard side can accommodate the door edge and the sealant. The manufacturing constraints are induced from manufacturing limitations such as the fact that difference of the thicknesses of two or more plates connected by spot welds cannot exceed a maximum value.

In this study, we considered 13 packaging constraints and 6 manufacturing constraints, respectively. They are listed and explained in the following. In the following expressions of constraints there are some terms of the form *Max_criterion_name* or *Min_criterion_name*. The prefixes *Max_* and *Min_* are the maximum and minimum values of the corresponding criterion, whereas the *criterion_name* usually explicitly tells the meaning of the criterion. For instance, *Max_rocker_width* is the maximum value of the width of the rocker cross section that is denoted by *rocker_width*. The constraints are normalized against some nominal values of the variables involved.

- Packaging constraints (g(1) to g(13)):

1) The width of door should be equal to (B2+C1),

$$g(1) = B2 + C1 - Door\_width = 0 \tag{7.2}$$

where $Door\_width$ is the width of the door (Figure 7.1).

2-3) The width of rocker cross section should not exceed a maximum value, Max_rocker_width (Figure 7.1) ,

$$g(2) = \frac{-(B2 + C2)}{Max\_rocker\_width} + 1 \geq 0 \tag{7.3}$$

$$g(3) = \frac{-(B2 + C3)}{Max\_rocker\_width} + 1 \geq 0 \tag{7.4}$$

4) The height of rocker should not exceed a maximum value, Max_rocker_height (Figure 7.1),

$$g(4) = \frac{-(H3 + \frac{C2}{\tan(\alpha_2)} - H6)}{Max\_rocker\_height} + 1 \geq 0 \tag{7.5}$$

5) (B2-B4) (Figure 7.1) should be sufficiently large so that step H5 in the outboard side can accommodate the door edge and the sealant.

$$g(5) = \frac{B2 - B4}{Door\_edge\_width + Sealant\_width} - 1 \geq 0 \tag{7.6}$$

where $Door\_edge\_width$ is the width of the lower edge of the door and $Sealant\_width$ is the width of the door sealant as shown in Figure 7.1.

6) The slope of step H5 should be less than an upper bound,

$$g(6) = \frac{-\tan(\frac{B4 - B1}{H5})}{Max\_H5\_slope} + 1 \geq 0 \tag{7.7}$$

where Max_H5_slope is the upper bound of the slope.

7) We set up the following constraint based on the styling consideration of the rocker outboard panel (Figure 7.1)

$$g(7) = \frac{-\alpha_3}{Max\_\alpha_3} + 1 \geq 0 \tag{7.8}$$

where Max_α_3 is the upper bound of α_3. The latter angle is defined as,

$$\alpha_3 = \tan^{-1}(\frac{H1}{B2 - B4}) \tag{7.9}$$

The following requirements are dictated by the shape of lower edge of the door (Figure 7.2),

8) The vertical distance of E and D (see Figure 7.2) should be larger than a minimum allowable value. This value is dictated by the geometry and properties of the sealant.

$$g(8) = \frac{H2 - H1}{Door\_edge\_height} - 1 \geq 0 \tag{7.10}$$

where $Door\_edge\_height$ is the door edge height as shown in Figure 7.2.

9) Point E should be above D (Figure 7.2).

$$g(9) = \frac{\left(\frac{B2}{\tan(\alpha_2)} + H1 + H5 + \frac{B1}{\tan(\alpha_1)}\right)}{H3} - 1 \geq 0 \tag{7.11}$$

10) The part of the section between points D and F must be concave (Figure 7.2):

$$g(10) = D(z) + \frac{F(z) - D(z)}{F(y) - D(y)}(E(y) - D(y)) - E(z) \geq 0 \tag{7.12}$$

where $D(z)$ and $D(y)$ are the z and y coordinates of point D (Figure 7.2).

11) The rocker must not be too tall so that it is easy to step out of the car,

$$g(11) = \frac{-H3 - C2/\tan(\alpha_2) + H6 + H4}{Max\_stepout\_height} + 1 \geq 0 \tag{7.13}$$

where $Max\_stepout\_height$ is the maximum value of $stepout\_height$ (Figure 7.1).

12-13) Continuity of the shape of the door and the rocker outboard panel,

$$g(12) = \varepsilon - (\alpha_4 - \alpha_3) \geq 0 \tag{7.14}$$

$$g(13) = \varepsilon + (\alpha_4 - \alpha_3) \geq 0 \tag{7.15}$$

where α_3 and α_4 are angles shown in figure 7.2. ε is the tolerance between these two angles.

- Manufacturing Constraints (g(14) to g(19))

14-19) The difference of the thicknesses of the two plates connected by spot welds can not be too large,

$$g(14) = -|T1 - T2| + \Delta T \geq 0 \tag{7.16}$$

$$g(15) = -|T2 - T3| + \Delta T \geq 0 \tag{7.17}$$

$$g(16) = -|T3 - T4| + \Delta T \geq 0 \tag{7.18}$$

$$g(17) = -|2T1 - T5| + \Delta T1 \geq 0 \tag{7.19}$$

$$g(18) = -|2T1 - T6| + \Delta T1 \geq 0 \tag{7.20}$$

$$g(19) = -|T1 - T3| + \Delta T \geq 0 \tag{7.21}$$

where ΔT is the minimum value of the difference of the thickness between two plates to be spot welded together. $\Delta T1$ is the minimum value of the difference of the thicknesses of the B-pillar outboard panel and its reinforcement (Figure 3.2 and Figure 3.9).

7.3.3 Constraints on Performance Targets

In this study, we consider constraints on the performance targets such as moments of inertia in vertical and horizontal directions, twist rigidity of rocker and I/O bending stiffness of a joint. We consider 5 such constraints in this study (g(20) to g(24)).

20-21) Constraints on moments of inertia of rocker section

$$g(20) = \frac{I_y}{Min\_I_y} - 1 \geq 0 \tag{7.22}$$

$$g(21) = \frac{I_z}{Min\_I_z} - 1 \geq 0 \tag{7.23}$$

where I_y, I_z are moments of inertia of rocker section about Y and Z axis (figure 7.2) and Min_I_y, Min_I_z are their minimum values, respectively.

22) Constraints on twist rigidity of rocker section

$$g(22) = \frac{J}{Min\_J} - 1 \geq 0 \tag{7.24}$$

J and $J\_\min$ are the torsional constant of rocker section and the corresponding minimum value of torsional constant.

23-24) Constraints on stiffness of joint

Both the stiffnesses predicted by the response surface polynomials and the neural network should be larger than a minimum acceptable value,

$$g(23) = \frac{stiff\_poly}{Min\_stiff\_poly} - 1 \geq 0 \tag{7.25}$$

$$g(24) = \frac{stiff\_nn}{Min\_stiff\_nn} - 1 \geq 0 \tag{7.26}$$

where $stiff\_poly$ and $stiff\_nn$ are stiffness predictions from polynomial and neural network, respectively and Min_stiff_poly and Min_stiff_nn are the corresponding minimum values. Since there is some error in predicting stiffness that is usually less than 10%, we suggest to increase the minimum allowable values for these quantities by 10% to assure that the joint obtained from optimization meets the stiffness target.

7.4 Results

We assume that the design variables can vary in narrow ranges. Hence, we choose to vary all thickness by ±30% from the values of the baseline joint (see Table 3.1), RPL

by ±18.75% and the remaining design variables by ±10%. Table 7.1 shows the design variables and their corresponding ranges. The allowable packaging and manufacturing constraint criteria are chosen assuming that the constraint criteria can vary by ±10% about the baseline values. Table 7.3 depicts the allowable constraint criteria and their corresponding values used in this study.

For the above specified ranges of design variables and the values of the allowable constraint criteria, we tried to solve the optimization problem by using random research method and Sequential Quadratic Programming method. The flow chart of Random Research Method is shown in Figure 7.3. The algorithm of Sequential Quadratic Programming used is from an IMSL subroutine developed by Schittkowski (1986)

7.4.1 Random Research Method

For random research method, all of the 21 design variables are varied uniformly in their ranges. We created 100,000 random designs of which 2506 were found to be feasible (i.e., satisfying all the constraints). Then, we ranked these 2506 designs by the values of the objective function. The top six designs in the ranking and their corresponding values of performance targets predicted by both optimization scheme and FEA are given in Table 7.4.

From Table 7.4 we can see that the mass of the design in rank #1 is 5% less than that of the baseline joint. There is an offset between the stiffness predicted by neural network and the stiffness predicted by FEA. Rank #6 has the largest offset that is about

11%. All six designs have lower mass than that of the baseline joint and their moment of inertia and section moduli exceed those of the baseline joint. Some designs (rank #1, #2 and #3) are significantly stiffer than the baseline design.

It is up to the designer to choose the most suitable design for a car among the above six designs. Note that the obtained best design is not the optimum one because we considered only a finite number of designs.

7.4.2 Sequential Quadratic Programming

The optimum designs obtained by SQP might be different for different initial guesses of the design variables. Since the optimization problem is nonlinear, there is no guarantee that the optimizer will find the global optimum. To increase the possibility of getting a good optimum design, we used several different initial guesses. We used the top 10 feasible designs of 100,000 random generated designs as the initial guesses. We found that the optimizer converge to the same design for the 9 of these 10 initial guesses and did not converge for only one of these initial guesses.

Table 7.5 compares the mass and stiffness of this optimum design with those of the baseline joint. We observe that the stiffness of this design predicted by FEA is less than that of the baseline joint. Hence, on the basis of FEA prediction, this design is not feasible. The reason for this is that there is an offset (usually less than 10%) of the stiffness predicted by neural network and response surface polynomial with respect to the FEA results (Section 6.4). Therefore, the design that satisfies the stiffness constraints obtained

by neural network and response surface polynomial might violate the stiffness constraint obtained by FEA. To overcome this problem, we increase the stiffness criteria by 10% and redo the optimization. By using the same 10 initial designs, we found that the optimizer converged to the three different designs. Table 7.6 compares the values of masses and the design variables of these three designs. We can see that the relative errors of mass for these two design is only 0.004% to 0.005%. However, some of the design variables of the two designs are different. The different design variables are T1, C2, α_1, H3 and RPL for these three designs. We choose the design with the least mass as the optimum design (case I in Table 7.6).

Table 7.7 compares the mass and stiffness of this optimum design against those of the baseline joint. We can see that the stiffness predicted by FEA also satisfies the constraint on minimum stiffness. Thus, we call this design "baseline optimum design". We notice from Table 7.7 that the mass of the baseline optimum design is 12.8% lower than the mass of the baseline design.

Table 7.8 and Table 7.9 give the values of design variables and constraints of the baseline optimum, respectively. Figure 7.4 depicts the rocker cross section of the baseline optimum design and the baseline design. We can see from Table 7.8 that the thickness of outboard panel (T1), shear panel (T2) and inboard panel (T3) are reduced by 10%, 30% and 15%, respectively from the values of the baseline design. T2 has the largest reduction (reaching its lower bound) because it has relatively less effect on the joint stiffness, twist rigidity J and moment of inertia I_y, I_z of the rocker section than T1 and T3. We may also conclude that the optimum design tends to put the mass as far away from the center of the

rocker center as possible. T1 was reduced less than T3 because stiffness is more sensitive to T1 than T3. Sakurai and Kamada (1988) reached the same conclusion.

We also observe from Table 7.8 that B1/B2 increases about 10.3% from the baseline joint. This is because B1/B2 affects stiffness significantly and the stiffness constraint is active at the baseline optimum design.

From Table 7.9 we observe that there are 5 active packaging constraints (g(1), g(4), g(5), g(11) and g(12)), 1 active manufacturing constraint (g(16)) and 5 performance constraints (g(20 to g(24)). Packaging constraint g(1) is an equality constraint. Since C1 is at its lower bound (Table 7.8), B2 takes the maximum allowable value. Active packaging constraint g(4) means that, at the optimum, the rocker height will be as large as it is allowed by the packaging constraint. Active packaging constraint g(5) means that (B2-B4) takes the smallest possible value (Figure 7.1). Active packaging constraint g(11) means that the step out height (Figure 7.2) affects the optimum design of the joint. Active packaging constraint g(12) means that continuity of door panel with the rocker outboard panel also affects the optimum design. There is only one active manufacturing constraint, g(16), which means that the thickness difference between T3 and T4 take the maximum allowable value 0.5. All performance constraints are active for the baseline optimum. This means that all of the performance targets affect the optimum design.

We also increased the stiffness constraint criterion up to 150% of the value of the baseline optimum and optimized the joint for several values of that criterion in the range from 100 to 150%. The constraint criteria for moments of inertia and torsional modulus

were kept same as those of the baseline optimum. After obtaining the optimum designs for each value of the stiffness criteria, we used FEA to estimate the stiffness of these designs with better accuracy. The results are shown in Table 7.10. Figure 7.5 depicts the mass of the optimum designs normalized by the mass of the baseline optimum joint versus the normalized stiffness. The curve with cross corresponds to the stiffness obtained using the approximate methods, while the curve marked with circles corresponds to the stiffness estimated using FEA. It is observed that the mass of the joint increases almost linearly as the minimum allowable stiffness increases. We also observed that the approximate methods used in optimum design tend to overestimate the stiffness. However, no such trend was observed when testing these methods using random designs (Chapter 6, Figure 6.9). We believe that the reason for the above observations is that optimization tends to take advantage of the weaknesses of the model and yield design whose stiffness is overestimated by the approximate methods. To overcome this problem we recommend to increase stiffness criterion by 10% to compensate for the modeling error of the approximate methods.

We created another set of randomly generated data (29 points) by arbitrarily varying the same 21 parameters used in optimization (Table 7.1). We used this data set to test the prediction of the approximate methods again. Figure 7.6 compares the prediction of polynomials, neural networks and FEA for this set of testing data when 7 parameters are used. Since some of the parameters that describe the B-pillar part do not vary in this case (Section 7.2), we should expect a smaller value of *cov* than that of the 50 point testing data in Section 6.5.3 (Figures 6.8 and 6.9). We observed that the *cov*'s of the predictions of the response surface polynomial and neural network are 0.042 and 0.036,

respectively, which are less than that of the set of 50 testing data (All 27 variables in Table 4.2 are varying). Hence, the prediction of neural network is still slightly better than that of the response surface polynomial in this case.

In the following, we summarize the observations from the optimization process:

1. Random search method can give several feasible designs whose mass is about 5% lower than that of the baseline design. If we consider more random designs the mass is expected to drop further.

2. Sequential quadratic programming can give a design whose mass is about 12.8% lower than the baseline design.

3. The optimizer tends to put the material of the rocker section as farther away from the center of rocker section as possible.

4. Rocker section tends to take the maximum allowable height for the optimum design.

5. B1/B2 increases about 10.3% from the baseline joint for the optimum design.

6. All performance constraints are active for the optimum design.

7. We need to increase the minimum allowable stiffness by 10% in order to cover the offset between the stiffness predicted by neural network and response surface polynomial with respect to the FEA. This will ensure that the optimum design has acceptable stiffness.

8. The predictions of neural network is slightly more accurate than those of response surface polynomial for the set of 29 randomly generated data in this Chapter.

Note that in this example we only considered stiffness in the I/O direction. We expect that weight savings would have been lower than what was achieved in this example (12.8%) if we had considered stiffness in the forward-afterward direction and also in torsion. Moreover, although the constraints were obtained on the basis of extensive discussion with the engineers and designers from the auto industry, it is possible that we have not considered some constraints. Therefore, this example only intends to demonstrate that the general approach proposed in this dissertation can allow designers to design more efficient joints faster.

8. Concluding Remarks

8.1 Conclusions

A methodology for developing tools for design guidance of joints in car bodies was presented. The methodology was demonstrated on the B-pillar-to-rocker joint of a car. Only out-of-plane (I/O) bending was considered. The following steps were completed in the demonstration.

The deformation mechanisms of a B-pillar-to-rocker joint subassembly under I/O bending were studied. These mechanisms are:

- Bending deflection of the B-pillar
- Twist deflection of the rocker
- Shear deflection of the cross section of the rocker
- Deformation due to imperfections such as the spot welds and weld access holes

Parameterization of a joint was performed. The joint was represented by a set of physical design variables that are meaningful to the designers. These parameters represent the major characteristics of the geometry of a joint.

The sensitivities of the joint stiffness with respect to the physical design parameters were studied using the one-parameter-at-a-time method.

Design modifications that aim at increasing the I/O stiffness of the joint were proposed based on the study of deformation mechanisms and the sensitivity of the I/O stiffness with respect to the parameters.

Approximate methods, response surface polynomials and neural networks, were used to predict the I/O stiffness of a joint with a few most important parameters to the this stiffness.

A design-oriented translator that maps given requirements on the performance of a vehicle joint to the physical design parameters of a feasible joint design was developed. An optimization scheme was used to obtain the optimum joint (having lowest mass) that satisfies the constrains on packaging, manufacturing and performance.

The following conclusions are based on the example considered in this study:

- The shear deformation of the rocker is the most important deformation mechanism in the deflection of the joint in I/O bending (it contributes about 87% of total deflection). This conclusion agrees with that of Sunami (1987) (Section 2.4).

- The joint used in this study can be represented by 35 independent physical design parameters that are meaningful to the designer (Section 3.3). Generally, the number of parameters depends on the geometry of the joint.

- The most important parameters to the I/O stiffness of the joint are B1/B2, T1, B4/B1, RPL, B2, α_1 and H3 (Section 4.3).

- The following design modifications for T-shaped joints are proposed (Section 5.2):
  - Introduce 2 transverse bulkheads in the outboard cell of the rocker (Figure 5.2). These bulkheads can be spot welded or seam welded to the outboard panel of the rocker.

  - Extend the B-pillar so that it forms a cap inside the rocker (Figure 5.3).

  - Add a plate in the rocker as shown in Figure 5.4. This plate will reinforce the linkage between the rocker and the B-pillar thereby reducing the shear deformation of the rocker.

  All the above modifications increase stiffness dramatically without increasing the weight of the joint significantly.

- The I/O stiffness of the joint considered in this example can be predicted using response surface polynomials and neural networks. Reasonably accurate predictions are obtained using the 7 most important parameters. The performance of neural networks is slightly more accurate than that of polynomials. The coefficient of variation of the ratio of FEA results and predictions is about 8% for the neural network and 10% for polynomials, for a group of 50 designs used to test the approximate methods (Section 6.5.3).

- In some cases, the translator that finds a joint that satisfies a given performance target can reduce weight significantly. In the example in this study, we found a design whose weight is 12.8% lower than that of the current used design.

8.2 Future Work

The methodology for developing translators for design guidance could be applied to other B-pillar-to-rocker joints with different types of construction (different internal reinforcements) and also to the remaining joints of a car body.

A database that contains the most suitable joint designs for various combinations of performance targets and packaging and manufacturing constraints can be established using the developed translators. This database should be of great help to the designers.

The methodology can be also extended to other components such as the joints of a truck frame. The joint of a truck frame usually consists of intersection of close section or open section beams. In this case, the translators will find the dimensions of the lightest beams that have the given cross-sectional properties (for example, moments of inertia, and section modulus), and satisfy the stiffness constraints of the joints.

We believe that all the above translators will significantly help automotive manufactures reduce cost and the time it takes to design the components of a car body because they will replace current trial-and-error, semi-empirical design procedures.

The methodology for developing translators for design guidance could be applied to gage and shape optimization of a car body structure.

As mentioned in the introduction currently we optimize the car body using simplified models, which represent components using engineering parameters. This procedure yields optimum values of the engineering parameters of the components. This procedure is not always affective because there is no tool available to link engineering parameters with physical design parameters of a component, and therefore a feasible design for the optimum values of the engineering parameters might not exist.

The methodology (translators) developed in this study can be used to link the engineering parameters of the simplified model with physical design parameters defining the geometry of components, such as plate gages, and dimensions. These translators provide realistic estimates of the effects of a design change on the mass of a car body and ensure that the optimization procedure yields a feasible final design.

We propose to use two types of translators. The first, called "type A translator", finds the engineering parameters of a given design from the physical design parameters and checks if that design is feasible. The second type, called "type B translator", finds the physical design parameters of a component that has the given engineering parameters and satisfies packaging and manufacturing constraints.

We propose to use the following three steps to optimize the car body structure:

- Step 1: Find initial guesses of the simplified model variables

First we find realistic initial guesses of the variables of the simplified model that are consistent with the packaging constraints imposed by the clay model. For this purpose we use a translator for each body component (joints and beams) that checks if there exists a manufacturable design of a component that has given dimensions and satisfies packaging and manufacturing constraints, and calculates the engineering parameters of this design. For example it checks if there is a manufacturable beam cross section that fits within a given envelope and finds the section properties of that beam.

- Step 2: Optimize the simplified model

Here we optimize the simplified body model to find the values of the engineering variables of the optimum body. Since we cannot directly use engineering parameters to define the geometry of a design, calculate its mass, and check if the design satisfies packaging, styling and manufacturing constraints, we use translators to link the engineering parameters with physical design parameters defining the geometry of a design.
These translators find the physical design parameters (dimensions, thicknesses) of a component that has given engineering parameters, and satisfies given packaging and manufacturing constraints. For example, the translator for a beam finds the dimensions of a beam whose cross section has given moment of inertia and fits within a given envelope. Figure 8.1 shows how to interface the simplified model of the car body with the translators. Using these translators, the optimizer can also find how the masses of the

components and of the overall body change if we change the engineering parameters of the simplified model. The calculated change in the mass will be accurate and realistic because it will correspond to components that are manufacturable and satisfy packaging constraints.

It is important to account for the fact that adjacent components share some dimensions, which means the translators cannot change these dimensions independently. For example, the thickness of the outer plate of the B-rocker joint and the rocker are same in most new cars because these plates are parts of the same shell.

- Step 3: Determine dimensions of optimum components

Optimization of the overall car body yields optimum values of the engineering parameters of all the components. In the last step we use translators to find the dimensions of the optimum components of the optimum car body.

Bibliography

Berke, L., Hafez, W. and Pao Y.-H., 1992, "Neural Networks for Structural Design: An Integrated System Implementation", 4th AIAA/USAF/NASA/OAI Symposium on Multidisciplinary Analysis and Optimization, Cleveland, Ohio, pp. 915-923.

Borowski, V. J., Steury, R.L. and Lubkin, J.L., 1973, "Finite Element Dynamic Analysis of an Automobile Frame", Paper 730506, SAE Automobile Engineering Meeting, Detroit, Michigan.

Box, G. E. P. and Behnken, D. W., 1960, "Some New Three Level Designs for the Study of Quantitative Variables", Technometrics, Vol. 2, No. 4, pp. 455-475.

Caudill, M., 1992A, "What is a Neural Network," Neural Networks Special Report, AI Expert, pp. 7-14.

Caudill, M. and Butler, C., 1992B, Understanding Neural Networks: Computer Explorations, Vol. 1 Basic Networks; Vol. 2 Advanced Networks, MIT Press.

Chang, D. C., 1974, "Effects of Flexible Connections on Body Structural Response", SAE Transactions, Vol. 83, pp. 233-244.

Elliot, J. G., 1987, "Statistical Methods and Applications", Allied Signal Corporation.

Fox, E. P., Pratt and Whitney, 1993, "Methods of Integrating Probabilistic Design within An Organization's Design System Using Box-Behnken Matrices", AIAA-93-1380-CP.

Han, S. P., 1977 "A Globally Convergent Method for Nonlinear Programming", J. Optimization Theory Appl. 22, 297-309.

Hajela, P. and Berke, L., 1992, "Neural Networks in Structural Analysis and Design: An Overview", 4th AIAA/USAF/NASA/OAI Symposium on Multidisciplinary Analysis and Optimization, Cleveland, Ohio, pp. 902-911.

Hecht-Nielsen, R., 1990, Neurocomputing, Addison-Wesley.

Lee, K. and Nikolaidis, E., 1991, "Identification of Flexible Joints in Vehicle Structures", AIAA Journal, Vol. 30, No. 2, pp. 482-489.

Lee, K., 1991, "Modeling And Identification of Flexible Joints in Vehicle Structure", Ph.D. Dissertation, Virginia Polytechnic Institute and State University.

MATLAB, 1992, "User's Guide of Neural Network TOOLBOX", The MATH WORKS Inc.

Montgomery, D. C., 1976, "Design and Analysis of Experiments", John Wiley & Sons, Inc.

Nikolaidis, E. and Zhu M., 1991, "Analysis the I/O Bending of T-Shaped Joint by Using Vlasov's Theory", Report to Ford, Virginia Polytechnic Institute and State University.

Nikolaidis, E. and Lee, K., 1992, "A 3-D Joint Model for Automotive Structures", 8th International Conference on Vehicle Structural Mechanics and CAE, Traverse City, Michigan.

Obermeier, K.K., and Baron, J.J., 1989, "Time to Get Fired Up", Byte, August, pp. 217-224.

Powell M. J. D. 1977, A Fast Algorithm for Nonlinearly Constrained Optimization Calculations, in Numerical Analysis Proceedings, Dundee. Lecture Notes in Mathematics, (edited by G. A. Watson), 630, Springer-Verlag, Berlin, Germany, 144-157, New York 1978.

Rao, M. K., Zebrowski, M. P. and Crabb, H.C., 1983, "Automotive Body Joint Analysis for Improved Vehicle Response", Proceedings of International Symposium on Automotive Technology and Automation, Vol. 2. pp. 953-973.

Rumelhart D. E., Hinton G. E. and Williams R. J., 1986, "Learning internal Representations by error propagation", Rumelhart D. E. and McClelland J. L., editors. Parallel Data Processing, Vol. 1, Chapter 8, the M.I.T. Press, Cambridge, MA pp. 318-362.

Sakurai, T. and Kamada, Y., 1988, "Structural Joint Stiffness of Automotive Body", SAE paper 880550, International Congress and Exposition, Detroit, Michigan.

Schaefer, H.G., 1979, "MSC/NASTRAN Primer: Static and Normal Modes Analysis", 2_nd edition.

Schittkowski, K. 1986, NLPQL: A FORTRAN subroutine solving constrained nonlinear programming problems, (edited by Clyde L. Monma), Annals of Operations Research, 5, 485-500

Sharman, P.W., 1982, "The Effect of Joint Flexibility on the Torsion of A Vehicle Body", Proceedings of Institution of Mechanical Engineers, Vol. 196, pp. 191-197.

Sunami, Y., Yugawa, T. and Yoshida, Y., 1987, "Analysis of the Joint Rigidity In-Plane Bending of Plane-Joint Structures", JSAE Review, Vol. 9, No. 2, pp. 44-51.

Sunami, Y., Yugawa, T. and Yoshida, Y., 1990, "Analysis of the Joint Rigidity of the Automotive Body Structure - Out-of-Plane Bending of Plane-Joint Structures", JSAE Review, Vol. 11, No. 3, pp. 59-66.

Swift, R. and Batill, S., 1991, "Application of Neural Networks to Preliminary Structural Design", AIAA Paper No. 91-1038, Proceedings of the 32nd AIAA/ASME/ASCE/AHS/ASC SDM Meeting, Baltimore, Maryland.

Vlasov, V. Z. 1961, "Thin-Walled Elastic Beams", (2nd edition), Published for National Science Foundation and the Department of Commerce by the Israel program for scientific translation, Jerusalem.

Wilson, R. B., 1963, "A Simplicial Algorithm for Concave Programming". Ph. D. Dissertation, Graduate School of Business Administration, Harward University, Boston.

Yamazaki, I. and Inoue, T., 1989, "An Application of Structural-Acoustic Coupling Analysis to Boom Noise", SAE Paper No. 891996.

Table 2.1 Physical properties of the equivalent beam of the B-pillar

Area mm^2	(I/O) Moment of Inertia mm^4	(F/A) Moment of Inertia mm^4
725.165	487480	3136000

Table 2.2 Summary of constraints and results for spot weld model when rocker clamped at F2 and R2 (Figure 2.4)

Case No.	Make up for the openings	Constraint shear deformation at F3 & R3	Φ_{tip} $10^{-3} rad.$	Φ_{root} $10^{-3} rad.$
1	-	-	6.0925	5.9755
2	Yes	-	6.0525	5.9355
3	-	Yes	0.7982	0.6812

Φ_{tip} and Φ_{root} are the tip and the root deflection of B-pillar (Figure 2.4), respectively.

Table 2.3 Angular deflection at the free end of rocker due to twist moment M_x = 24,500 N.mm applied at the free end. The other end of rocker is clamped

Case No.	Model Constraints	Φ_{free} $10^{-3} rad.$
4	F2 clamped, R2 free (Figure 2.4)	0.5218

Table 3.1 Values of design variables of baseline model.

#	Variables	Baseline model
1	T1 (mm)*	0.80
2	T2 (mm)*	0.91
3	T3 (mm)*	1.00
4	T4 (mm)*	1.35
5	T5 (mm)*	0.80
6	T6 (mm)*	2.20
7	C1 (mm)*	28.99
8	C2 (mm)*	86.12
9	C3 (mm)*	78.61
10	C4 (mm)*	52.51
11	B1/B2*	0.7232
12	B2 (mm)*	78.62
13	B3 (mm)*	38.21
14	B4/B1*	1.060
15	H1 (mm)*	65.17
16	α_1 (°)*	72.614
17	H3 (mm)*	121.28
18	H4 (mm)*	62.260
19	H5 (mm)*	16.082
20	H6 (mm)*	6.3186
21	α_2 (°)*	71.514
22	AU (mm)**	163.64
23	BU/B4**	0.95
24	HL (mm)**	130.26
25	RP (mm)**	217.4
26	RPL (mm)**	300.00
27	X_ini (mm)***	618.75
28	ZZU (mm)*	18.61
29	ZZL (mm)*	24.94
30	ZZM (mm)*	31.09
31	W (mm)**	17.8
32	α_P (°)***	73.797
33	PF1 (mm)**	81.816
34	RL (mm)***	1350
35	PL (mm)***	697.6

***, * and ** refer to Figures 3.7, 3.8 and 3.9, respectively.

Table 3.2 Results of static response of generic model when rocker clamped at F2 and R2 (Figure 2.4)

Case No.	Constraint shear deformation at F3 & R3	Φ_{tip} $10^{-3} rad.$	Φ_{root} $10^{-3} rad.$
1	No	5.672	5.555
2	Yes	0.4415	0.3245

Φ_{tip} and Φ_{root} are the tip and the root deflection of B-pillar (Figure 2.4), respectively. There are no openings for both component and generic models.

Table 3.3 Angular deflection at the free end of rocker due to twist moment M_x = 24,500 N.mm applied at the free end and another end of rocker is clamped (for generic model)

Case No.	Model Constraints	Φ_{free} $10^{-3} rad.$
3	F2 clamped, R2 free (Figure 2.4)	0.3913

Table 3.4 Comparison of results of decomposition of generic model against those of component model

	Total		B-pillar		Twist		Shear		Residual	
Model	Value	%	Value	%	Value	%	Value	%	Value	%
C*	6.053	100	0.117	1.9	0.128	2.1	5.294	87.5	0.514	8.5
G**	5.672	100	0.117	2.1	0.092	1.6	5.230	92.2	0.233	4.1
Change	-6.9%		0%		-28%		1.21%		-51.8%	

Note: The opening is not considered here.
C* = Component model
G**= Generic model

$$\text{Change} = \frac{\text{deflection of generic - deflection of component}}{\text{deflection of component}} \times 100\%$$

Table 4.1 The 8 physical design parameters whose values are fixed in sensitivities and effects study

#	Variables	Values*
1	X_ini (mm)	618.75
2	ZZU (mm)	18.61
3	ZZL (mm)	24.94
4	ZZM (mm)	31.09
5	W (mm)	17.8
6	PL (mm)	802.
7	RL (mm)	1350.
8	α_p (°)	73.797

* The values are the same as those of the baseline joint.
Refer to Figures 3.7 to 3.9 for definition of variables.

Table 4.2 Values of physical parameters of baseline joint and their ranges for sensitivities and effects study.

#	Variables	Baseline joint	Ranges for Sensitivity study %	Ranges for effect study %
1	T1 (mm)	0.80	±5	±30
2	T2 (mm)	0.91	±5	±30
3	T3 (mm)	1.00	±5	±30
4	T4 (mm)	1.35	±5	±30
5	T5 (mm)	0.80	±5	±30
6	T6 (mm)	2.20	±5	±30
7	C1 (mm)	28.99	±5	±10
8	C2 (mm)	86.12	±5	±10
9	C3 (mm)	78.61	±5	±10
10	C4 (mm)	52.51	±5	±10
11	B1/B2	0.7232	±5	±15
12	B2 (mm)	78.62	±5	±10
13	B3 (mm)	38.21	±5	±10
14	B4/B1	1.060	±5	±6
15	H1 (mm)	65.17	±5	±10
16	α_1 (°)	72.614	±5	±4
17	H3 (mm)	121.28	±5	±5
18	H4 (mm)	62.260	±5	±10
19	H5 (mm)	16.082	±5	±10
20	H6 (mm)	6.3186	±5	±10
21	α_2 (°)	71.514	±5	±10
22	AU(MM)	163.64	±5	±10
23	BU(mm)	0.95	±5	±5
24	HL (mm)	130.26	±5	±10
25	RP (mm)	217.4	±5	±10
26	RPL (mm)	300.00	±5	±18.75
27	PF1(mm)	81.816	±5	±10

Refer to Figures 3.7 to 3.9 for definition of variables.

Table 4.3 Normalized sensitivities of parameters for ±5% ranges of variations obtained by central difference

Parameters	+5%	-5%	Normalized sensitivities	Rank*
B1/B2	1.2406	0.8091	4.3154	1
T1 (mm)	1.1064	0.8986	2.0778	2
B4/B1	1.0478	0.9453	1.0244	3
RPL (mm)	1.0331	0.9736	0.5959	4
B2 (mm)	1.0171	0.9825	0.3458	5
H1 (mm)	1.0103	0.9950	0.1538	6
T6 (mm)	1.0054	0.9940	0.1137	7
T2 (mm)	1.0051	0.9950	0.1017	8
T3 (mm)	1.0041	0.9960	0.0808	9
B3 (mm)	1.0033	0.9958	0.0748	10
BU/B4	1.0030	0.9964	0.0660	11
α_2 (°)	1.0056	0.9992	0.0646	12
α_1 (°)	1.0070	1.0124	-0.0546	13
H5 (mm)	1.0030	0.9977	0.0529	14
C2 (mm)	1.0015	0.9979	0.0357	15
T4 (mm)	1.0011	0.9987	0.0241	16
H3 (mm)	1.0108	1.0132	-0.0236	17
C1 (mm)	1.0011	0.9989	0.0216	18
AU (mm)	1.0007	0.9993	0.0140	19
T5 (mm)	1.0006	0.9994	0.0116	20
HL (mm)	1.0005	0.9994	0.0111	21
RP (mm)	0.9995	1.0005	-0.0100	22
H4 (mm)	1.0002	0.9998	0.0042	23
C4 (mm)	0.9999	1.0002	-0.0029	24
PF1 (mm)	0.9999	1.0001	-0.0024	25
H6 (mm)	1.0000	1.0003	-0.0022	26
C3 (mm)	1.0000	0.9999	0.0013	27

The rank is based on the normalized sensitivities as defined in equation (4.4).
Refer to Figures 3.7 to 3.9 for definition of variables.

Table 4.4 Normalized effects of parameters for actual ranges of variations obtained by central difference

Parameters	Upper ranges	Lower ranges	Normalized effects	Rank*
B1/B2	2.3177	0.4455	1.8721	1
T1 (mm)	1.7101	0.4725	1.22376	2
RPL (mm)	1.1003	0.9046	0.1958	3
B4/B1	1.0621	0.9203	0.1418	4
T6 (mm)	1.0261	0.9496	0.0765	5
B2 (mm)	1.0328	0.9631	0.0698	6
T2 (mm)	1.0306	0.9698	0.0608	7
T3 (mm)	1.0261	0.9766	0.0495	8
H1 (mm)	1.0261	0.9946	0.0315	9
B3 (mm)	1.0058	0.9901	0.0158	10
T4 (mm)	1.0058	1.0000	0.0158	11
α_2 (°)	1.0148	1.0036	0.0113	12
H5 (mm)	1.0058	0.9968	0.0090	13
C2 (mm)	1.0036	0.9946	0.0090	14
BU/B4	1.0036	0.9968	0.0068	15
T5 (mm)	1.0036	0.9968	0.0068	16
α_1 (°)	1.0050	1.0101	-0.005	17
C1 (mm)	1.0013	0.9968	0.0045	18
H3 (mm)	1.0108	1.0132	-0.0024	19
HL (mm)	1.0013	0.9991	0.0023	20
AU (mm)	1.0013	0.9991	0.0023	21
H4 (mm)	1.0013	0.9991	0.0023	22
PF1 (mm)	0.9991	1.0013	-0.0022	23
RP (mm)	0.9991	1.0013	-0.0022	24
H6 (mm)	0.9991	1.0013	-0.0022	25
C4 (mm)	0.9991	1.0013	-0.0022	26
C3 (mm)	0.9991	0.9991	0.0000	27

* The rank is based on the effects of normalized stiffness as defined in equation (4.6). Refer to Figures 3.7 to 3.9 for definition of variables.

Table 4.5 Sensitivities of α_1 and H3 for ±5% variations obtained by forward and backward differences

Variables	Backward difference	Forward difference
α_1	0.140	0.248
H3	0.216	0.263

Refer to Figure 3.8 for definition of variables α_1 and H3.

Table 5.1 Effect of Proposed Modifications (Figure 5.8 to Figure 5.9) on Stiffness.

Modification from lower to upper bounds	Change (% of baseline)
Increase B1/B2 30%	187.4
Increase T1 60%	123.5
Increase RPL 37%	19.5

Note: All changes in the parameter values are normalized by the baseline values of the parameters.

Table 6.1 Box-Behnken's three level designs

No. of Variables	Design Matrix	No. of Points	No. of Runs
3	$\begin{bmatrix} \pm1 & \pm1 & 0 \\ \pm1 & 0 & \pm1 \\ 0 & \pm1 & \pm1 \\ 0 & 0 & 0 \end{bmatrix}$	12 3 N = 15	13
4	$\begin{bmatrix} \pm1 & \pm1 & 0 & 0 \\ 0 & 0 & \pm1 & \pm1 \\ 0 & 0 & 0 & 0 \\ \pm1 & 0 & 0 & \pm1 \\ 0 & \pm1 & \pm1 & 0 \\ 0 & 0 & 0 & 0 \\ \pm1 & 0 & \pm1 & 0 \\ 0 & \pm1 & 0 & \pm1 \\ 0 & 0 & 0 & 0 \end{bmatrix}$	8 1 8 1 8 1 N = 27	25
5	$\begin{bmatrix} \pm1 & \pm1 & 0 & 0 & 0 \\ 0 & 0 & \pm1 & \pm1 & 0 \\ 0 & \pm1 & 0 & 0 & \pm1 \\ \pm1 & 0 & \pm1 & 0 & 0 \\ 0 & 0 & 0 & \pm1 & \pm1 \\ 0 & 0 & 0 & 0 & 0 \\ 0 & \pm1 & \pm1 & 0 & 0 \\ \pm1 & 0 & 0 & \pm1 & 0 \\ 0 & 0 & \pm1 & 0 & \pm1 \\ \pm1 & 0 & 0 & 0 & \pm1 \\ 0 & \pm1 & 0 & \pm1 & 0 \\ 0 & 0 & 0 & 0 & 0 \end{bmatrix}$	20 3 20 3 N = 46	41
7	$\begin{bmatrix} 0 & 0 & 0 & \pm1 & \pm1 & \pm1 & 0 \\ \pm1 & 0 & 0 & 0 & 0 & \pm1 & \pm1 \\ 0 & \pm1 & 0 & 0 & \pm1 & 0 & \pm1 \\ \pm1 & \pm1 & 0 & \pm1 & 0 & 0 & 0 \\ 0 & 0 & \pm1 & \pm1 & 0 & 0 & \pm1 \\ \pm1 & 0 & \pm1 & 0 & \pm1 & 0 & 0 \\ 0 & \pm1 & \pm1 & 0 & 0 & \pm1 & 0 \\ 0 & 0 & 0 & 0 & 0 & 0 & 0 \end{bmatrix}$	56 6 N = 62	57

Table 6.2 Top 7 ranking of parameters based on their effects on I/O stiffness in section 4.3

Parameters	Ranking	Effects*
B1/B2	1	1.8744
T1 (mm)	2	1.2353
RPL (mm)	3	0.1951
B4/B1	4	0.1411
B2 (mm)	5	0.0704
H3 (mm)	**	**
α_1 (°)	**	**

Refer to Figures 3.7 to 3.9 for definition of variables.

* Definition of effects

$$\text{Effects} = \frac{K_{I/O}(x_i + \Delta x_i) - K_{I/O}(x_i - \Delta x_i)}{K_{I/O}(0)}$$

where $K_{I/O}$ is I/O stiffness of a joint; $K_{I/O}(0)$ is the I/O stiffness of the baseline model of the joint.

** H3 and α_1 are not monotonic at the region near the baseline design. They should be ranked in 5 to 7 positions based on the discussions in section 4.3.

Table 6.3 The number of regression coefficients of second order complete polynomials

No. of Parameters	No. of Regression Coefficients	No. of Runs of Box-Behnken Designs
3	10	13
4	15	25
5	21	41
7	36	57

Table 6.4 The number of neurons in the inner layer and weights of neural networks

No. of Parameters	No. of Neurons in the Inner Layer	No. of Weights of Neural Networks	No. of Runs of Box-Behnken Designs
3	2	11	13
4	4	19	25
5	5	36	41
7	6	55	57

Table 6.5 Values of *cov* for 26 testing data sets selected from 50 testing data points for 7 parameter case

Data Set #	Polynomial %	Neural Network %
1	11.79	7.64
2	11.74	7.59
3	11.71	7.59
4	11.77	7.60
5	11.81	7.58*
6	11.78	7.60
7	11.67	7.66
8	11.64	7.67
9	11.62	7.67
10	11.69	7.70
11	11.66	7.71
12	11.57	7.67
13	11.54*	7.66
14	11.65	7.72
15	11.84	7.80
16	11.78	7.82
17	11.81	7.88
18	11.80	7.88
19	11.84	7.89
20	11.81	7.87
21	11.87	7.90
22	11.87	7.91
23	11.85	7.90
24	11.88	7.93
25	12.03**	8.01**
26	11.98	7.96

* and ** correspond to minimum and maximum values of *cov*.

Table 7.1 Values of design variables of baseline joint and their upper and lower bounds.

#	Variables	Baseline joint	Ranges %	Upper Bound	Lower Bound
1	T1 (mm)	0.80	30	1.040	0.560
2	T2 (mm)	0.91	30	1.183	0.637
3	T3 (mm)	1.00	30	1.300	0.700
4	C1 (mm)	28.99	10	31.889	26.091
5	C2 (mm)	86.12	10	94.732	77.508
6	C3 (mm)	78.61	10	86.471	70.749
7	C4 (mm)	52.51	10	57.761	47.259
8	B1/B2	0.7232	15	0.7955	0.6147
9	B2 (mm)	78.62	10	86.482	70.758
10	B3 (mm)	38.21	10	42.031	34.389
11	B4/B1	1.060	5.6	1.119	1.000
12	H1 (mm)	65.17	10	71.687	58.653
13	α_1 (°)	72.614	4	75.518	69.709
14	H3 (mm)	121.28	5	127.34	115.22
15	H4 (mm)	62.260	10	68.486	56.034
16	H5 (mm)	16.082	10	17.690	14.474
17	H6 (mm)	6.3186	10	6.950	5.687
18	α_2 (°)	71.514	10	78.665	64.363
19	HL (mm)	130.26	10	143.29	117.23
20	RP (mm)	217.4	10	239.14	195.66
21	RPL (mm)	300.00	18.75	356.25	243.75

Refer to Figures 3.7 to 3.9 for definition of variables.

Table 7.2 The rest 14 of physical design parameters whose values are fixed in optimization problem

#	Variables	Values*
1	X_ini (mm)	618.75
2	ZZU (mm)	18.61
3	ZZL (mm)	24.94
4	ZZM (mm)	31.09
5	W (mm)	17.8
6	α_p (°)	73.797
7	PF1 (mm)	81.816
8	T4 (mm)	1.35
9	T5 (mm)	0.80
10	T6 (mm)	2.20
11	AU (mm)	163.64
12	BU/B4	0.95
13	PL (mm)	802.
14	RL (mm)	1350.

* The values are the same as those of the baseline joint.
Refer to Figures 3.7 to 3.9 for definition of variables.

Table 7.3 The constraint criteria of optimization problem - baseline constraint.

Constraint Type	Constraint Criteria	Values	Source
Packaging	Door_width (mm)	95.130	B
Packaging	Max_rocker_width (mm)	181.23	B
Packaging	Max_rocker_height (mm)	158.125	B
Packaging	Door_edge_width + Sealent_width (mm)	16.497	C
Packaging	Max_H5_slope	0.2376	B
Packaging	Max_α_3 (°)	64.018	B
Packaging	Min_door_edge_height (mm)	8.51	C
Packaging	Max_stepout_height (mm)	89.65	B
Packaging	α_4 (°)	63.198	*
Packaging	ε (°)	10	Given
Manufacturing	ΔT (mm)	0.5	Given
Manufacturing	$\Delta T1$ (mm)	1.0	Given
Performance	I_y_min (MM^4)	1864000	A
Performance	I_z_min (MM^4)	1467500	A
Performance	J_min (MM^4)	1573100	A
Performance	Min_stiff_poly (N.mm/rad.)	4445000	A
Performance	Min_stiff_nn (N.mm/rad.)	4396000	A

Note:

Source A: Value is the same as that of the baseline joints.
Source B: Value is 110% of the baseline joint.
Source C: Value is 90% of the baseline joint.

* : $\alpha_4 = \alpha_3$ of baseline joint + $\varepsilon/2$

Given : The value is given.

Table 7.4 The 6 best designs obtained by random search method

Ranks	Mass (kg.)	Stiffness 10^7N.mm/rad.			Moment of Inertia(E+7) $10^7 mm^4$		
		FEM	N.N.	POLY	Iy	Iz	J
1	7.973	0.531	0.574	0.588	0.201	0.167	0.170
2	7.996	0.582	0.562	0.592	0.191	0.153	0.180
3	7.996	0.566	0.551	0.575	0.191	0.160	0.171
4	8.053	0.486	0.484	0.477	0.190	0.148	0.176
5	8.055	0.429	0.455	0.442	0.189	0.149	0.167
6	8.128	0.476	0.425	0.447	0.187	0.158	0.181
Baseline joint	8.375	0.444	0.439	0.445	0.186	0.147	0.157

NN: Prediction of neural network.
POLY: Prediction of response surface polynomials.

Table 7.5 Comparison of objective function and joint stiffness of optimum (**stiffness constraints taken from baseline constraint**, Table 7.3) against those of FEM analysis

	Mass(kg.)	Stiffness 10^7 N.mm/rad.	
Baseline Optimum	7.237	0.4396(NN)	0.4445(POLY)
FEM	7.237	0.420E7	
Baseline Joint	8.375	0.444E7	

NN: Prediction of neural network.
POLY: Prediction of response surface polynomials.

Table 7.6 Values of design variables and mass of two designs obtained by SQP method when stiffness criterion increased by 10%

#	Variables	Design (I)	Design (II)	Design (III)	Error % (II)	Error % (III)
1	T1 (mm)	0.720	0.717	0.714	-0.4	-0.8
2	T2 (mm)	0.66	0.66	0.66	0	0
3	T3 (mm)	0.85	0.85	0.85	0	0
4	C1 (mm)	26.09	26.09	26.09	0	0
5	C2 (mm)	87.60	88.28	88.47	0.8	1.0
6	C3 (mm)	86.47	86.47	86.47	0	0
7	C4 (mm)	47.26	47.26	47.26	0	0
8	B1/B2	0.798	0.798	0.798	0	0
9	B2 (mm)	81.52	81.52	81.52	0	0
10	B3 (mm)	37.64	37.64	37.64	0	0
11	B4/B1	1.0	1.0	1.0	0	0
12	H1 (mm)	58.65	58.65	58.65	0	0
13	α_1 (°)	75.51	75.51	72.95	0	-3.4
14	H3 (mm)	124.33	125.24	125.24	0.7	0.7
15	H4 (mm)	68.49	68.49	68.49	0	0
16	H5 (mm)	14.47	14.47	14.47	0	0
17	H6 (mm)	6.95	6.95	6.95	0	0
18	α_2 (°)	65.28	65.28	65.28	0	0
19	HL (mm)	117.234	117.234	117.234	0	0
20	RP (mm)	195.66	195.66	195.66	0	0
21	RPL (mm)	250.13	244.03	247.57	-2.4	-1.0
	Mass	7.3068	7.3072	7.3071	0.005	0.04

Refer to Figures 3.7 to 3.9 for definition of variables.

Error (II) $= \frac{(II)-(I)}{I} * 100\%$, Error (III) $= \frac{(III)-(I)}{I} * 100\%$,

Table 7.7 Comparison of mass and joint stiffness of optimum (**minimum stiffness increased by 10% from the baseline**, Table 7.3) against those of FEA

	Mass(kg.)	Stiffness 10^7 N.mm/rad.	
Baseline Optimum	7.307	0.4835(NN)	0.4890(POLY)
FEM	7.307	0.448E7	
Baseline Joint	8.375	0.444E7	

NN: Prediction of neural network.
POLY: Prediction of response surface polynomials.

Table 7.8 Values of design variables of baseline optimum

#	Design Variables	Values	Comments	% Change wrt Baseline Joint
1	T1 (mm)	0.720		-10.0
2	T2 (mm)	0.660	Lower bound	-30.0
3	T3 (mm)	0.850		-15.0
4	C1 (mm)	26.091	Lower bound	-10.0
5	C2 (mm)	87.596		1.7
6	C3 (mm)	86.471	Lower bound	-10.0
7	C4 (mm)	47.259	Lower bound	-10.0
8	B1/B2	0.7976		10.3
9	B2 (mm)	81.519		3.7
10	B3 (mm)	37.638		-1.5
11	B4/B1	1.000	Lower bound	-5.6
12	H1 (mm)	58.653	Lower bound	-10.0
13	α_1 (°)	75.519	Upper bound	4.0
14	H3 (mm)	124.326		2.5
15	H4 (mm)	68.486	Upper bound	10.0
16	H5 (mm)	14.474	Lower bound	-10.0
17	H6 (mm)	6.950	Upper bound	10.0
18	α_2 (°)	65.285		-8.7
19	HL (mm)	117.234	Lower bound	-10.0
20	RP (mm)	195.660	Lower bound	-10.0
21	RPL (mm)	250.134	Lower bound	-16.6

Refer to Figures 3.7 to 3.9 for definition of variables.

Table 7.9 Constraints of baseline optimum

Constraint	#	Constraint Descriptions	Active
Packaging	1	Maximum width of door	Y
Packaging	2	Maximum rocker width	-
Packaging	3	Maximum rocker width	-
Packaging	4	Maximum rocker height	Y
Packaging	5	Minimum door edge width	Y
Packaging	6	Maximum slope of H5	-
Packaging	7	Maximum α_3	-
Packaging	8	Minimum door edge height	-
Packaging	9	Point E be above point D in Figure 6.3	-
Packaging	10	Point E above line $\overline{DF}$ in Figure 6.3	-
Packaging	11	Maximum step out height	Y
Packaging	12	Continuity of door with rocker outboard*	Y
Packaging	13	Continuity of door with rocker outboard**	-
Manufacturing	14	Maximum difference between T1 & T2	-
Manufacturing	15	Maximum difference between T2 & T3	-
Manufacturing	16	Maximum difference between T3 & T4	Y
Manufacturing	17	Maximum difference between T1 & T5	-
Manufacturing	18	Maximum difference between T1 & T6/2	-
Manufacturing	19	Maximum difference between T1 & T2	-
Performance	20	Minimum moment of inertia I_y	Y
Performance	21	Minimum moment of inertia I_z	Y
Performance	22	Minimum twist constant J	Y
Performance	23	Minimum stiffness predicted by polynomial	Y
Performance	24	Minimum stiffness predicted by neural net	Y

* This is for $g(12) = \varepsilon - (\alpha_4 - \alpha_3) \geq 0$ (Figure 7.3).

** This is for $g(13) = \varepsilon + (\alpha_4 - \alpha_3) \geq 0$ (Figure 7.3).

Table 7.10 Resultant mass of optimum program and FEA when increasing stiffness constraint up to 150% from that of baseline constraint (Table 7.3)

Normalized Stiffness		Normalized Mass
Optimization Program	FEM Analysis	
1.0	1.0	1.0
1.1	1.067	1.010
1.2	1.143	1.019
1.3	1.236	1.028
1.4	1.326	1.037
1.5	1.417	1.045

$$\text{Normalized Stiffness} = \frac{\text{Stiffness}}{\text{Stiffness of baseline optimum design}}$$

$$\text{Normalized Mass} = \frac{\text{Mass}}{\text{Mass of baseline optimum design}}$$

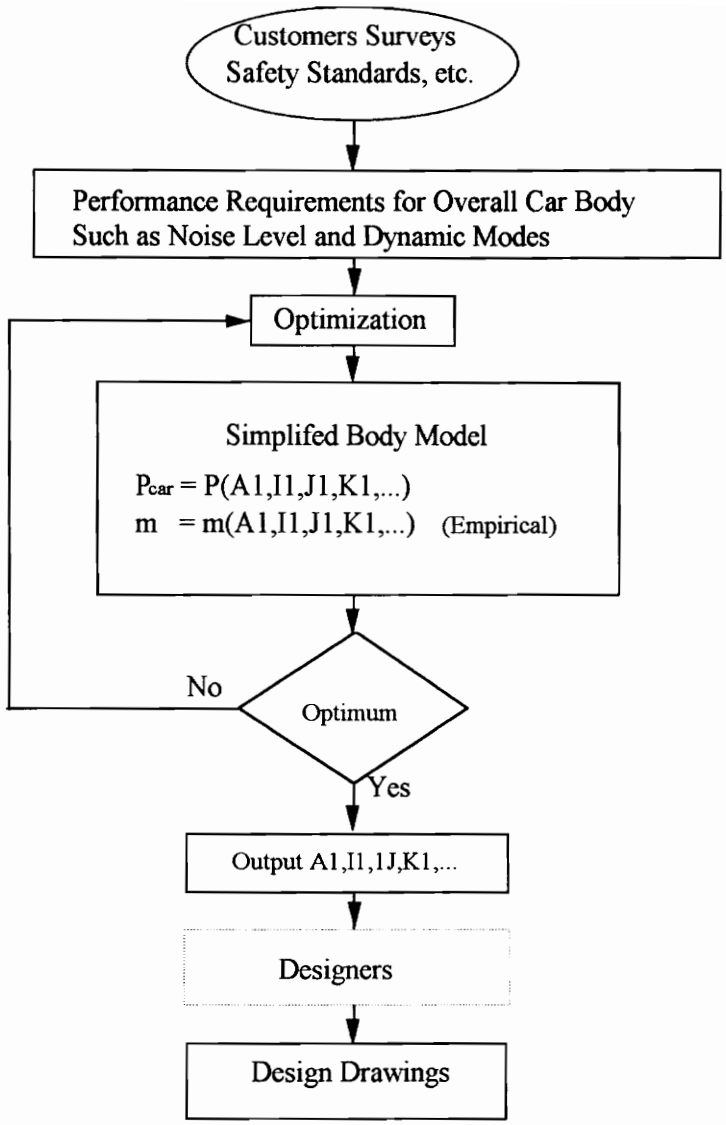

P_{car} :	Performance characteristics of car body (bending stiffness, noise level measured at drivers seat)
A1,I1,J1:	Area, moment of inertia, torsional constant of cross section of a beam
K1:	Stiffness of a joint
m:	Mass of body

Figure 1.1 Optimization of Car Body Using A Simplified Model

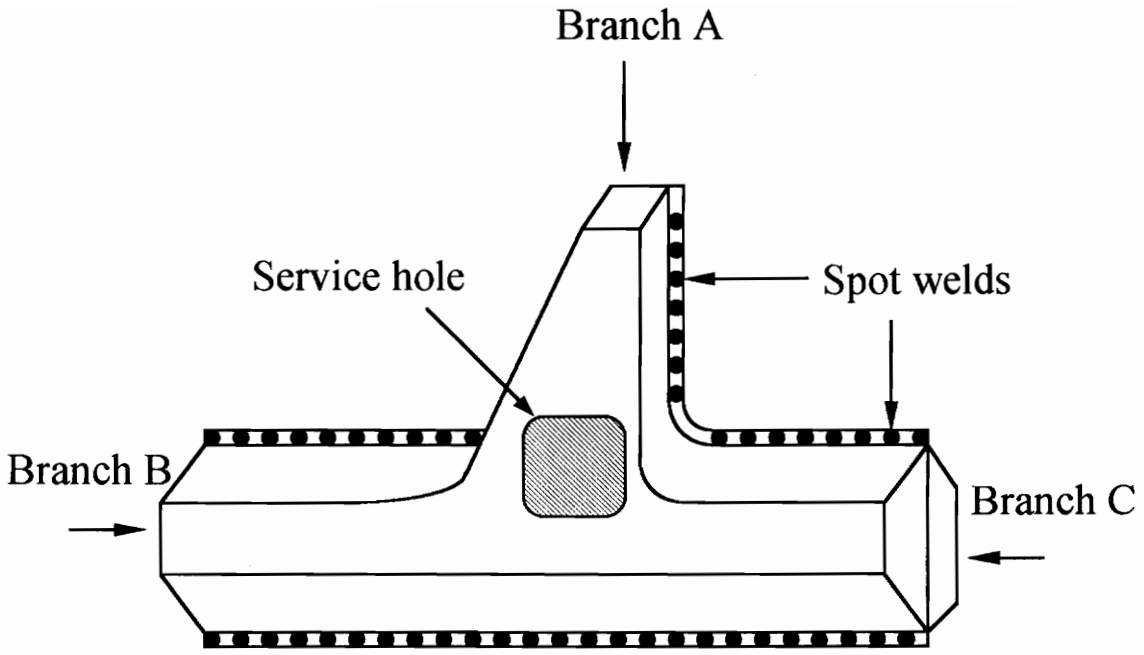

Figure 1.2 A Joint Model in A Car Structure

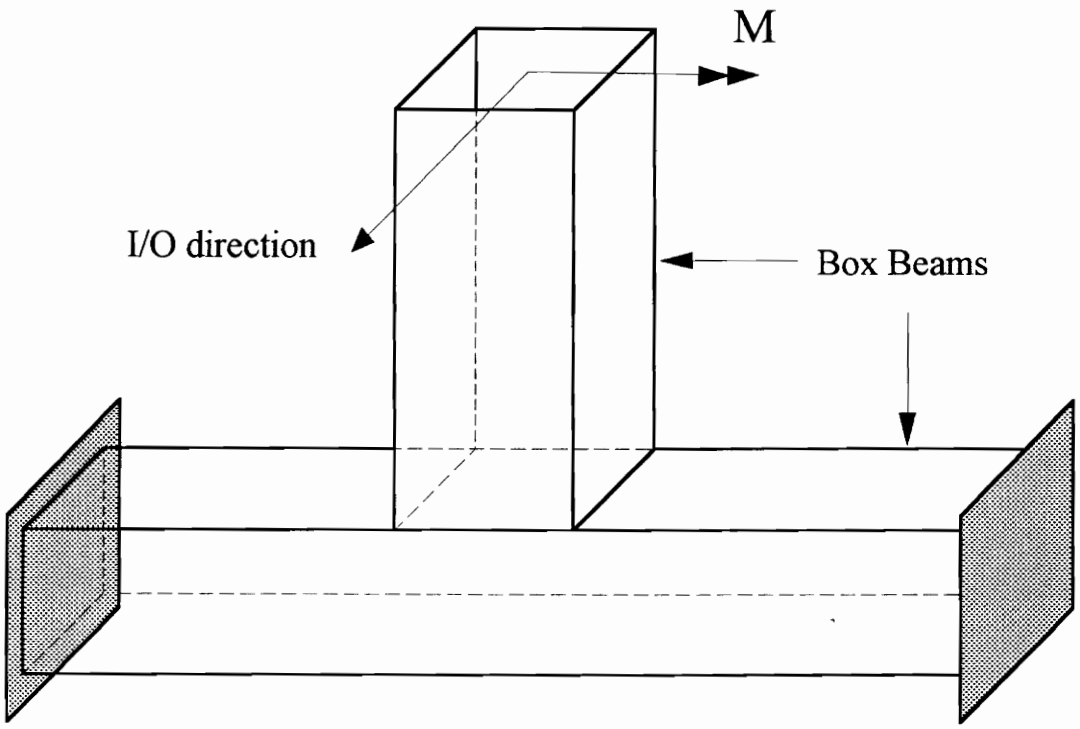

M = I/O Bending Moment

Figure 1.3 The Inboard-Outboard (I/O) Bending of T-Shaped Joint Made of Two Box Beams

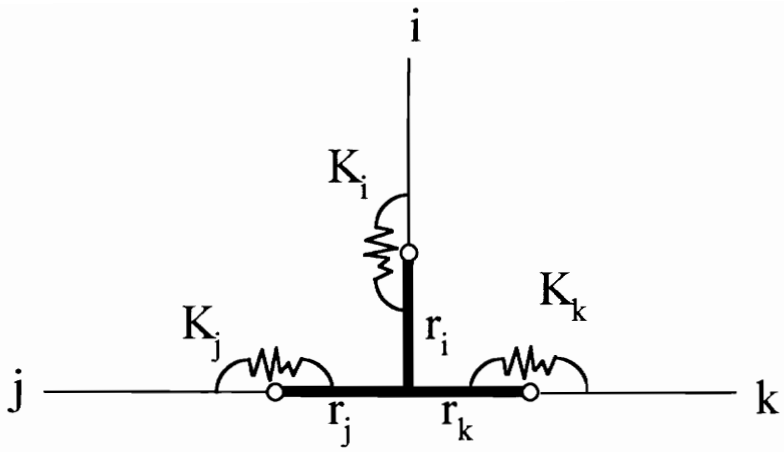

i, j, k = Branch Members

K_i, K_j, K_k = Stiffness

r_i, r_j, r_k = Rigid Elements

Figure 1.4 A Simplified 2-D Joint Model

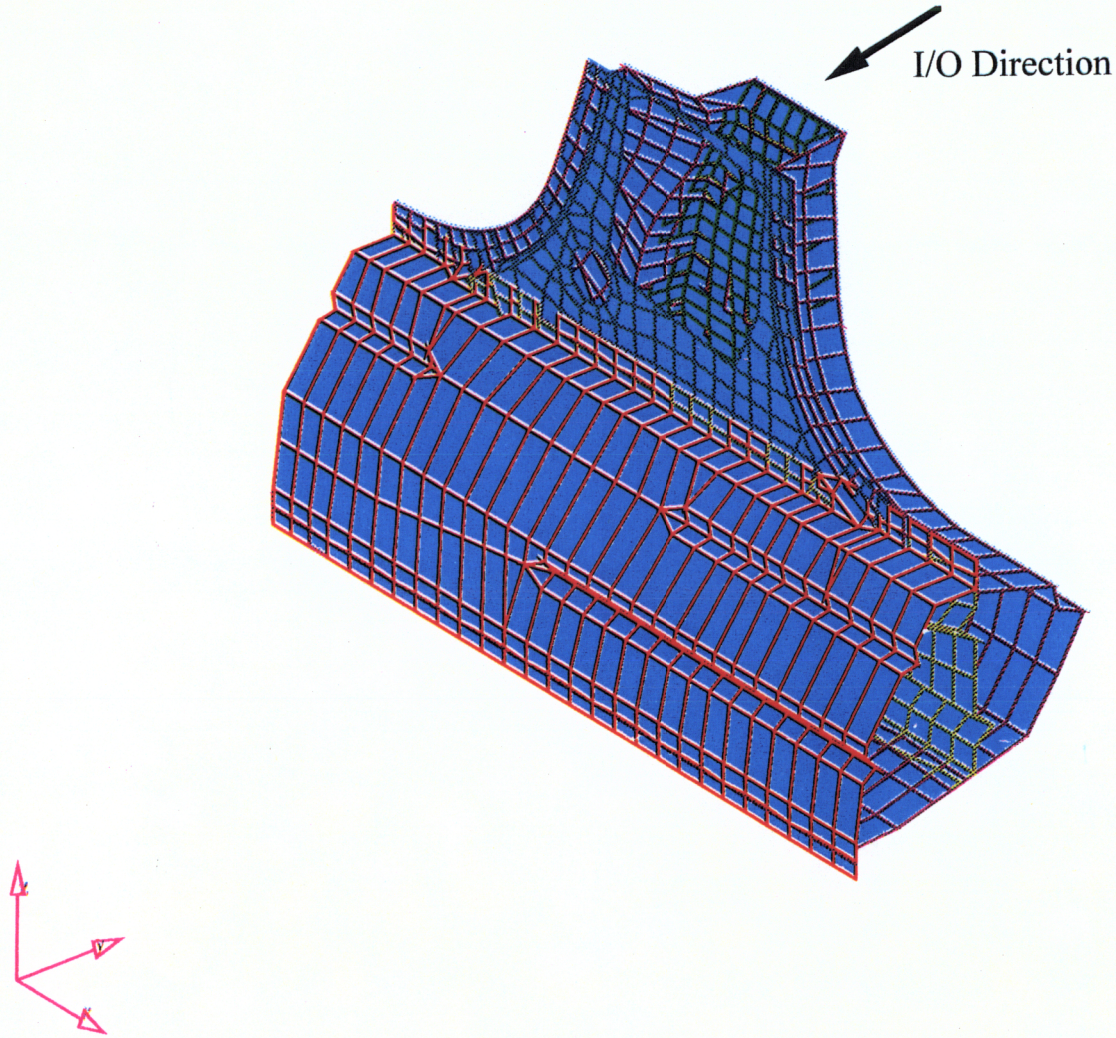

Figure 1.5 A Detailed FEM Model of B-pillar to Rocker Joint

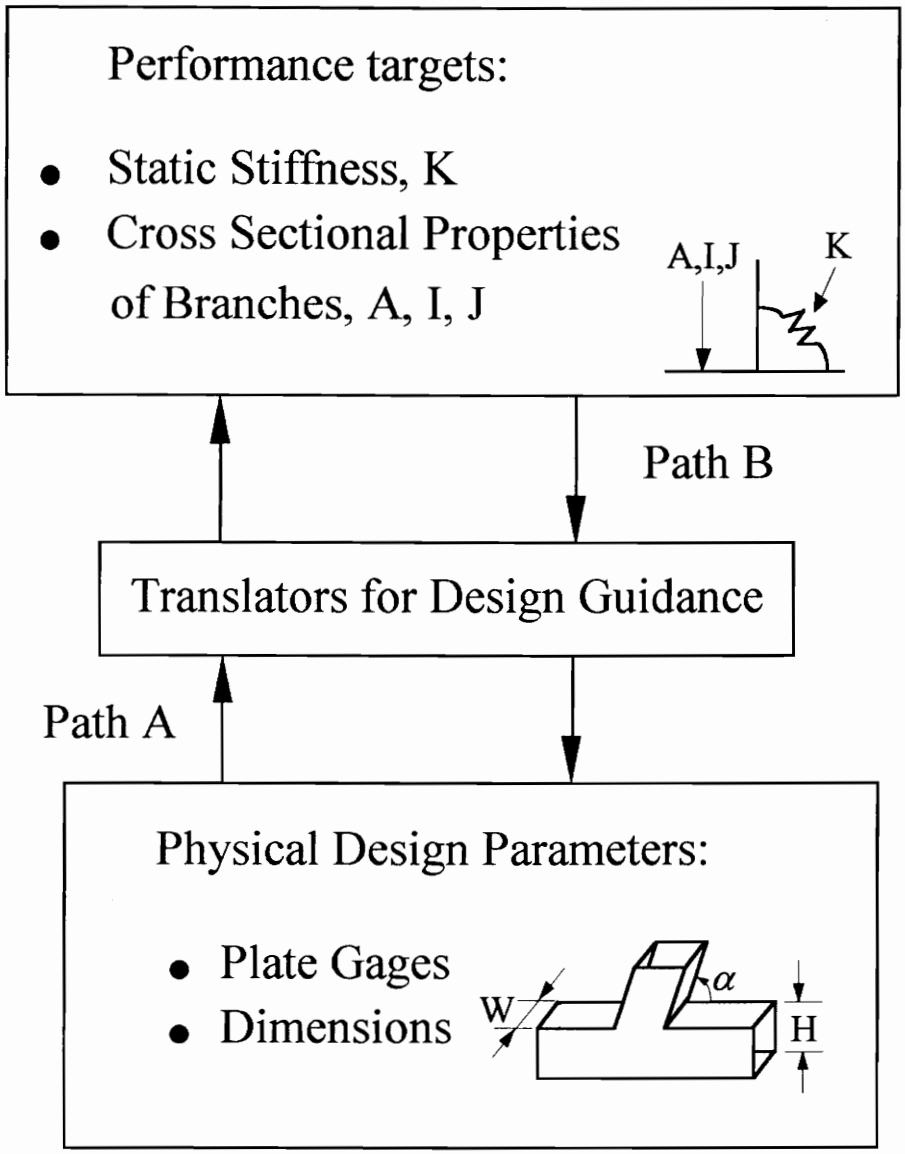

Figure 1.6 Translators for Design Guidance of Joints

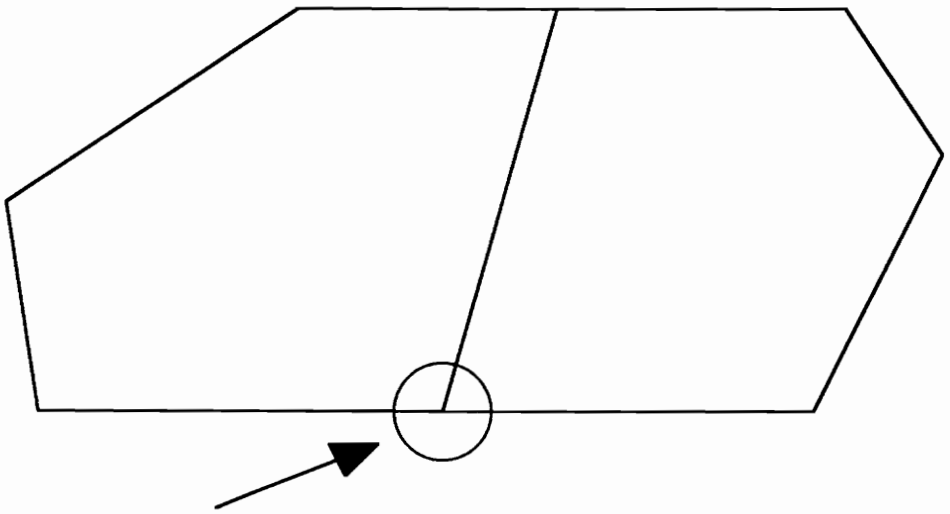

Figure 2.1 A 2_D Frame Structure of A car Body

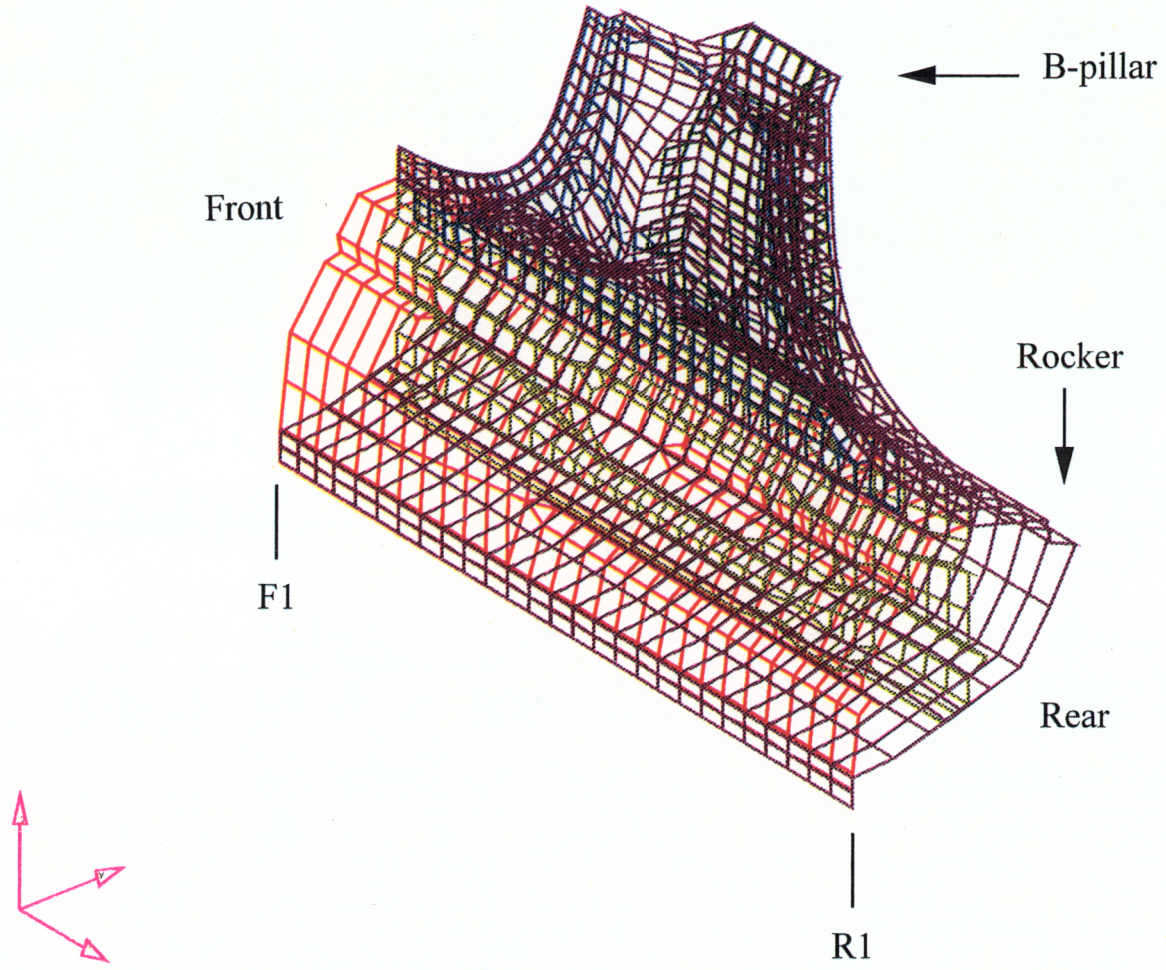

Figure 2.2 B-pillar to Rocker Joint Used in This Study

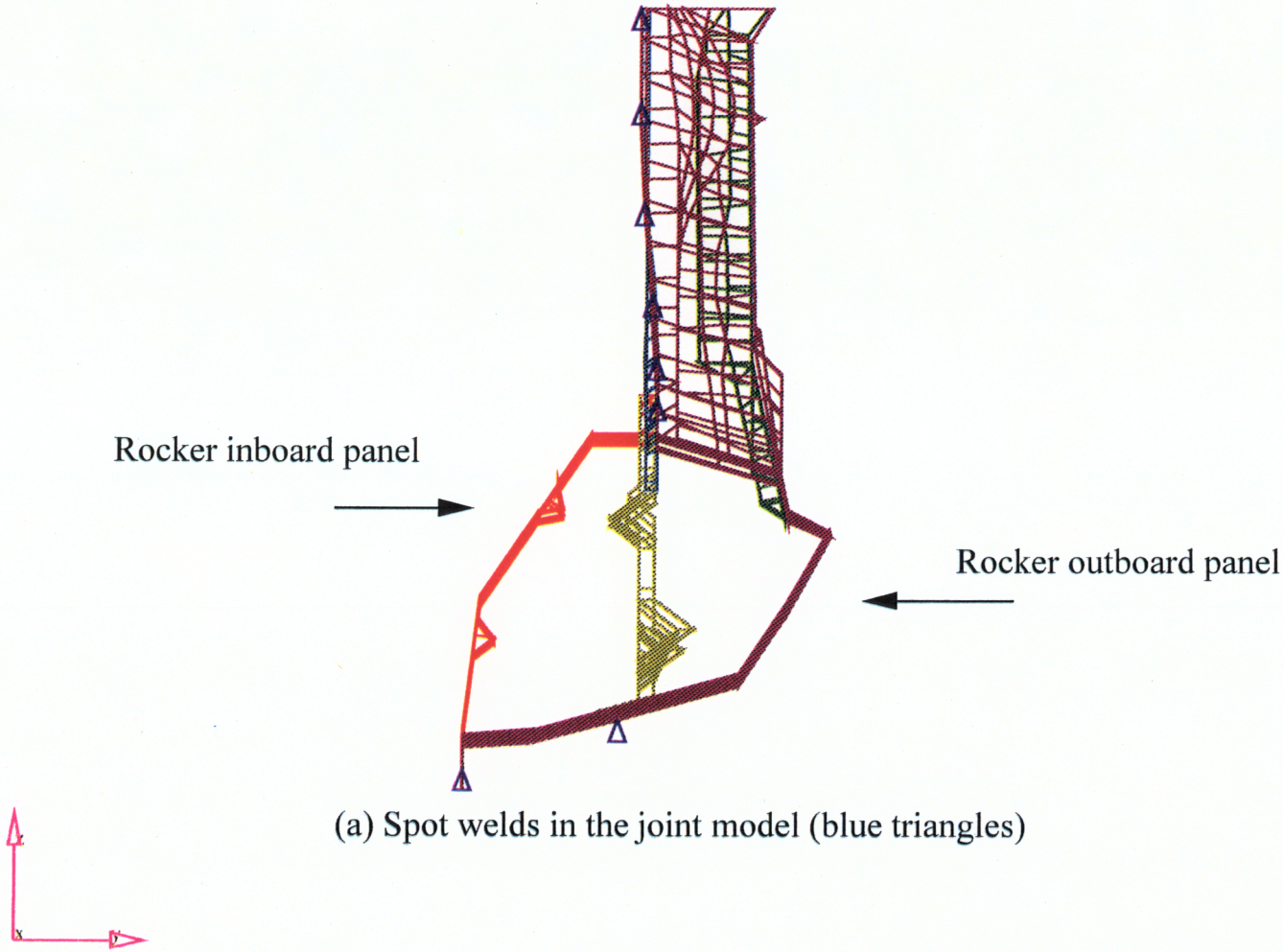

Figure 2.3 Imperfections of B-pillar to Rocker Joint Used in This Study

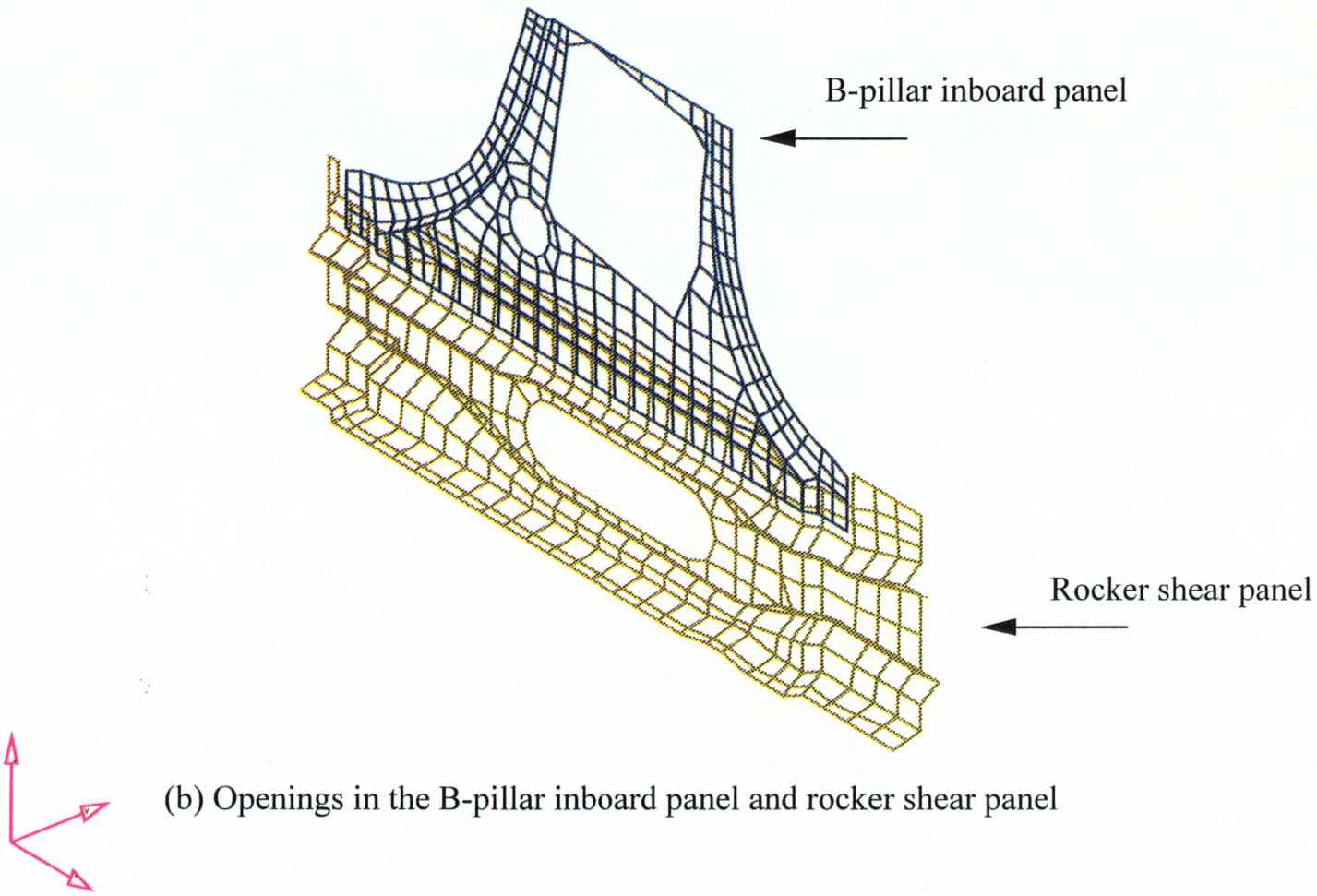

(b) Openings in the B-pillar inboard panel and rocker shear panel

Figure 2.3 (Continued)

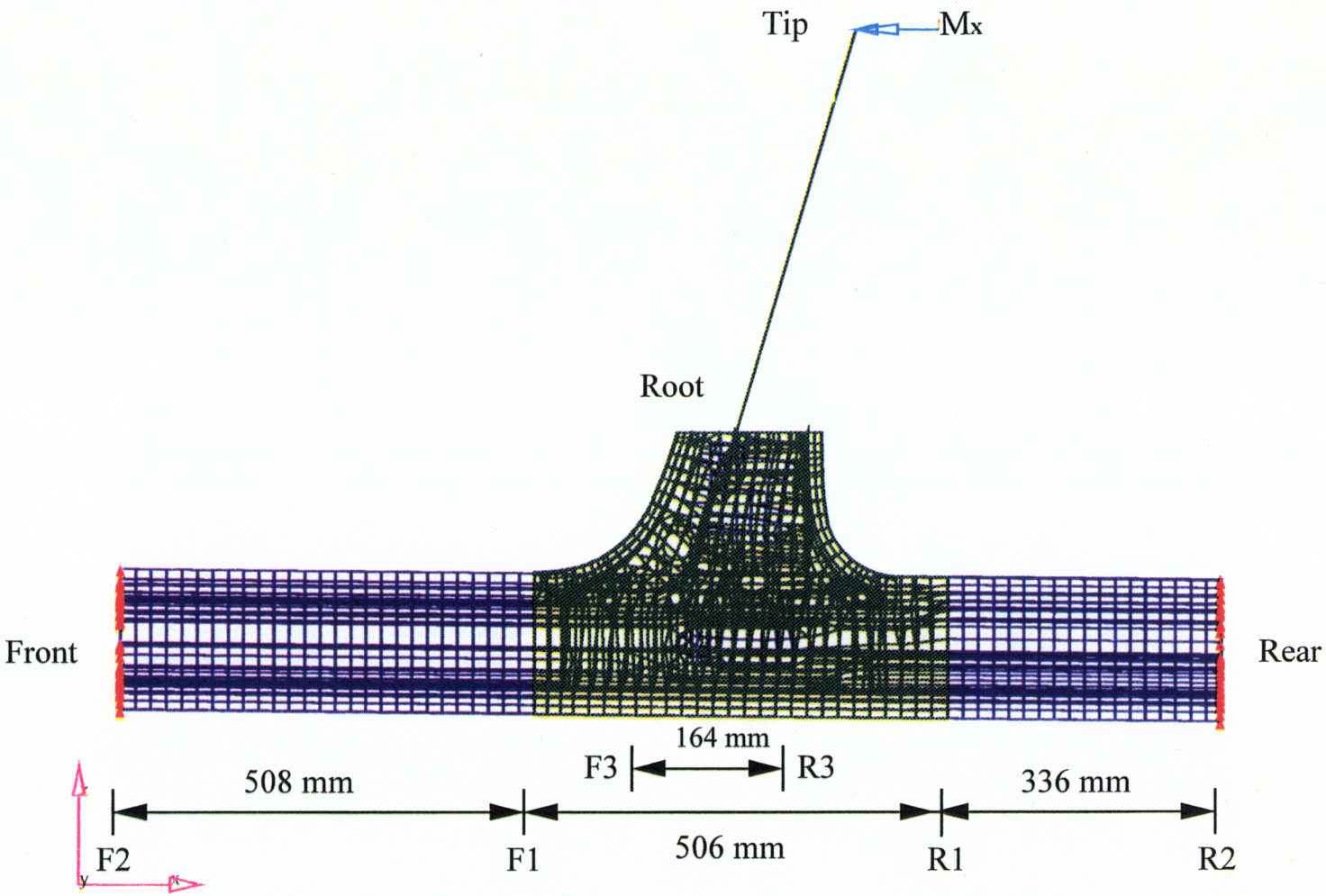

Figure 2.4 A Joint Subassembly of B-pillar to Rocker Joint

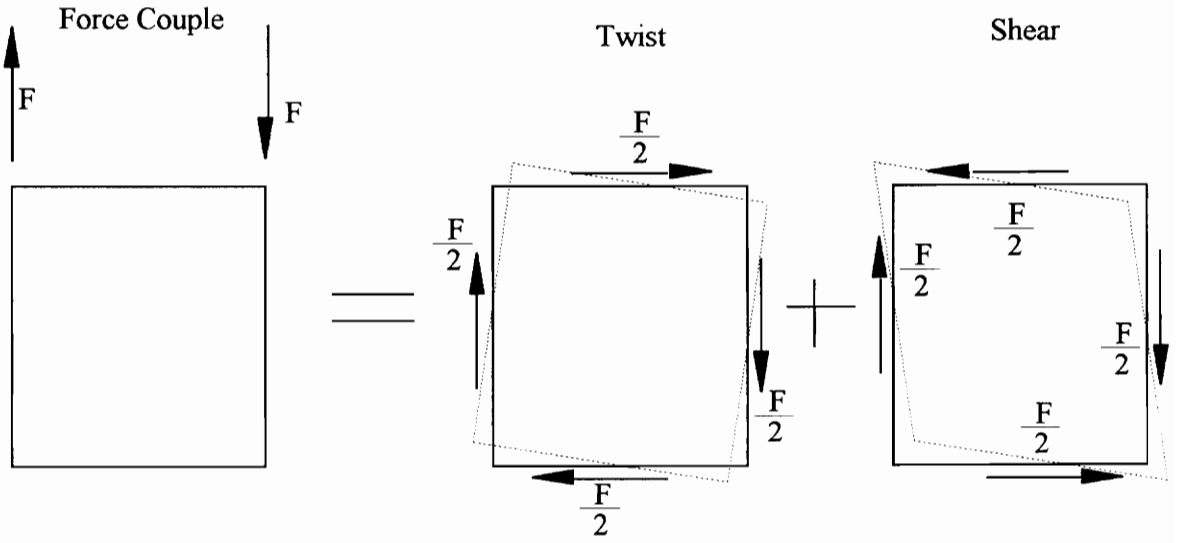

Figure 2.5 Shear and Twist Deformation of A Rectangular Rocker Section

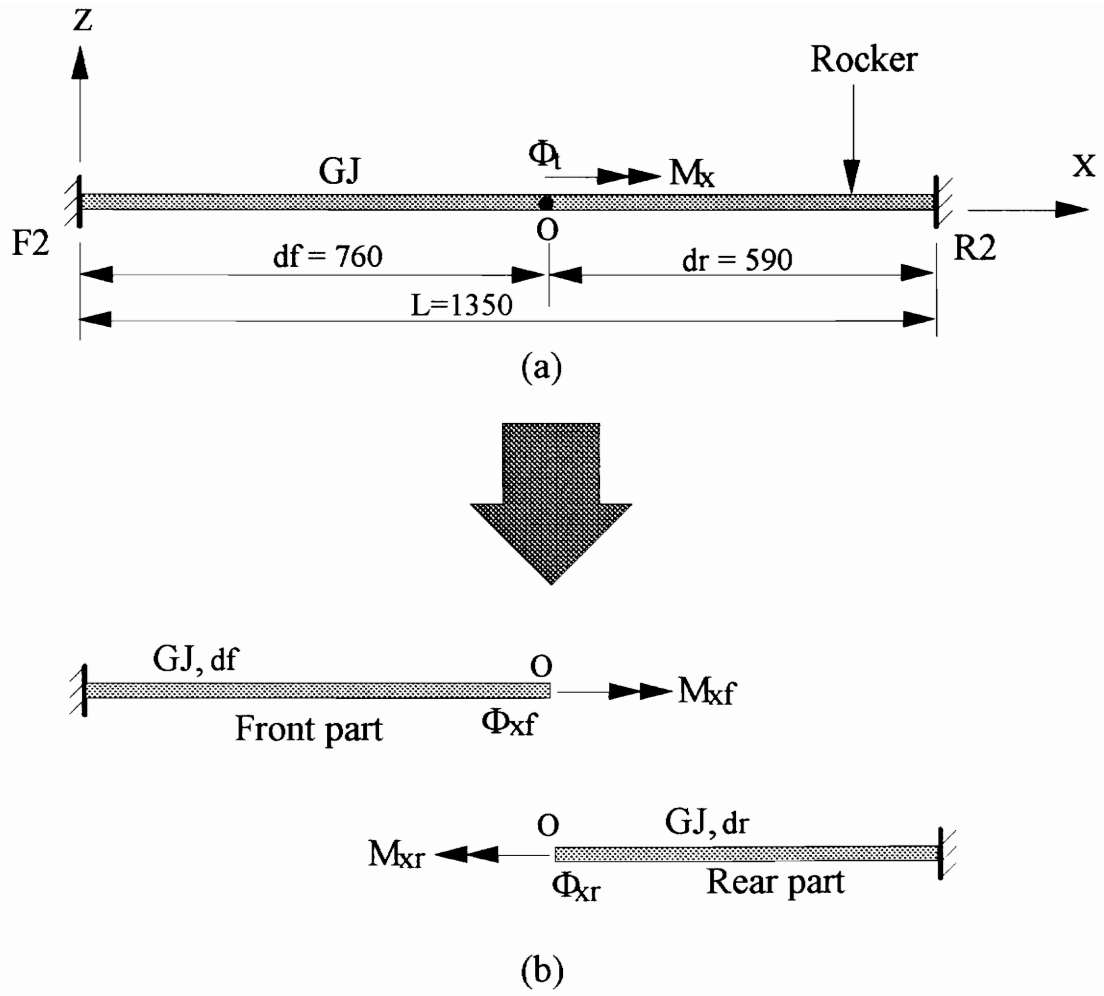

Section "O" passes the center of the joint.

M_x is the twist moment applied at point "O" in X direction.

Φ_t, Φ_{xf} and Φ_{xr} are angular deflection about X axis at point "O".

$\Phi_t = \Phi_{xf} = \Phi_{xr}$

Figure 2.6 Rocker Twist deflection Under A Twist Moment Applied at the Center of the Joint

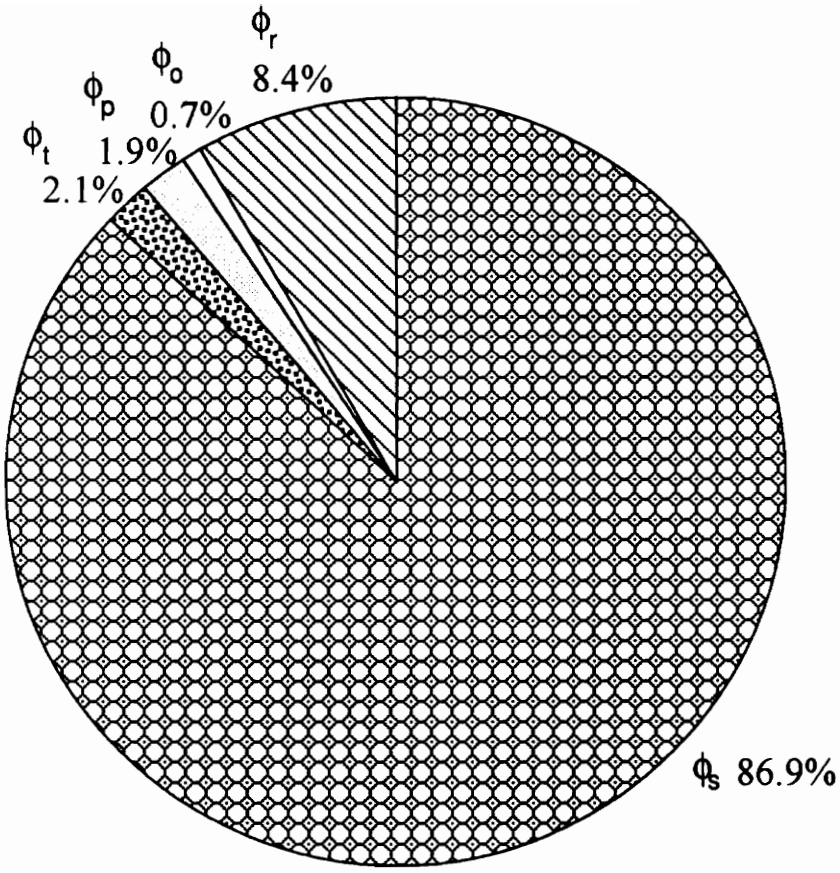

Total deflection = 6.093E-3 rad.

Figure 2.7 Contribution of Deflection of Deformation Mechanisms to I/O Deflection

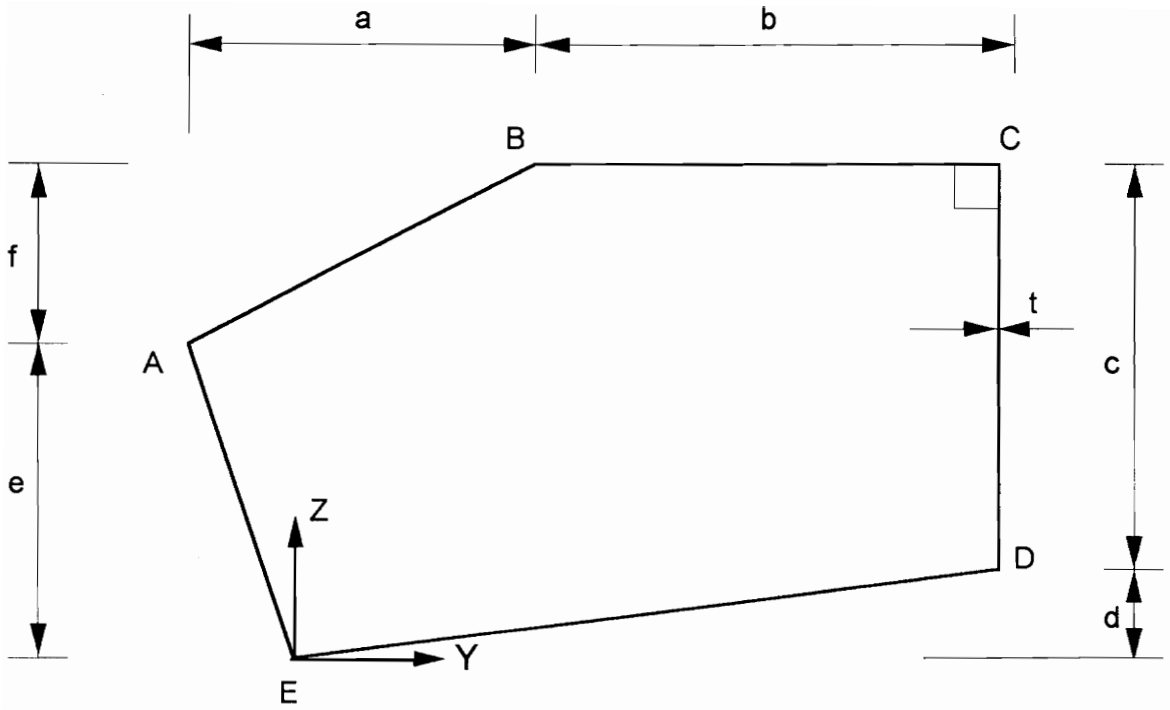

Figure 3.1 An Example of Rocker Cross Section

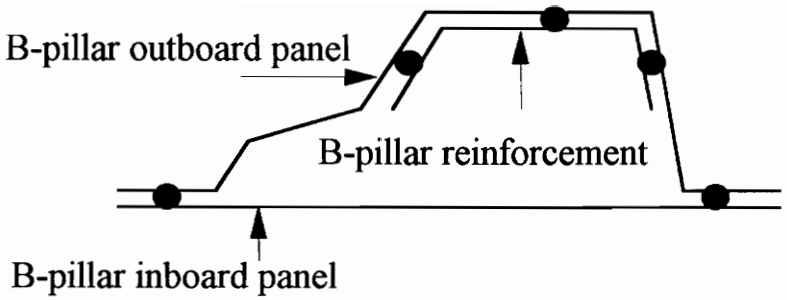

Cross section of B-pillar

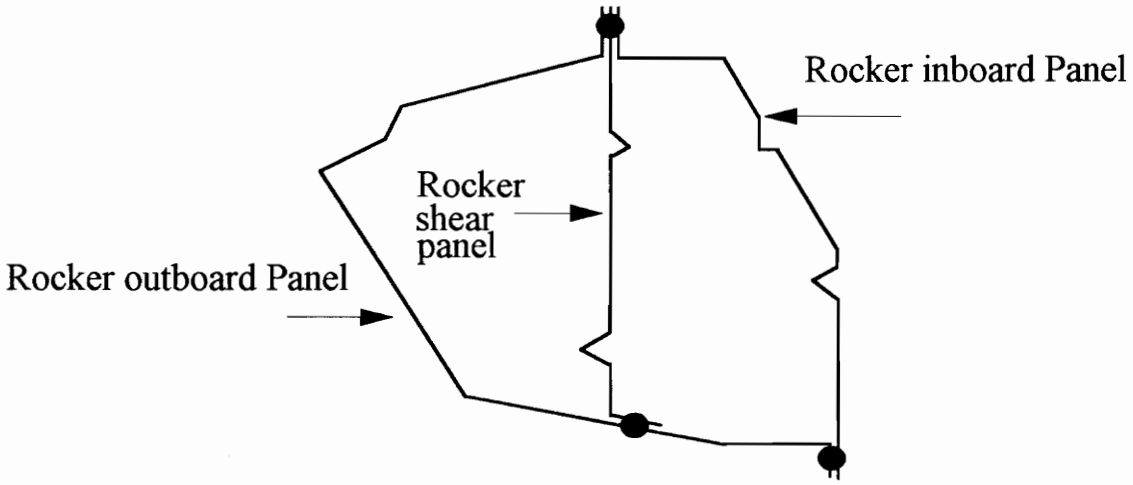

Cross section of rocker

● = Spot Weld

Figure 3.2 B-pillar and Rocker Sections of the Joint Model Used in This Study

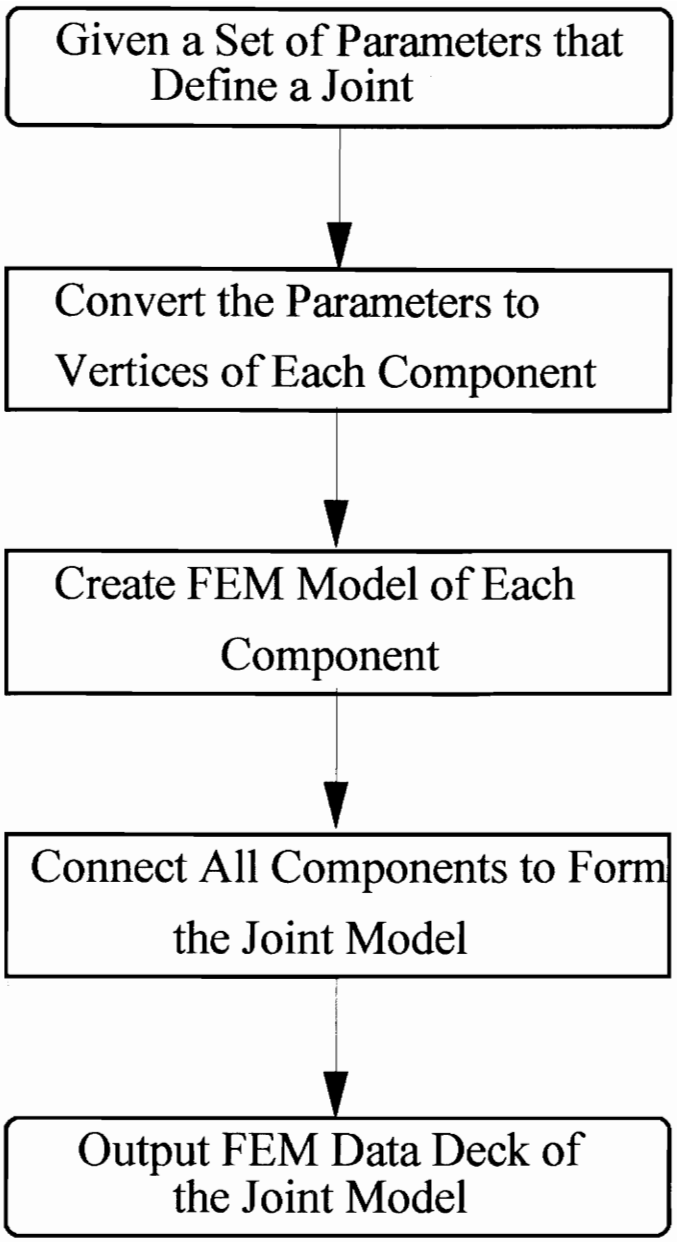

Figure 3.3 Flow Chart of Generic Model

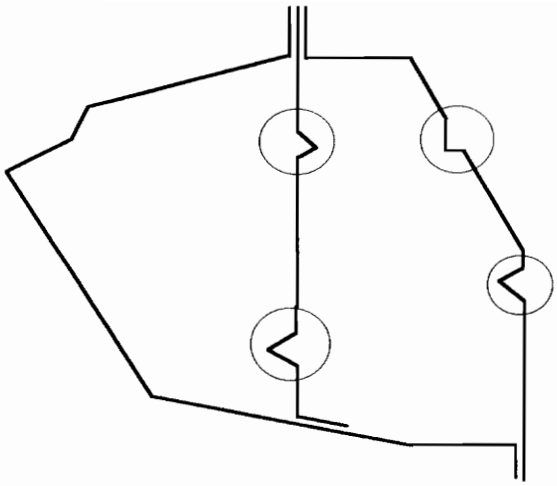

(a) Rocker Section of Joint Model Used In This Study

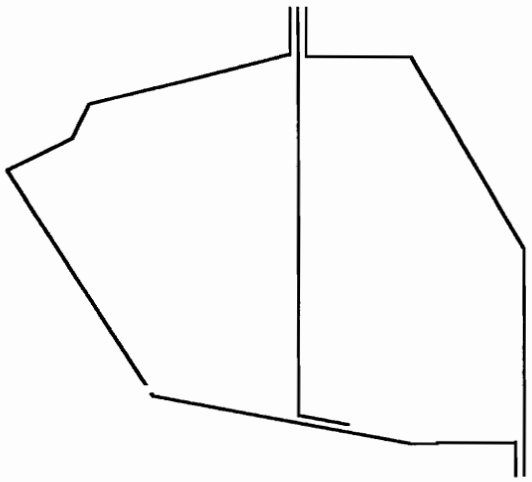

(b) Rocker Section after Simplification

Figure 3.4 Simplified Rocker Section for Parameterization

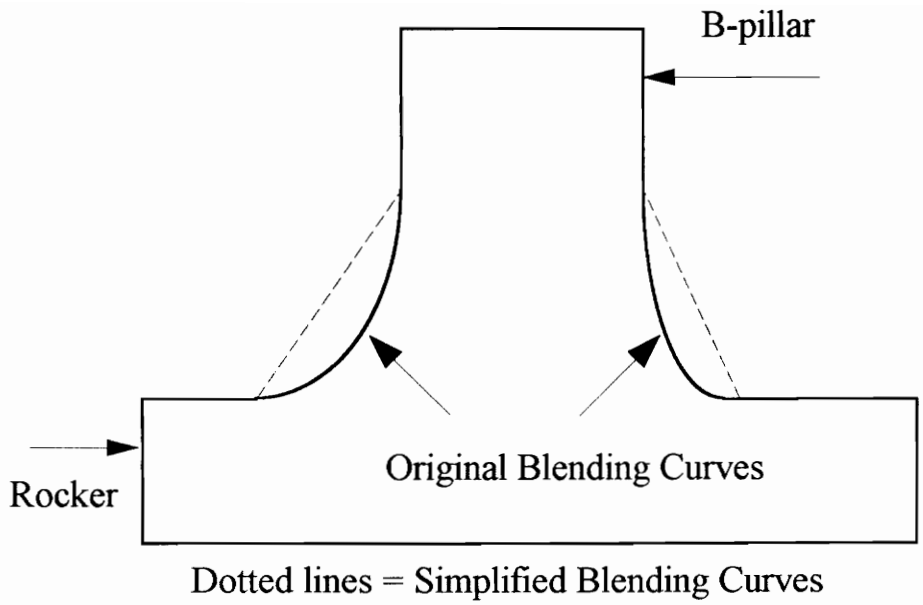

Figure 3.5 Simplified Blending Curves

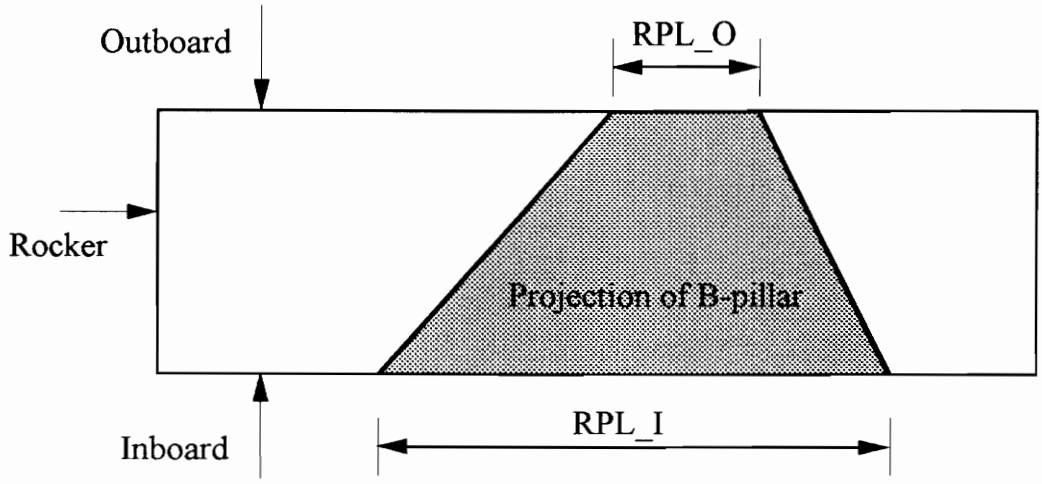

(a) Linkage Lengths of Original Joint Model (top view)

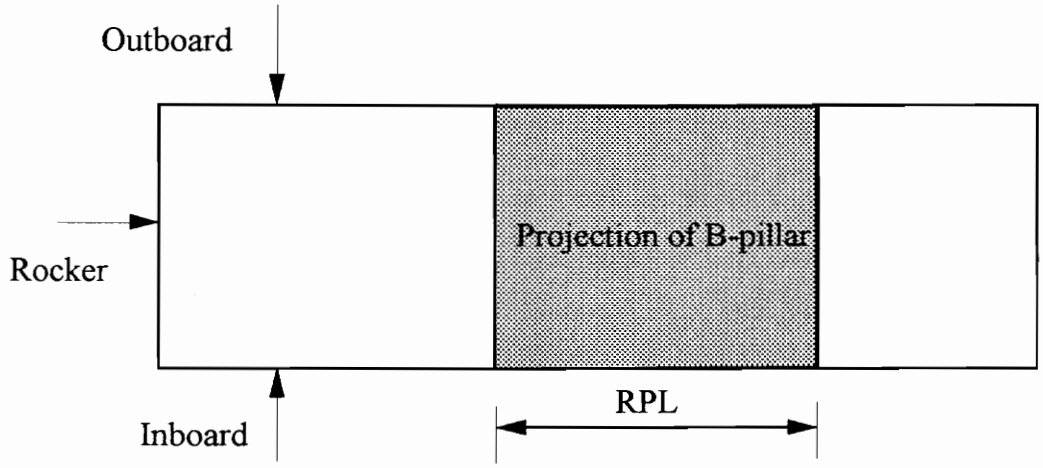

(b) Linkage Length after Simplification (top view)

RPL_O -- The linkage length at outboard of original model
RPL_I -- The linkage length at inboard of original model
RPL -- The linkage length used in parameterization
RPL= (RPL_O+RPL_I)/2

Figure 3.6 Simplified Linkage Length

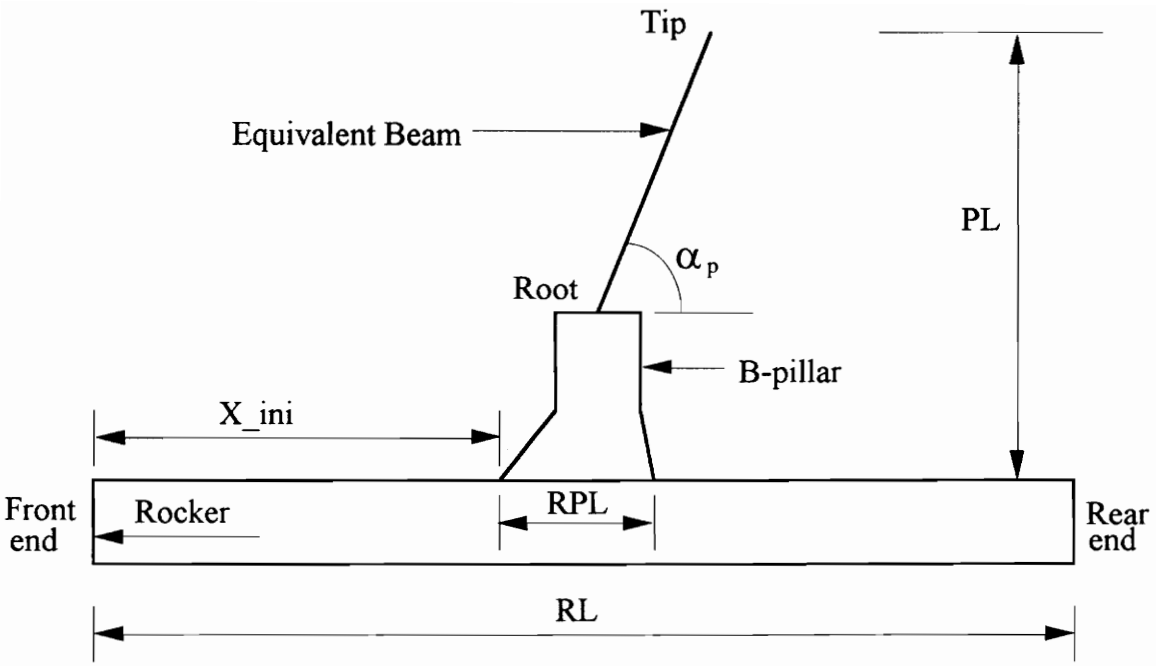

5 parameters:
RL, PL -- lengths of rocker and B-pillar, respectively
RPL -- B-pillar to rocker linkage length
X_ini -- The length between starting point of blending curve of B-pillar and the front end of rocker
α_p -- Inclined angle of shear axis of B-pillar with respect to that of the rocker

Figure 3.7 Parameters of Joint Side View

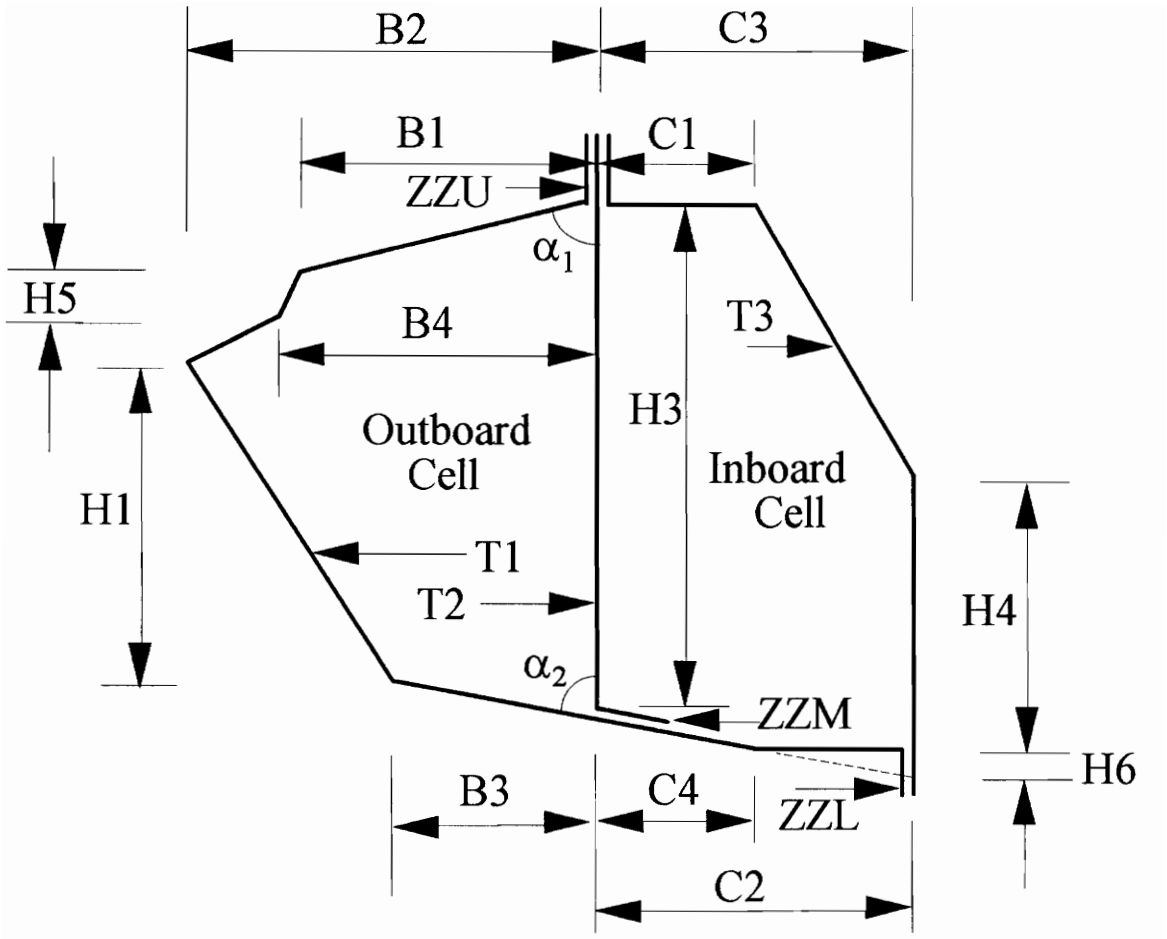

21 parameters:

α_1 and α_2	-- Two angles
B1, B2, B3, B4	-- Four widths of outboard cell
C1, C2, C3, C4	-- Four widths of inboard cell
H1, H3, H4, H5, H6	-- Five heights
T1, T2, T3	-- Three thickness
ZZU, ZZM, ZZL	-- Three widths of flanges

Figure 3.8 Parameters of Rocker Cross Section

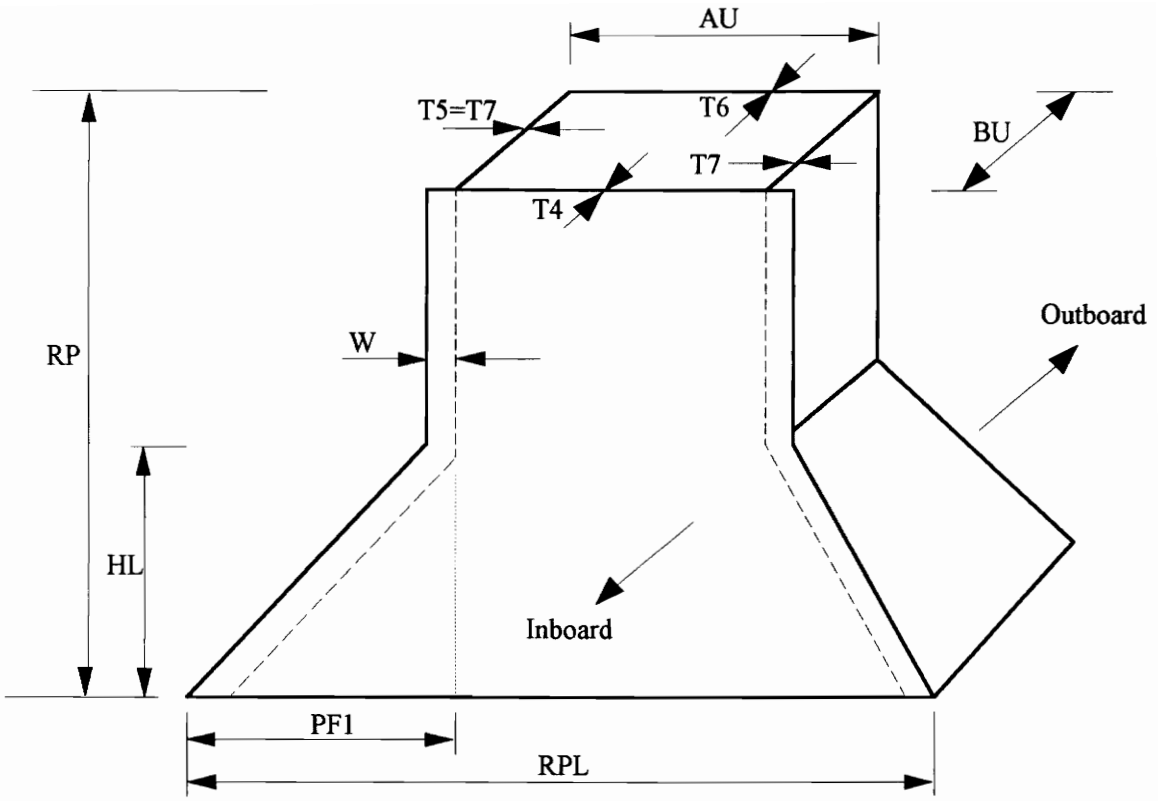

9 parameters:

HL, RP	-- Two Heights
PF1	-- Shrinking of bending curve
AU, BU	-- Two dimensions of B-pillar cross section at the root
T4	-- Thickness of pillar inboard panel
T5, T6	-- Thickness of B-pillar outboard panel and side panel (including thickness of the reinforcement)
W	-- width of the flange of B-pillar
RPL	-- B-pillar to rocker linkage length (the same as that in Figure 3.7)

Figure 3.9 Parameters of Transition Part of B-pillar to Rocker

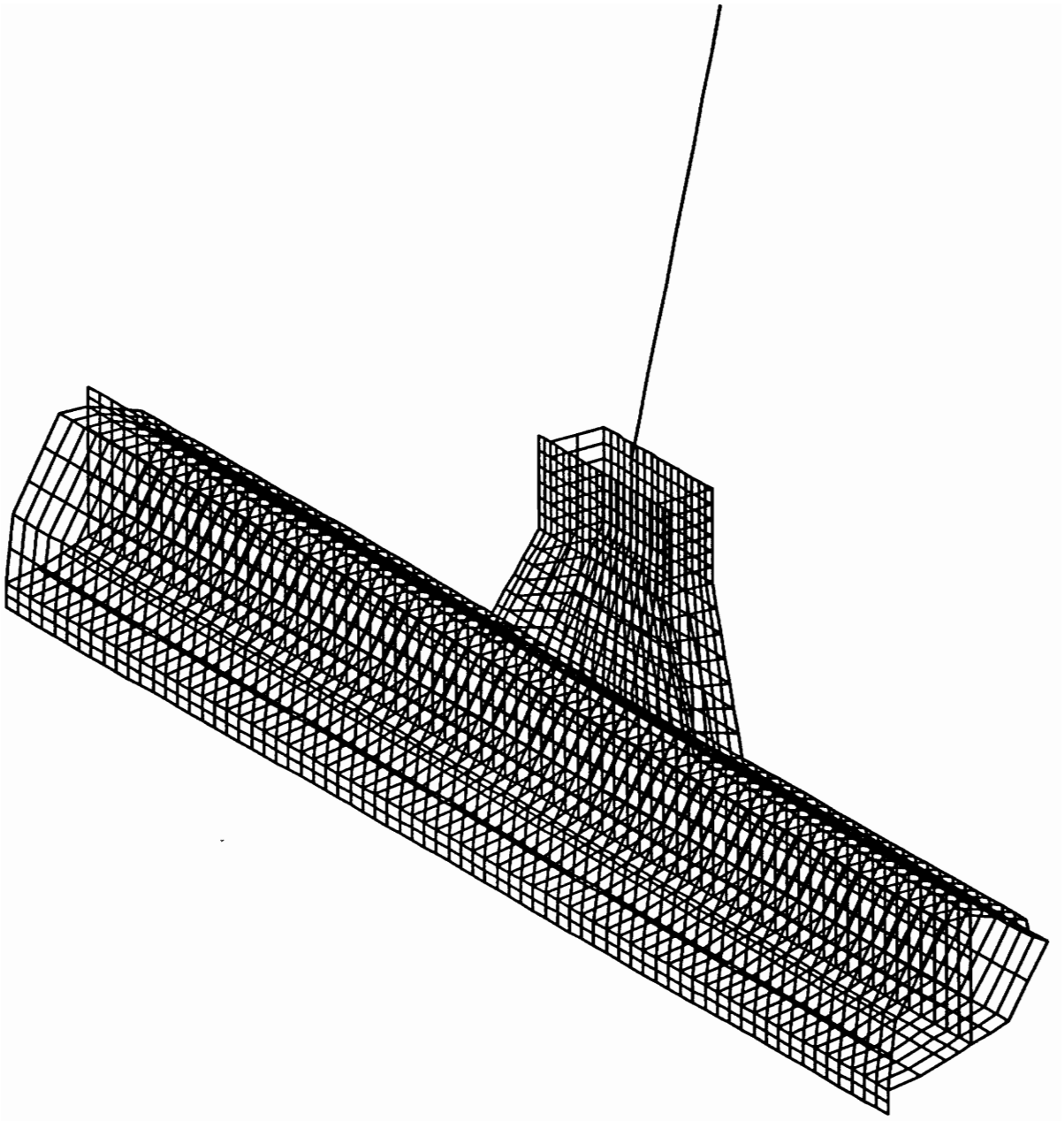

Figure 3.10 Generic Model of the Joint Subassembly Created by Converting Physical Design parameters into FEM Model

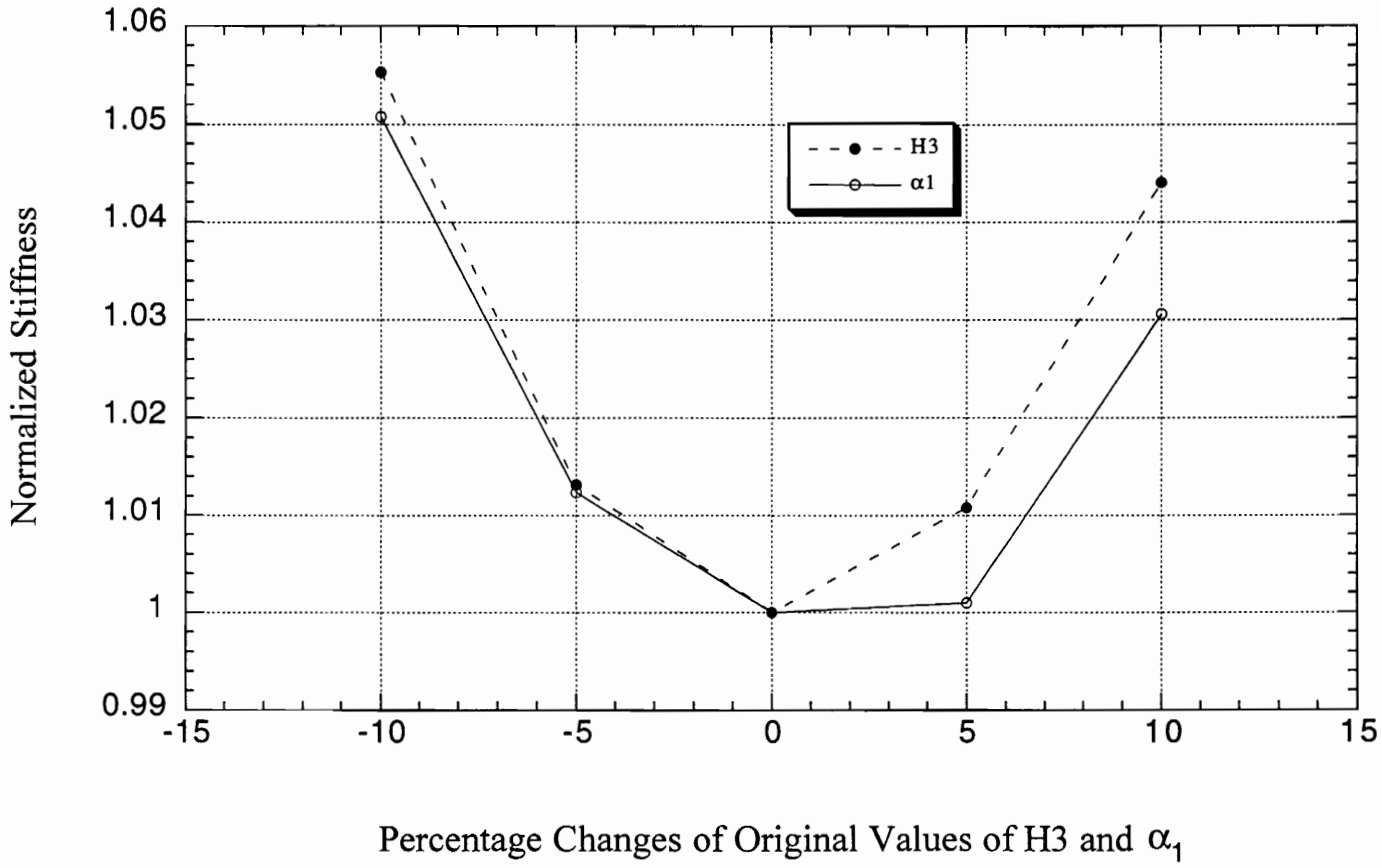

Figure 4.1 Normalized Stiffness versus H3 and α_1

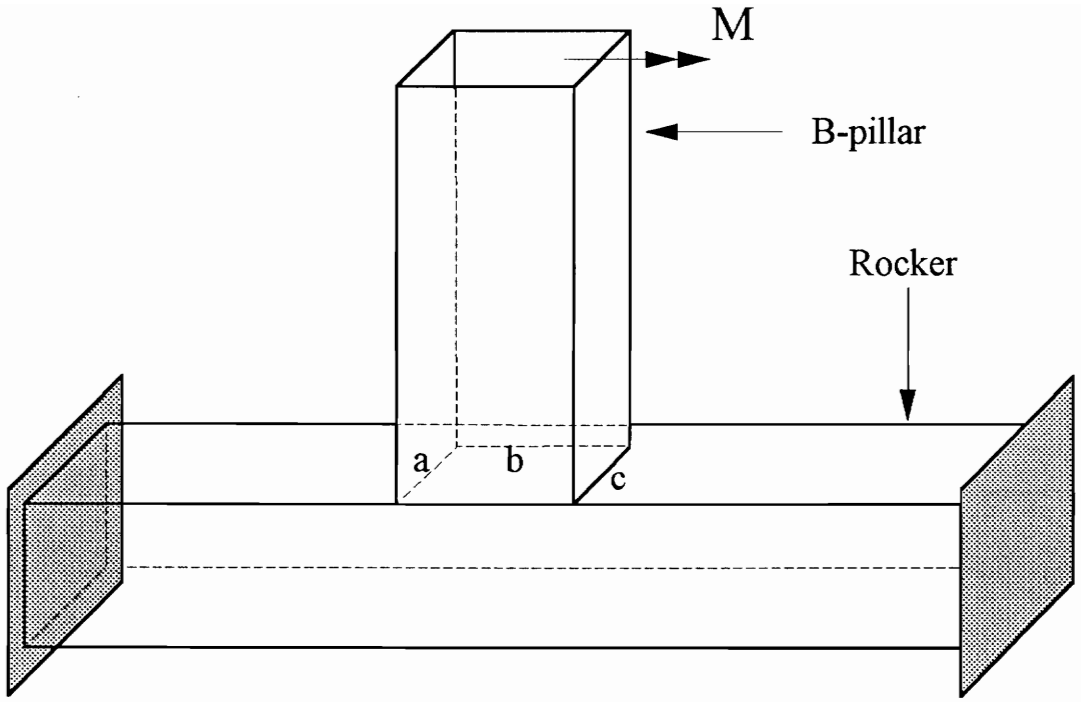

Along edges a, b and c, there is a discontinuity of load carrying from B-pillar to rocker.

Figure 5.1 The Discontinuity of Load Carrying from B-pillar to Rocker

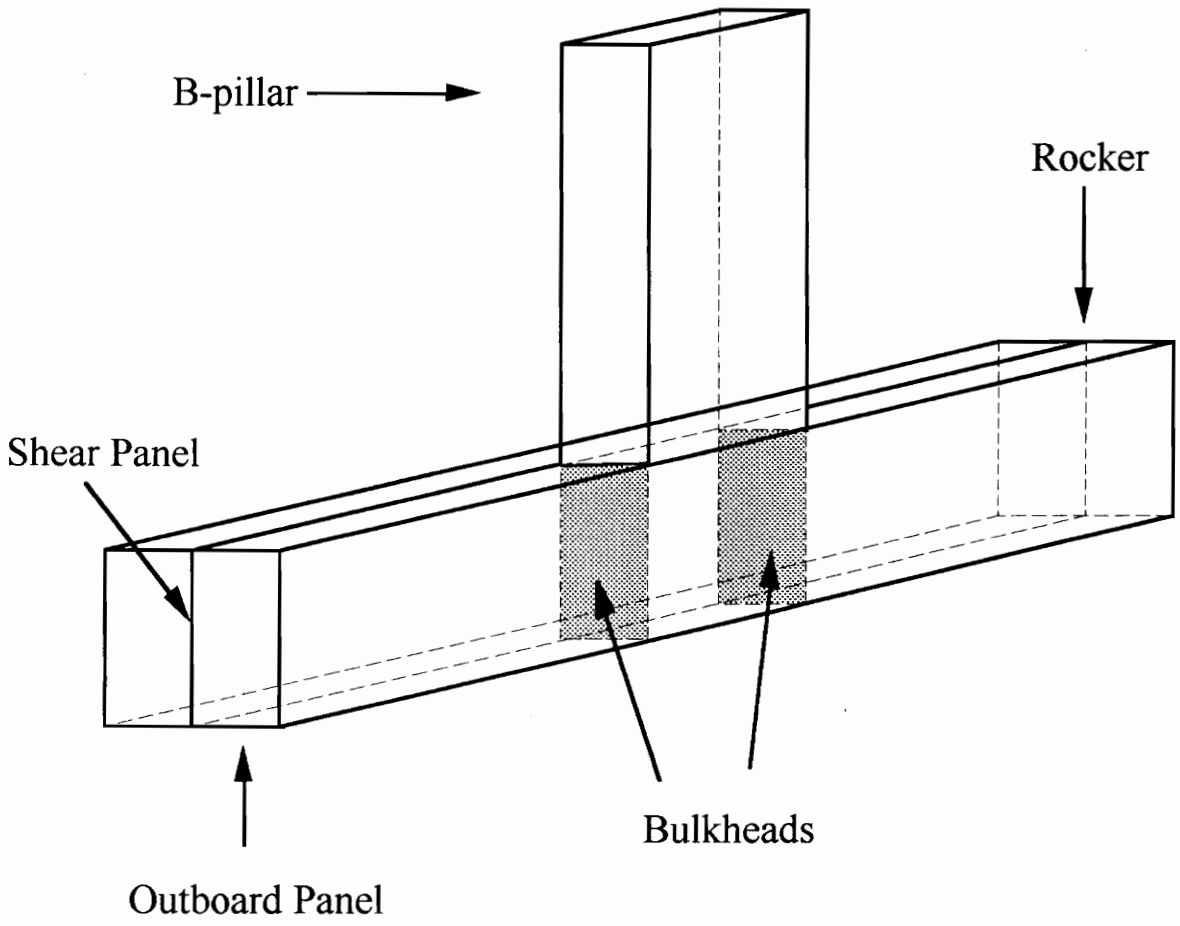

Figure 5.2 Design Modification: Transverse Bulkheads in Rocker

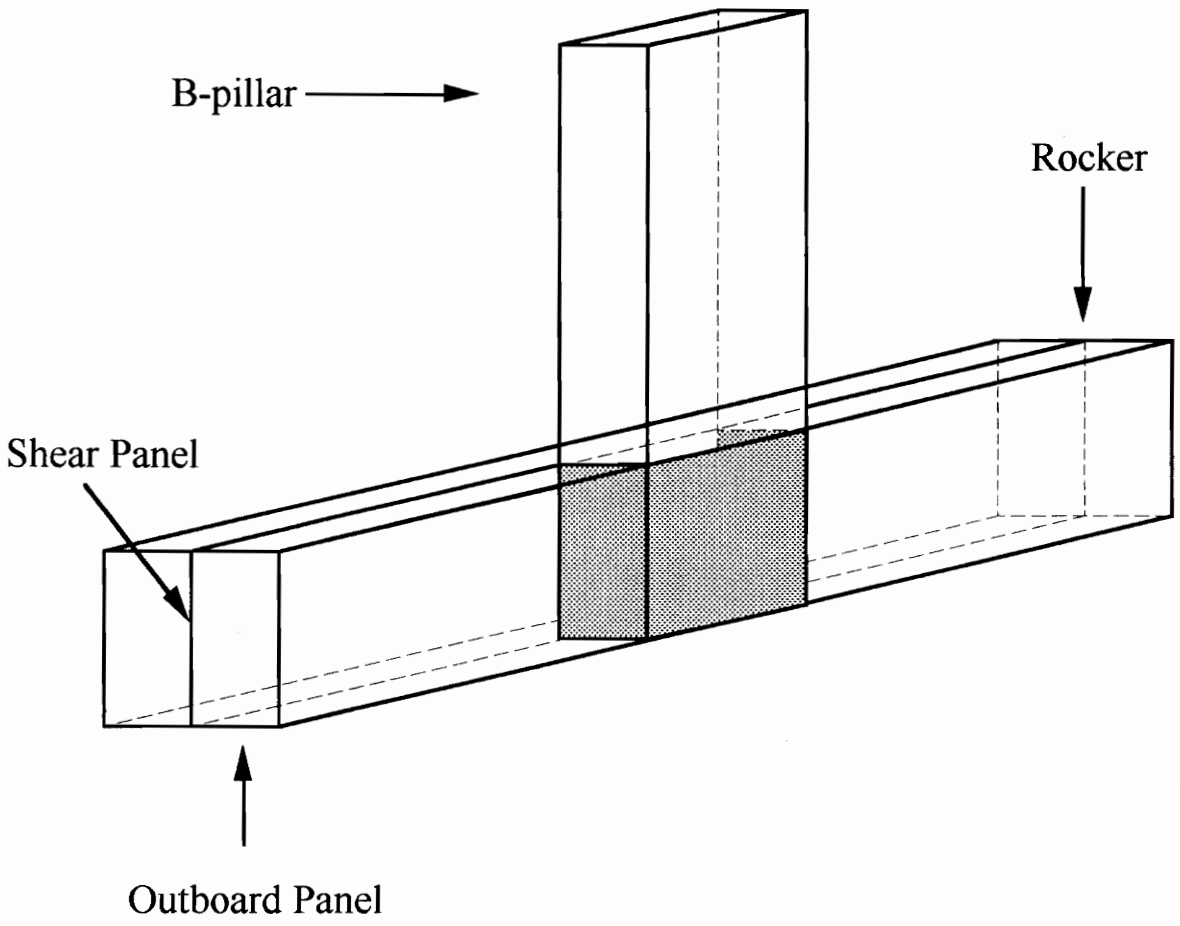

Figure 5.3 Design Modification: Extent B-pillar Inside the Rocker

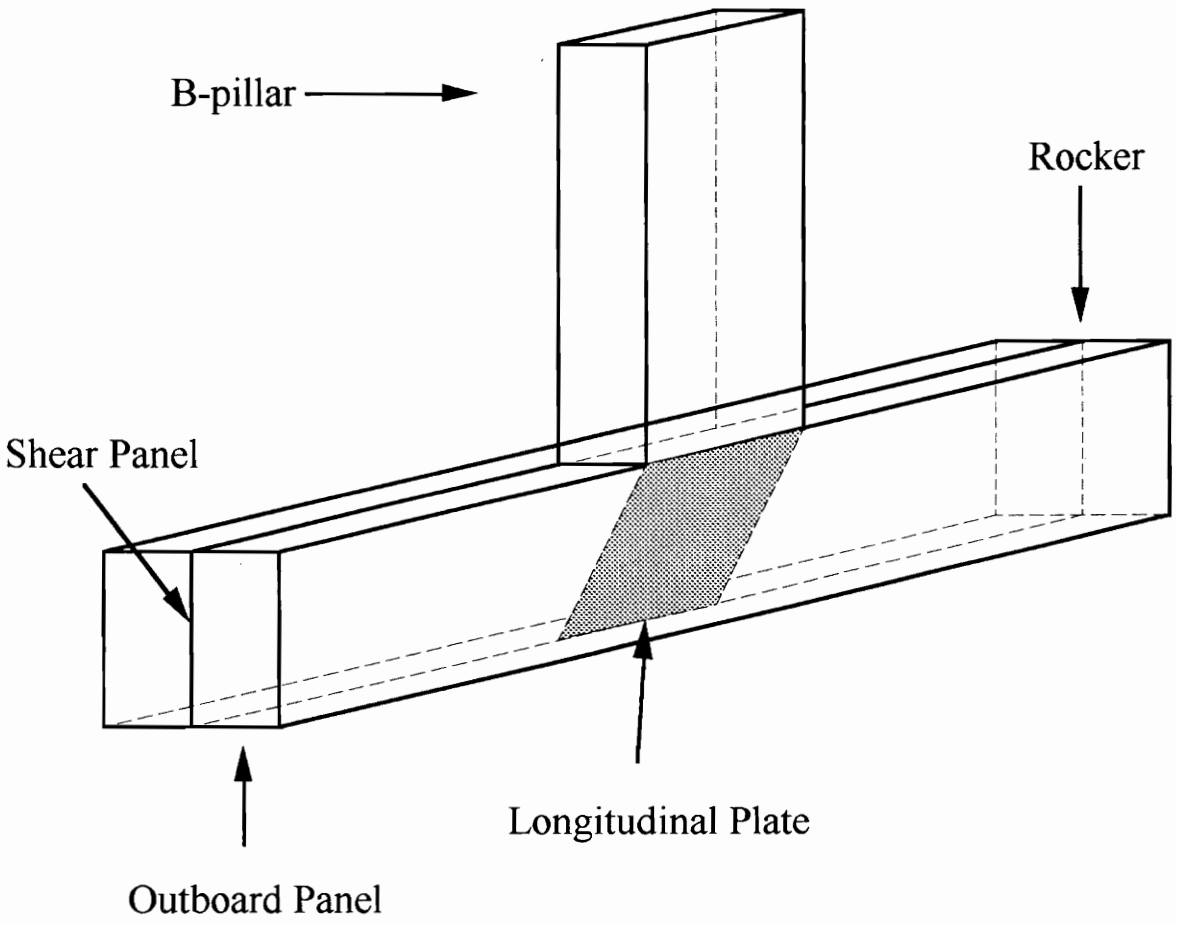

Figure 5.4 Design Modification: Longitudinal Plate in Rocker

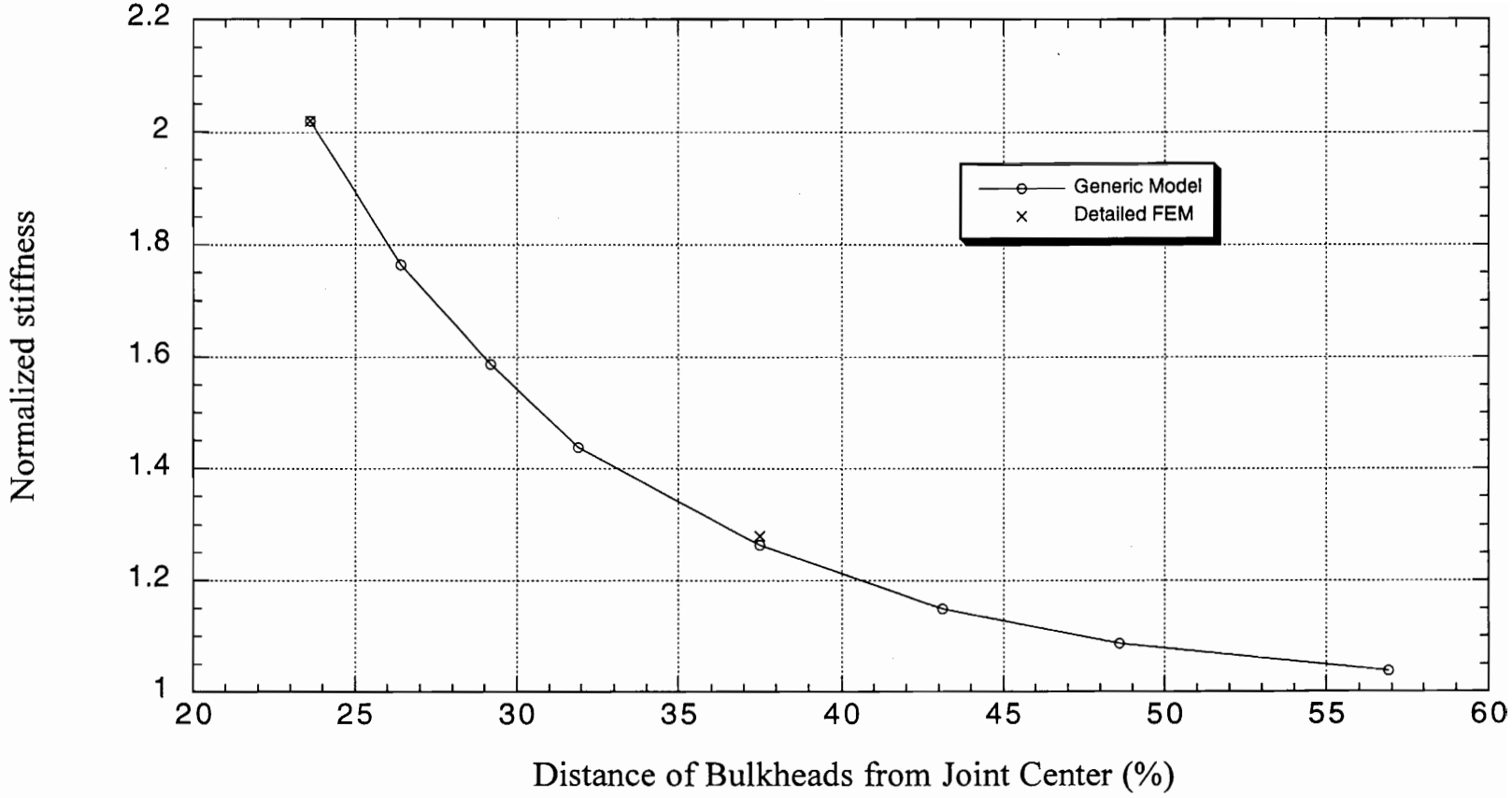

Normalized stiffness: Stiffness of modified joint with bulkheads over stiffness of original joint

Figure 5.5 Effects of Transverse Bulkheads on Joint Stiffness

(Transverse bulkheads are spot welded to the outboard rocker panel.)

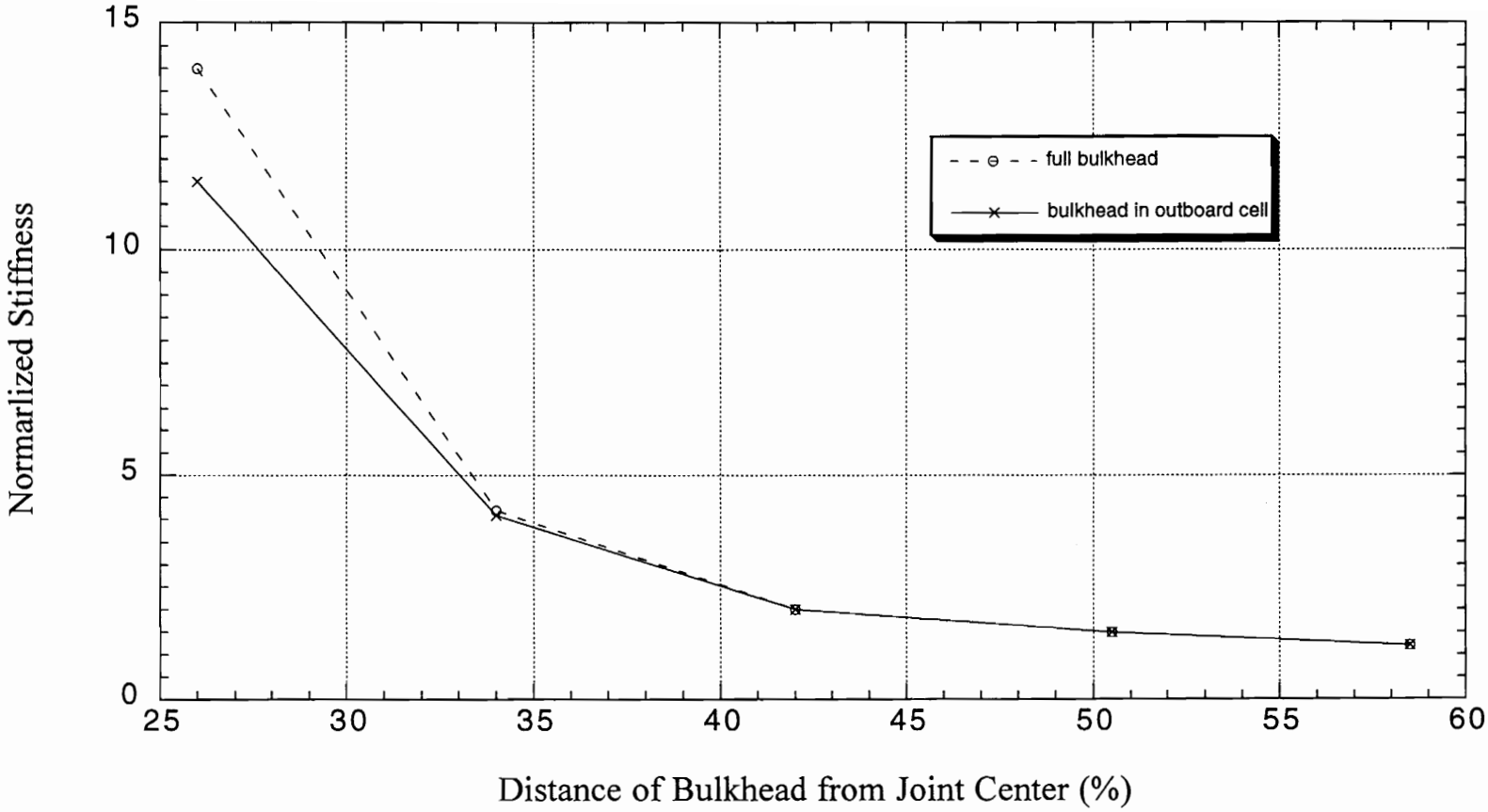

Normalized Stiffness: Stiffness of modified joint with bulkheads over stiffness of orginal joint

Figure 5.6 Effects of Transverse Bulkheads on Joint Stiffness

(Transverse bulkheads are continuously weled to all panels.)

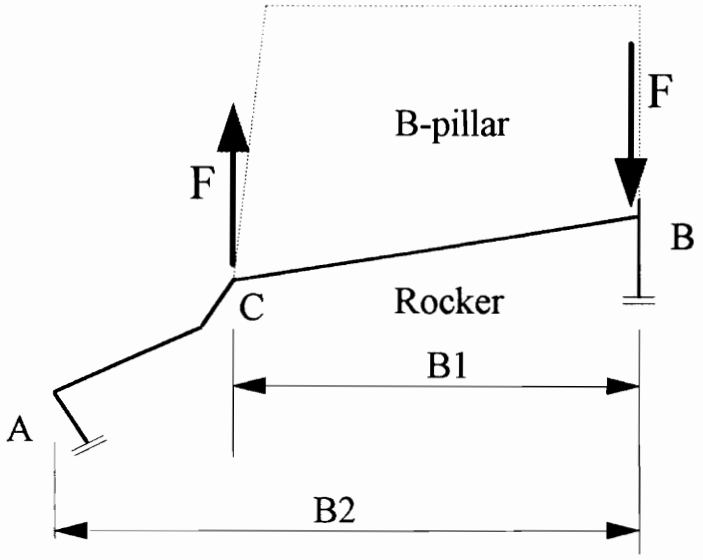

(a) Connection of B-pillar to top panel of rocker

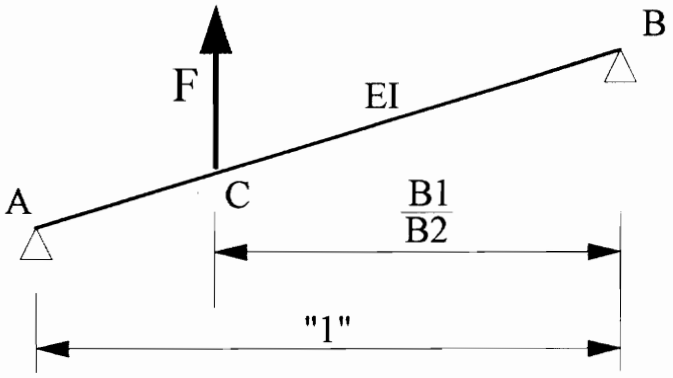

(b) Simplify the structure (a) as a simple supported beam and simplify the load from B-pillar to rocker as a concentrated force

Figure 5.7 Couple of Forces Applied to Top Plate of Rocker due to I/O Bending and Importance of Parameter B1/B2

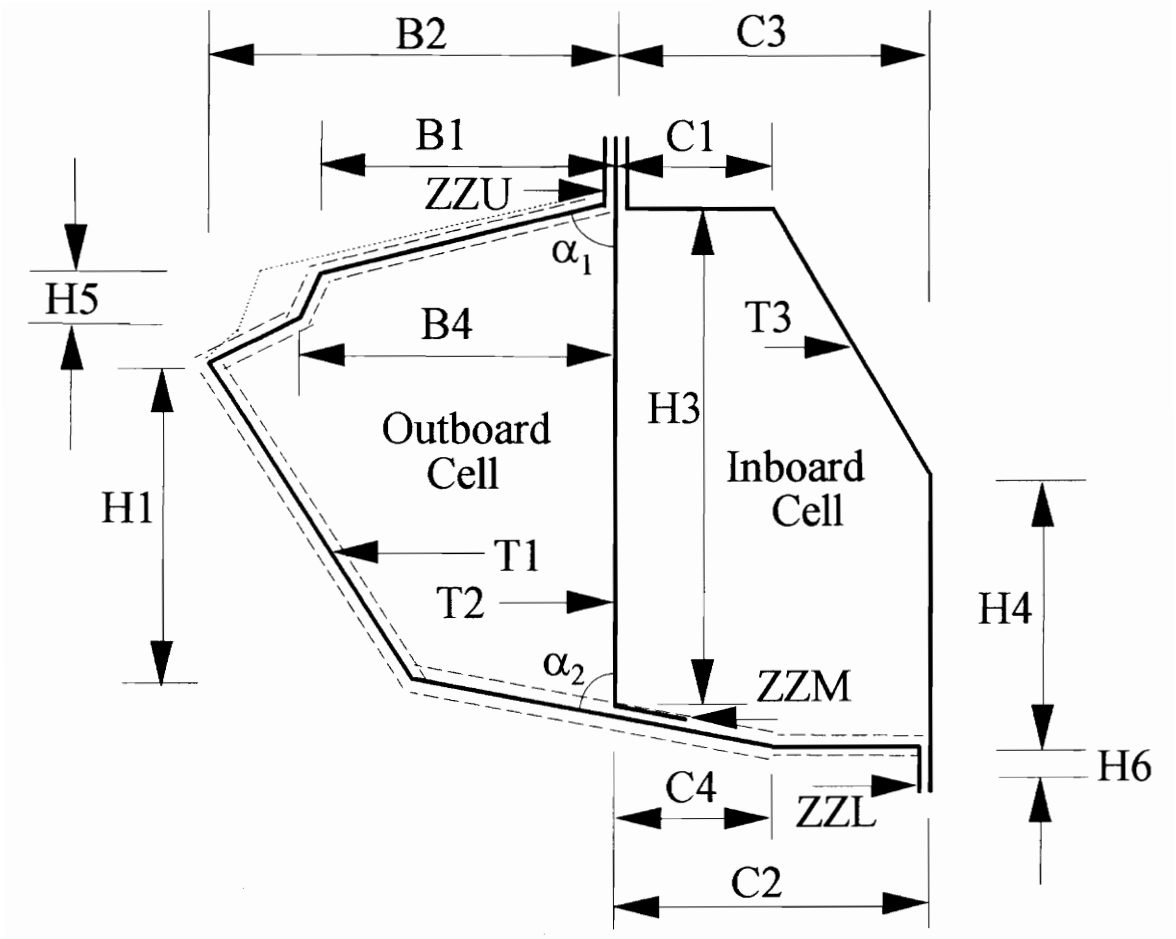

Figure 5.8 Proposed Modifications 1 and 2: Increasing B1/B2 and T1

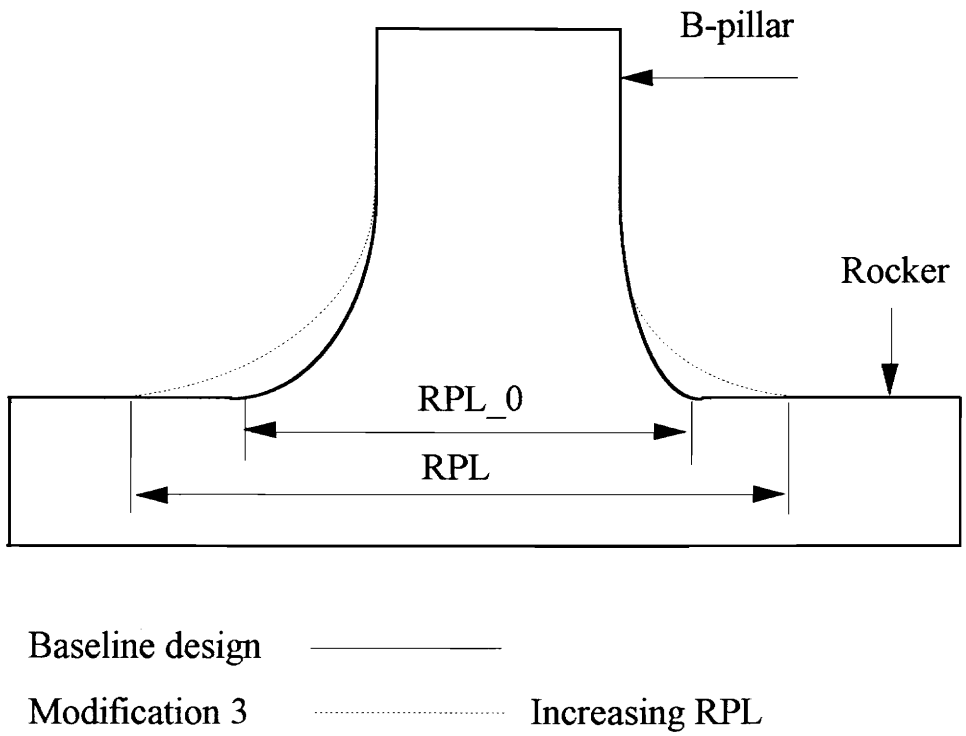

Figure 5.9 Proposed Modification 3: Increasing Linkage Length

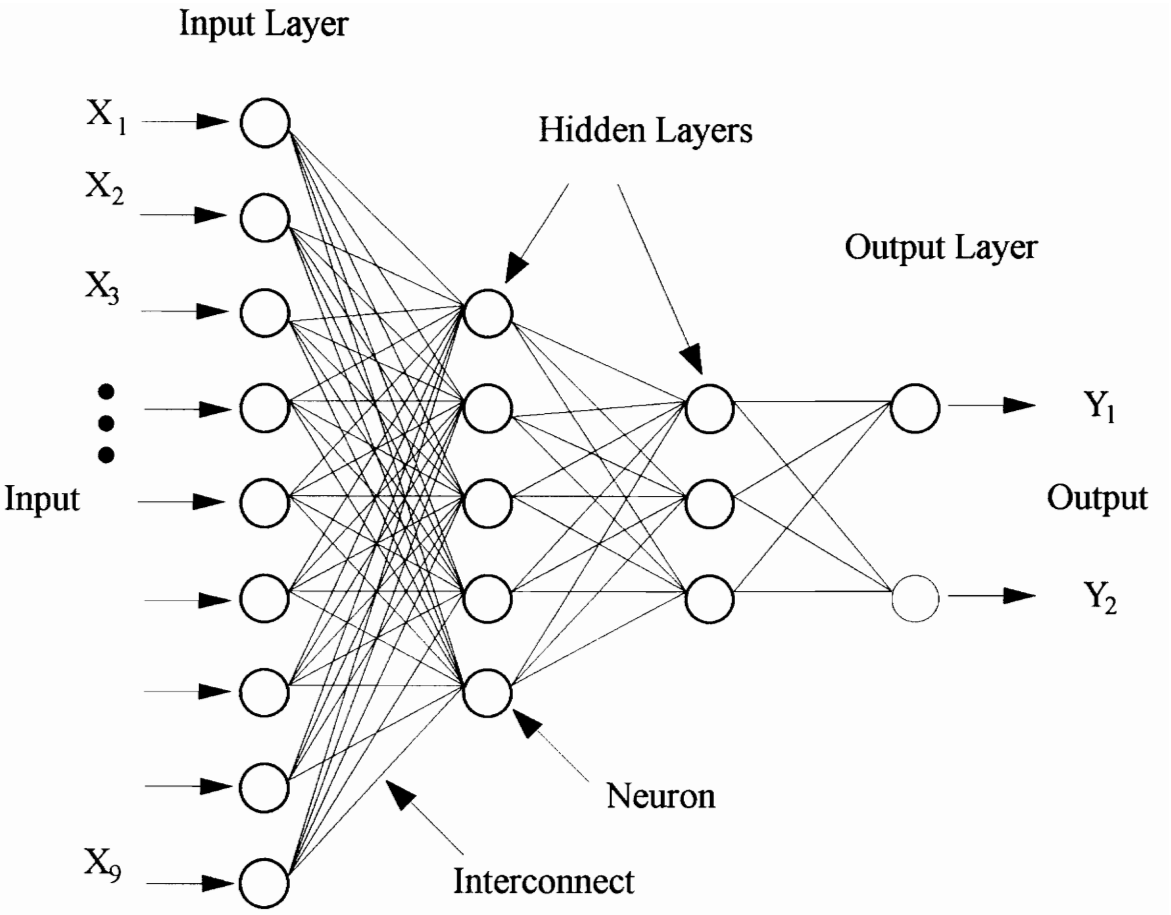

Figure 6.1 Artificial Neural Network

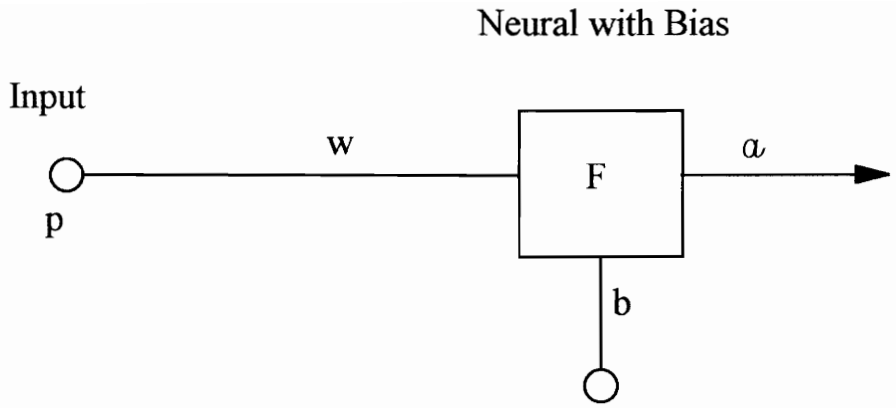

$$a = F(wp^T + b)$$

Figure 6.2 A Mathematical Model of A Neuron

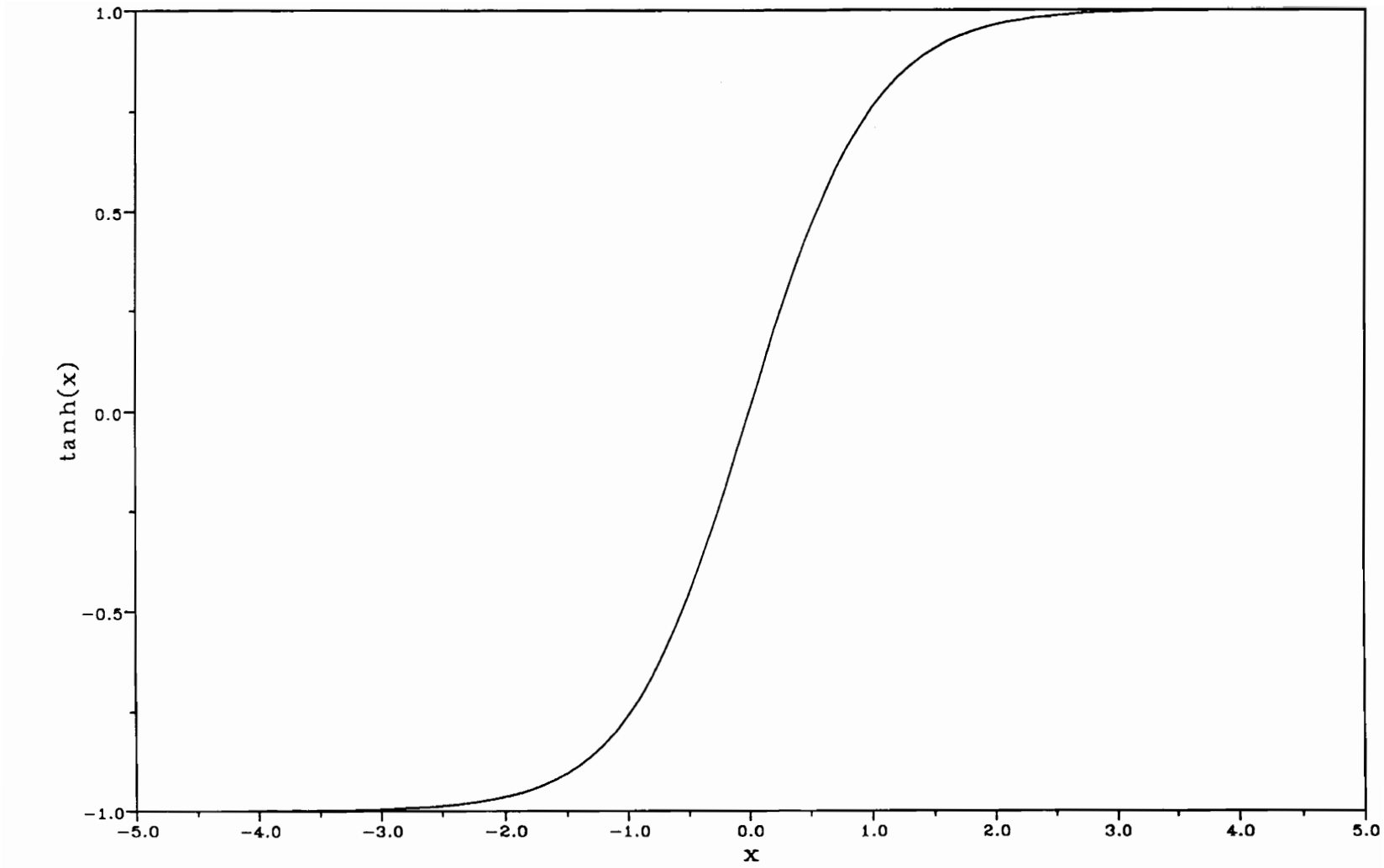

Figure 6.3 Hyperbolic Tangent Sigmoid Transfer Function

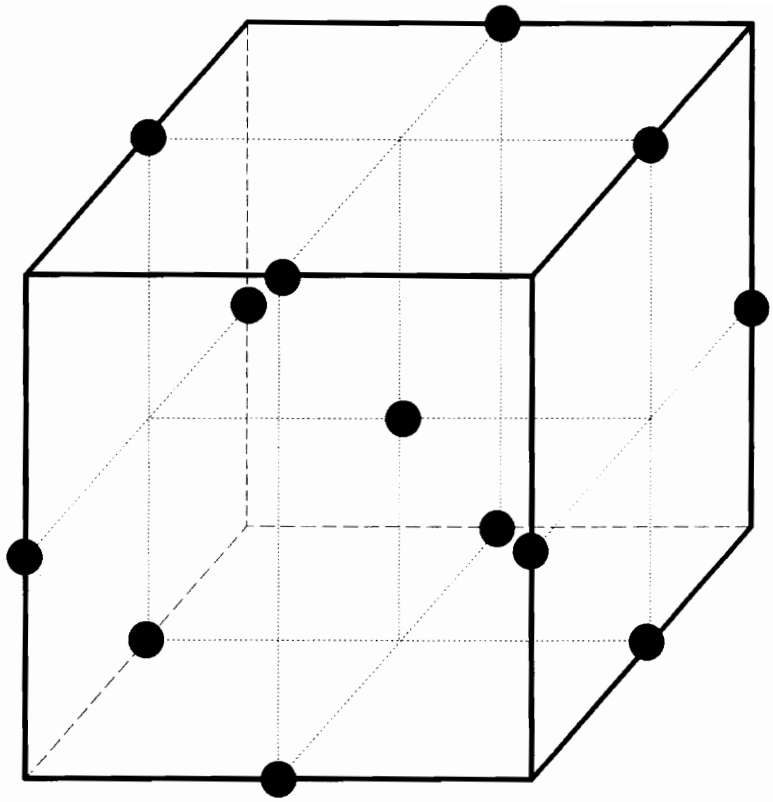

Figure 6.4 Box-Behnken Design for 3 Factors and 3 Levels

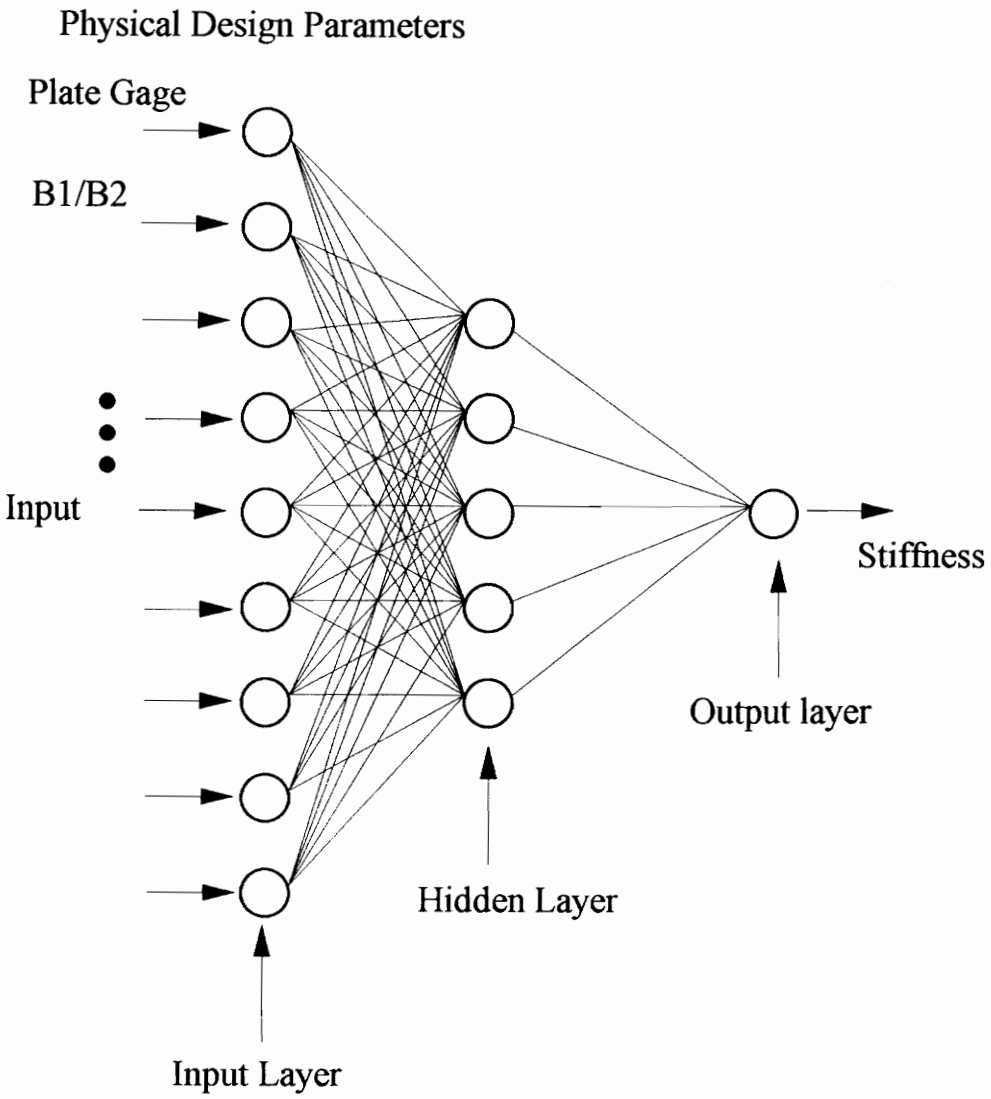

Figure 6.5 A Neural Network Used to Predict the I/O Stiffness of the Joint in This Study

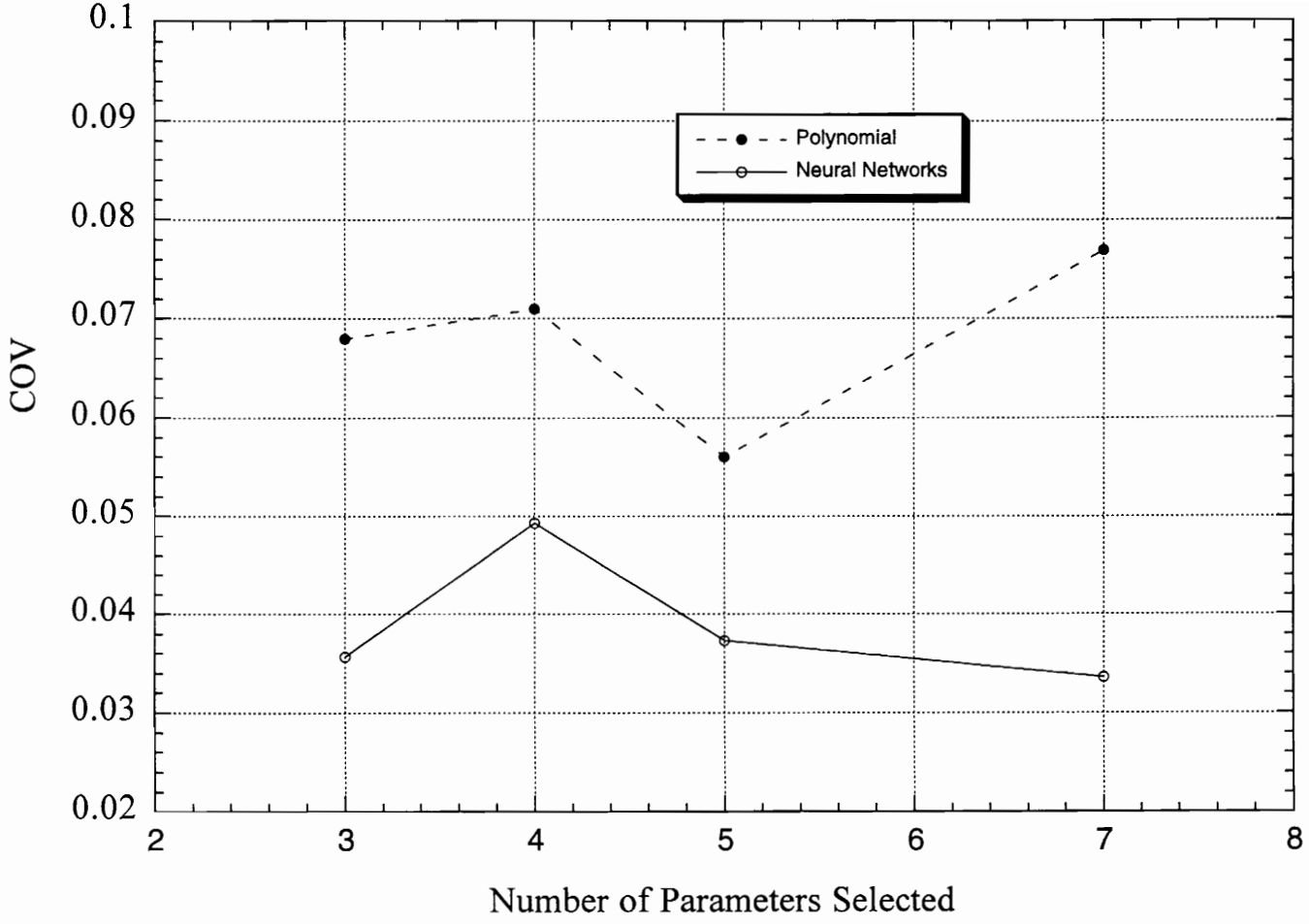

Figure 6.6 COV versus Number of Parameters for Fitting/Training Data Set

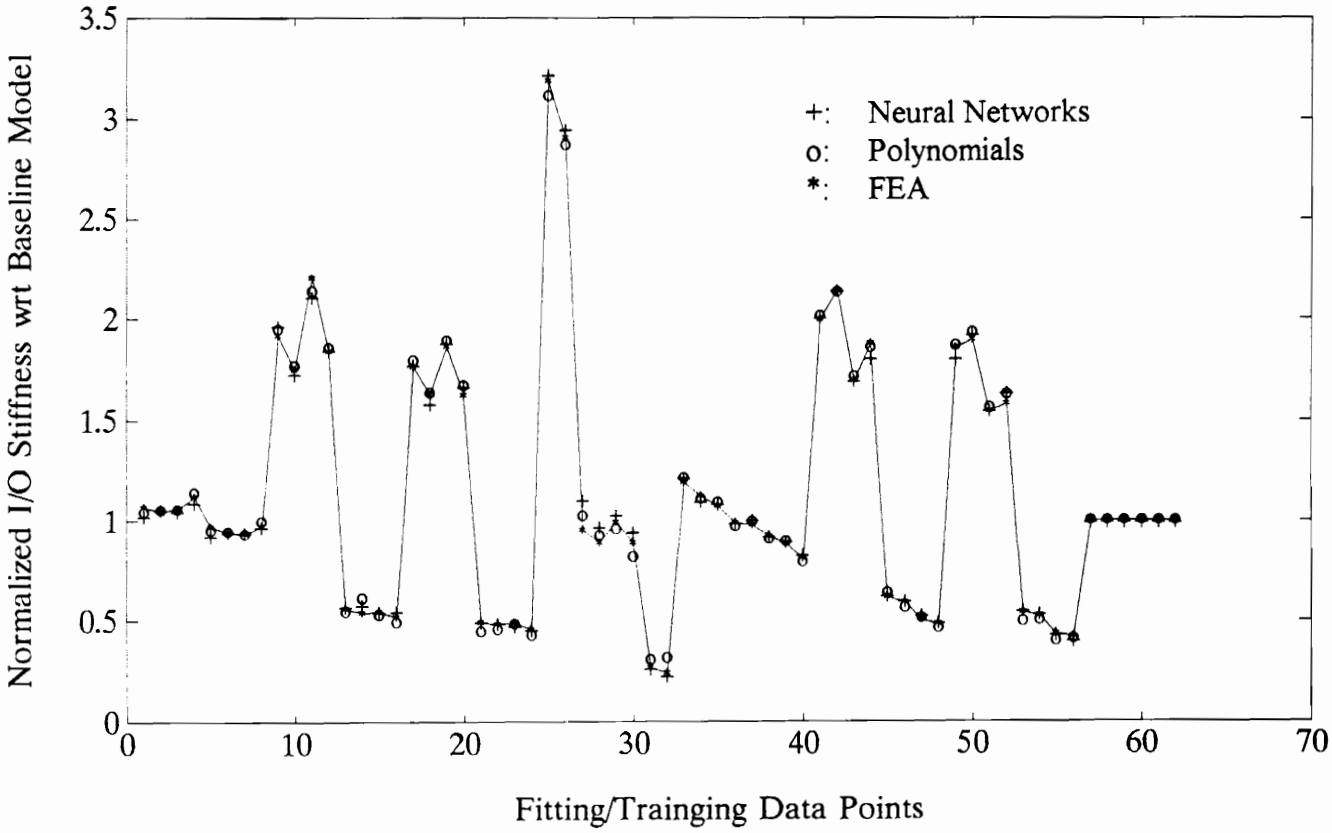

Figure 6.7 Prediction of Polynomials and Neural Networks for Fitting/Training when Using Top 7 Parameters

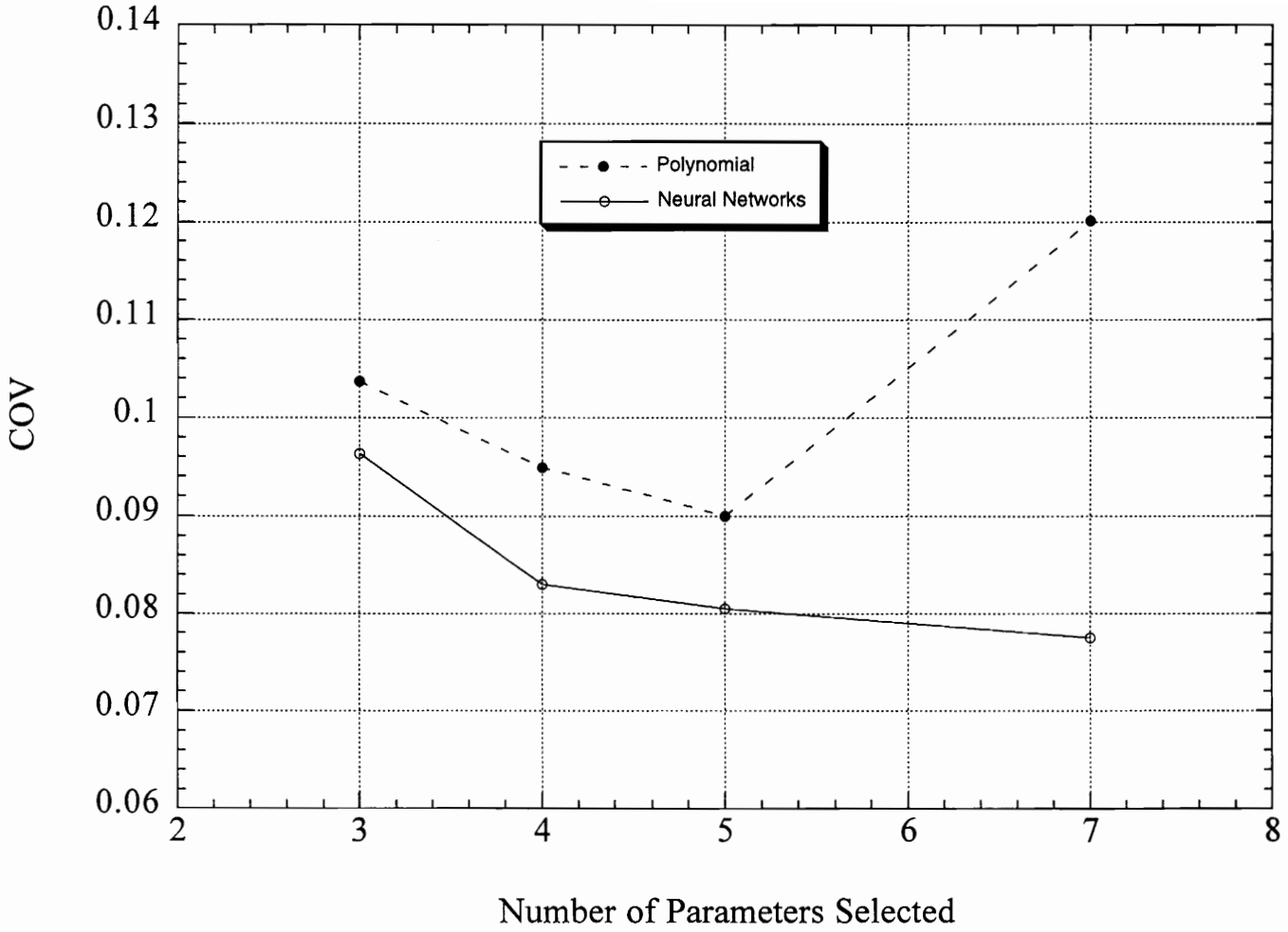

Figure 6.8 COV versus Number of Parameters for 50 Points Testing Data

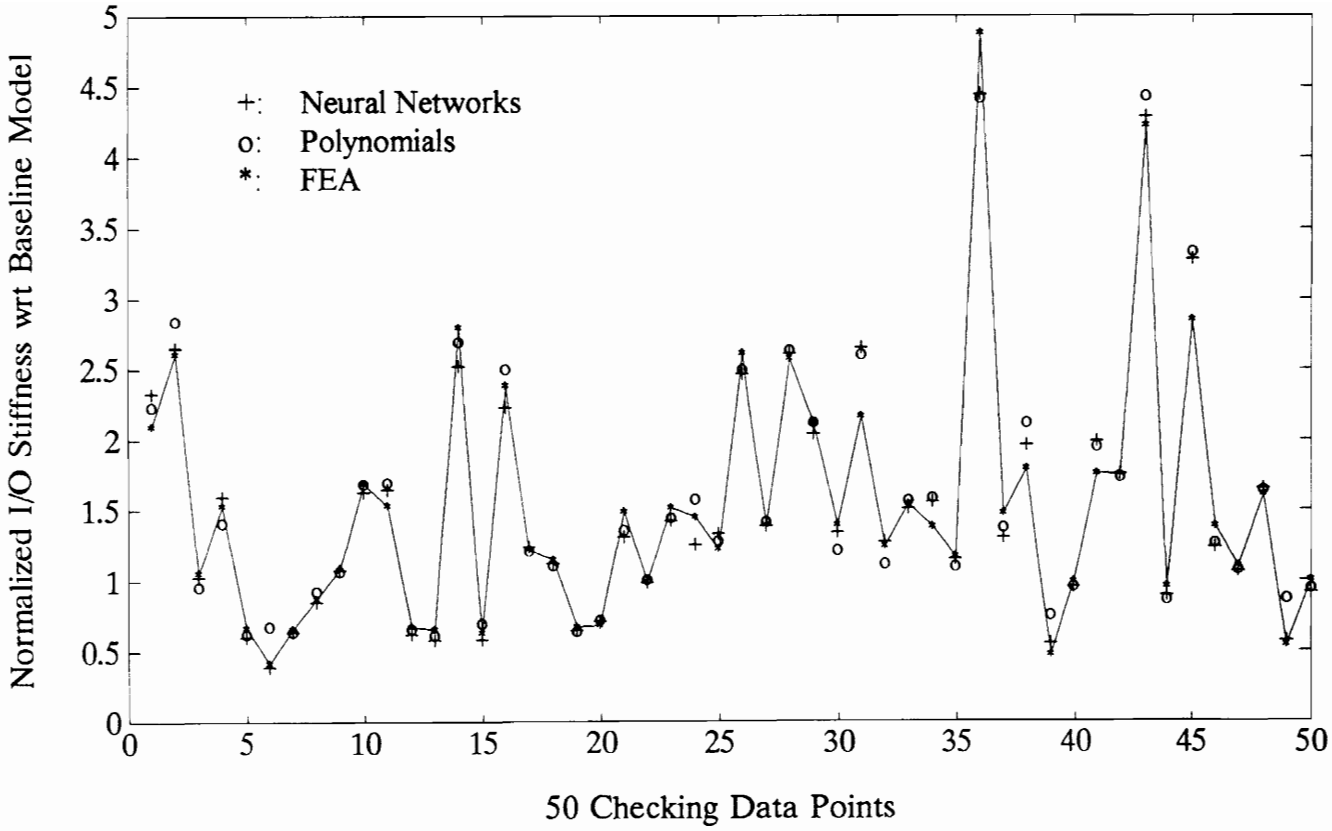

Figure 6.9 Predictions of Polynomial and Neural Network for 50 Points Testing Data When Using top 7 Parameters

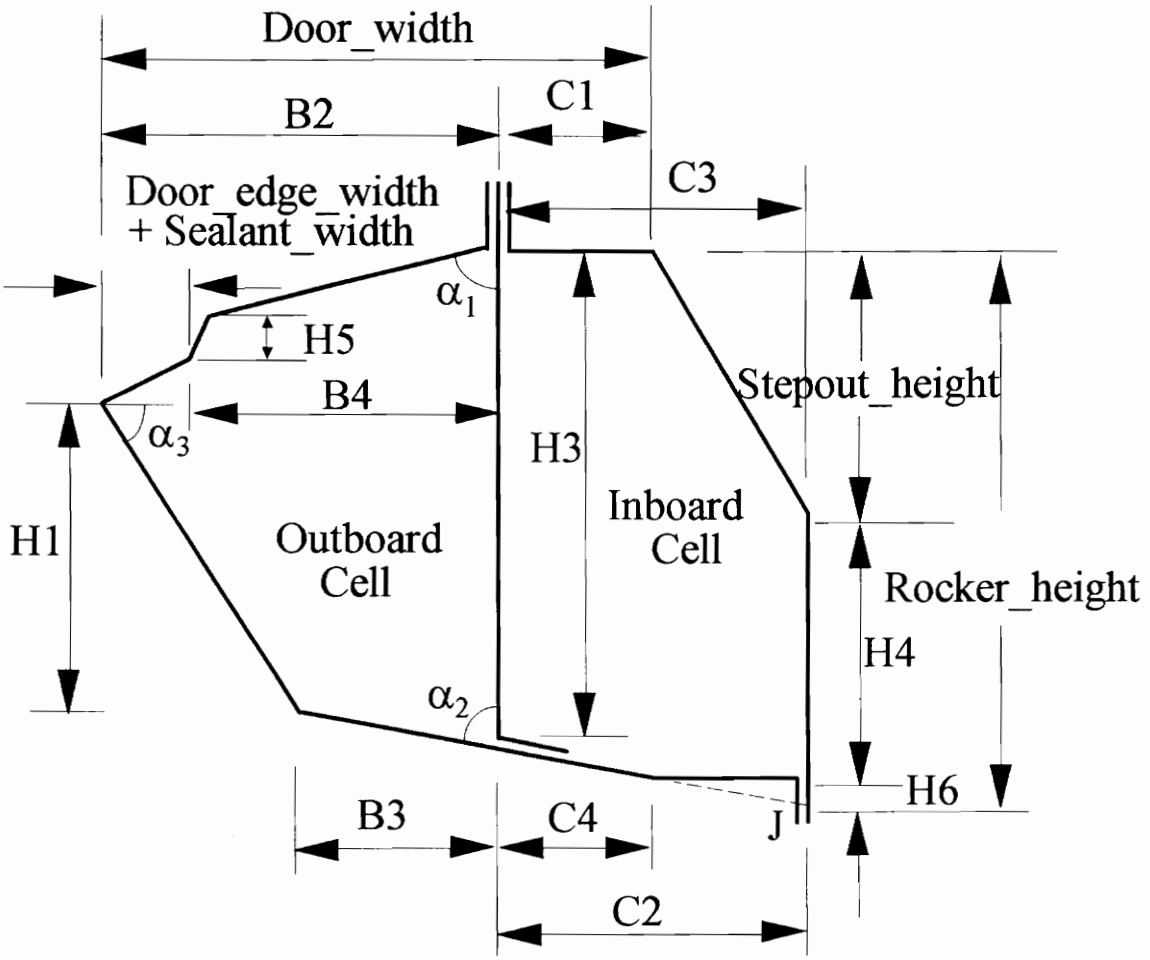

Rocker_height	-- rocker height
Rocker_width	-- rocker width
Door_width	-- door width
Door_edge_width	-- width of lower edge of door
Stepout_height	-- height of step out from the car

Figure 7.1 Some Packaging Constraint Criteria
(See Figure 3.8 for Detailed Parameters for Rocker Section)

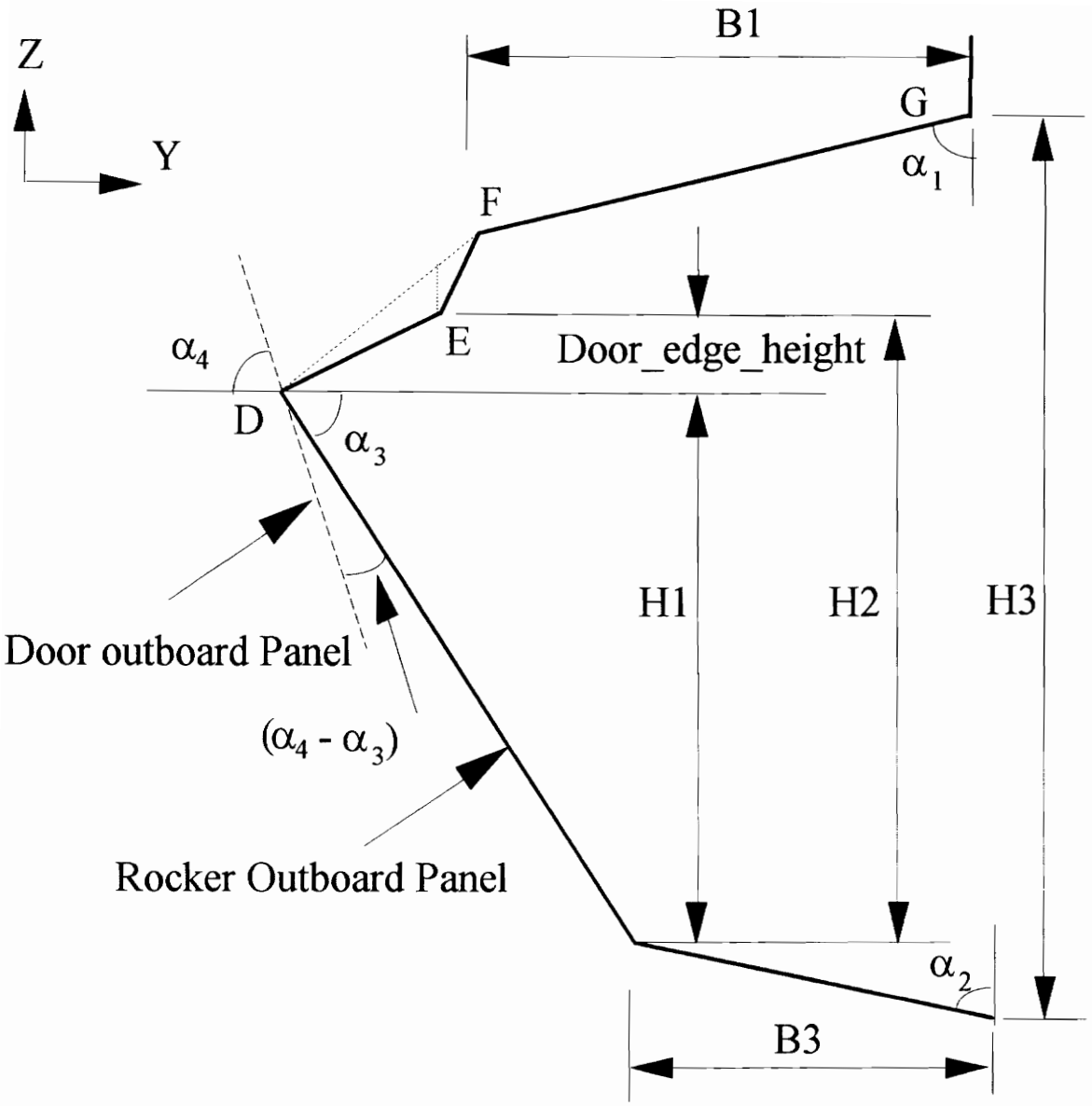

Where H2 = H3 - (H1 + B3/tan(α_2) + B1/tan(α_1)).

Figure 7.2 Packaging Constraints of Shape of Lower Edge of the Door

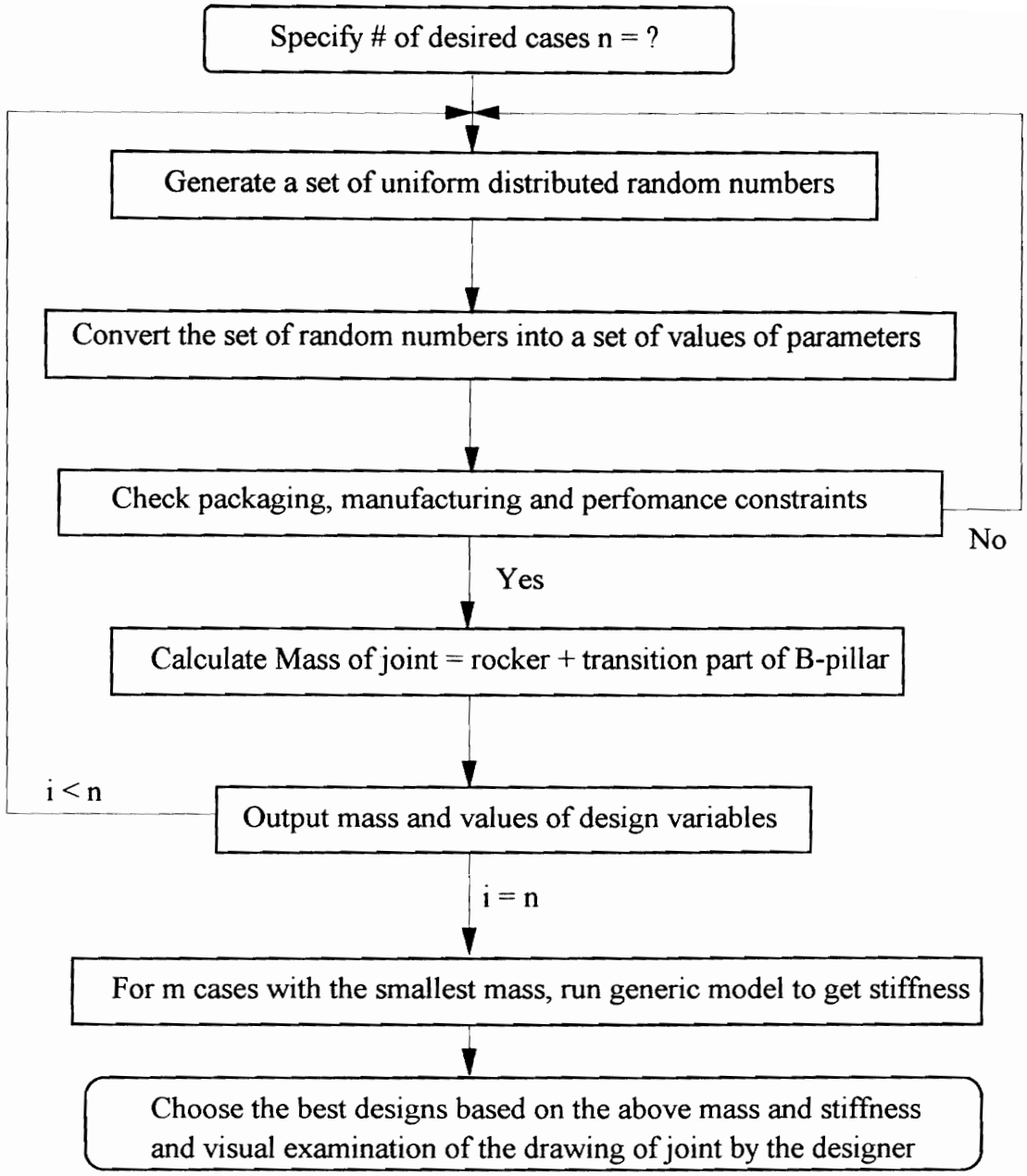

Figure 7.3 Flow Chart of Random Search Method

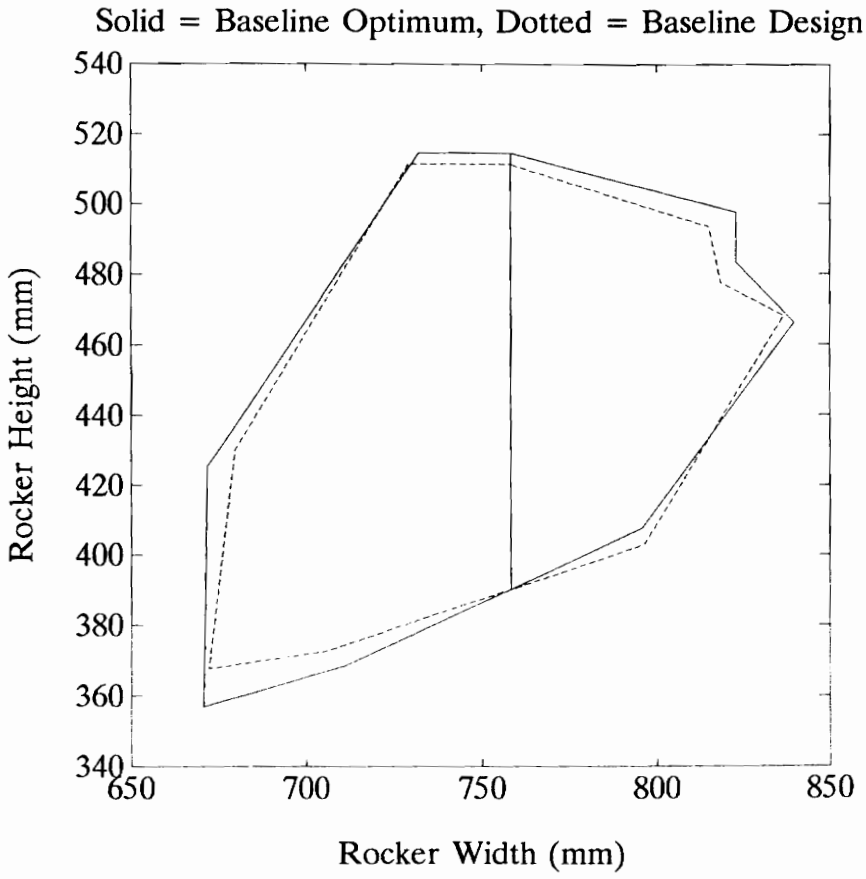

Figure 7.4 Rocker Section of Baseline Optimum versus Baseline Design

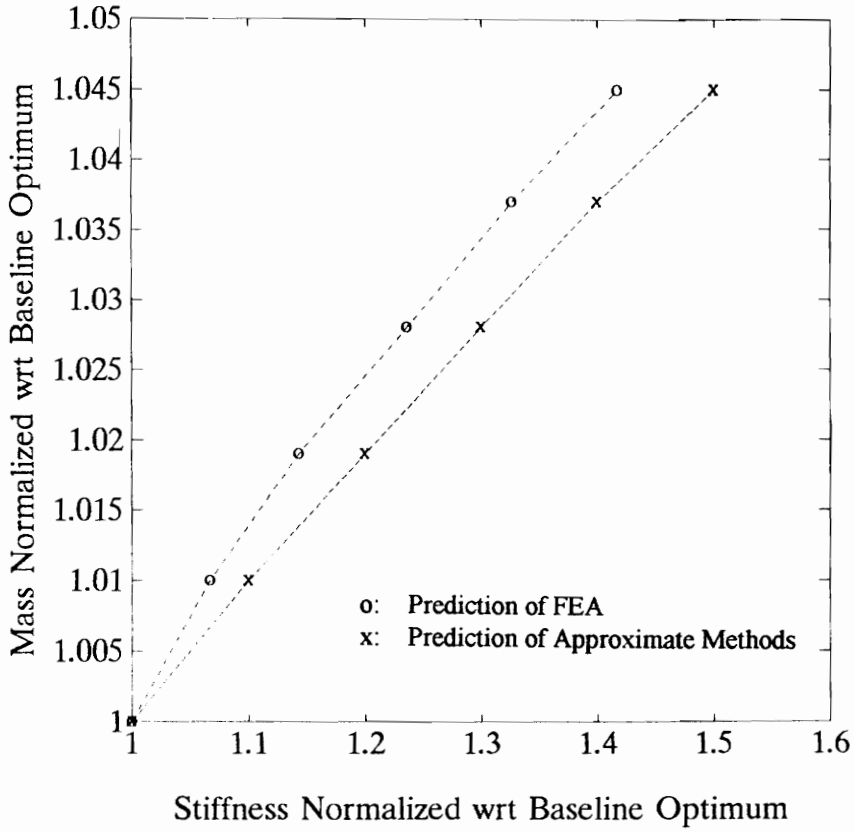

Figure 7.5 Normalized Mass versus Normalized Stiffness at Optimum

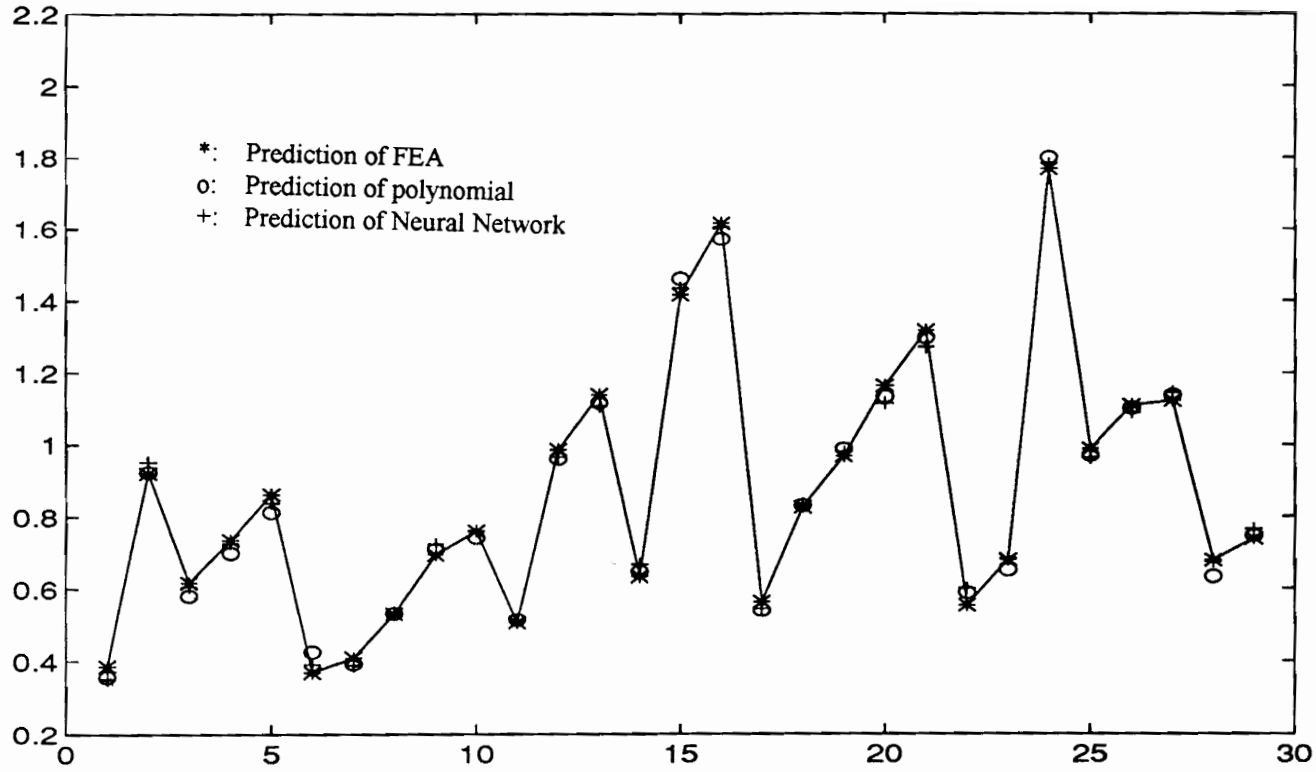

cov of the prediction of Neural network is 3.6%
cov of the prediction of Polynomial is 4.2%

Figure 7.6 Predictions of Polynomial and Neural Network for 30 Points Testing Data (Generated by Varying 21 Parameters) Using 7 Parameters

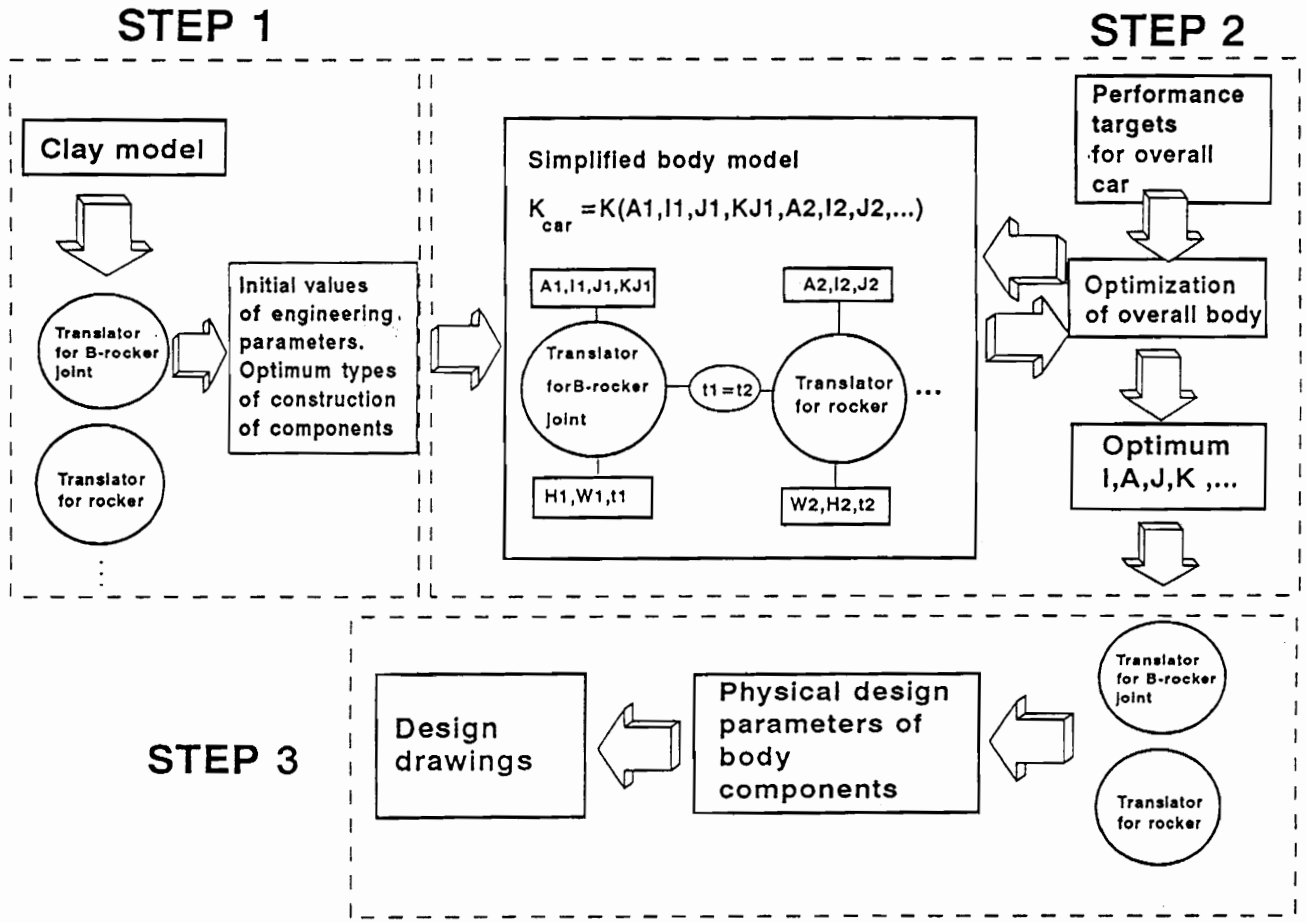

Figure 8.1 New Approach Proposed for Body Structure Gage and Shape Optimization

Vita

The author was born in China in 1962. He graduated from Department of Ship Architecture and Ocean Engineering, Shanghai Jiaotong University in 1983. Then, he worked in China Ship Scientific Research Center (CSSRC) as a research assistant for six years (1983 to 1989). He received an M.S. degree from CSSRC in 1988. He began to study for Ph.D. in Department of Aerospace and Ocean Engineering, Virginia Polytechnic Institute and State University in 1990.

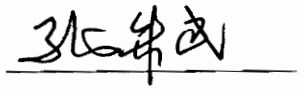

Min Zhu